Karin Tieber, BSc, BSc

Temperature distribution modelling of an automotive wet clutch disk

Master's Thesis

to achieve the university degree of

Diplom-Ingenieur

Master's degree programme: Mechanical Engineering

submitted to

Graz University of Technology

Supervisor

Assoc. Prof. Dipl.-Ing. Dr.techn. Michael Bader

Institute of Machine Components and Methods of Development
Head: Univ.-Prof. Dipl-Ing. Dr.techn. Hannes Hick

Graz, June 2018

Affidavit

I declare that I have authored this thesis independently, that I have not used other than the declared sources/resources, and that I have explicitly indicated all material which has been quoted either literally or by content from the sources used. The text document uploaded to TUGRAZonline is identical to the present master's thesis.

Date	Signature

Abstract

To optimize durability, reliability and efficiency of an automotive wet clutch, the temperature of the clutch disks is one of the most important variables. In this thesis, a semi-physical model is developed, that is capable of estimating the disk temperature online during clutch operation with little computational effort and only a few sensors available.

The model is based on a detailed theoretical analysis of the physical phenomena influencing the clutch temperature. Under consideration of a radially grooved friction layer, the oil flow between the disks is described analytically. From this, phenomena like the forming of rivulets, the drag torque and finally the convective heat transfer from the disk to the oil is derived. For the generation and distribution of the friction heat, simple relations based on physical and empirical relationships are formulated. To efficiency compute the derived relations in each time step, numerical procedures are proposed. To obtain an estimate of the temperature and its distribution in radial and axial direction, the finite difference method is used.

The developed model is validated qualitatively under consideration of empirical, numerical and analytical results from literature and an analysis of stability. Also, a quantitative validation with measurement data is conducted. In all considered scenarios, the model shows good performance and provides a temperature estimation that is accurate enough for its destined application.

Zusammenfassung

Um die Lebensdauer, Zuverlässigkeit und Effizienz einer nasslaufenden Lamellenkupplung zu optimieren, ist die Temperatur der Kupplungsscheiben einer der wichtigsten Parameter. In dieser Arbeit wird ein semi-physikalisches Modell entwickelt, das in der Lage ist, die Scheibentemperatur während des Kupplungsbetriebs mit geringem Rechenaufwand und nur wenigen verfügbaren Sensoren online zu berechnen.

Das Modell basiert auf einer detaillierten theoretischen Analyse der physikalischen Phänomene, die die Kupplungstemperatur beeinflussen. Unter Berücksichtigung eines radial gerillten Reibbelags wird der Ölfluss zwischen den Scheiben analytisch beschrieben. Daraus ergeben sich Phänomene wie unvollständige Benetzung, das Schleppmoment und schließlich die konvektive Wärmeübertragung von der Scheibe auf das Öl. Für die Entstehung und Verteilung der Reibungswärme werden einfache Beziehungen auf der Basis physikalischer und empirischer Zusammenhänge formuliert.
Um die abgeleiteten Beziehungen in jedem Zeitschritt effizient zu berechnen, werden numerische Verfahren präsentiert. Für die Berechnung der Scheibentemperatur und ihrer Verteilung in radialer und axialer Richtung wird die Finite-Differenzen-Methode verwendet.

Das entwickelte Modell wird unter Berücksichtigung empirischer, numerischer und analytischer Ergebnisse aus der Literatur und einer Stabilitätsanalyse qualitativ validiert. Außerdem wird eine quantitative Validierung mit Messdaten durchgeführt. In allen betrachteten Szenarien zeigt das Modell eine gute Performance und liefert eine Temperaturschätzung, die ausreichend genau für die vorgesehene Anwendung ist.

Acknowledgment

Contents

Contents

List of Figures

List of Tables

1 Introduction

1.1 Motivation

Wet multi disk clutches are used in most automated gearboxes. One of the reasons is the better controllability compared to dry clutches. Also, due to the oil cooling, they can be constructed more compact and with a higher durability.

These clutches are used in all main categories of geared automated transmissions for on-road vehicles, namely:

- automated manual transmission (AMT)
- dual clutch transmission (DCT)
- automatic transmission (AT)

The AMT is basically a common manual transmission with hydraulic or electro mechanical actuators to control the clutch, where often a wet multi disk clutch is used as a launching clutch.
The DCT consists of two sub-transmissions for odd and even gear sets and a dual clutch connecting the sub-transmissions with the gearbox input shaft. With the dual clutch, a gear shift without interruption of tractive power is possible.
In an AT, a torque converter acts as the launching clutch. For higher efficiency, a lock-up torque converter can lock the pump and turbine of the torque converter together. Planetary gears connect the torque converter with the output of the AT. The gear ratio can be switched by changing the power flow in the planetary gears.

Wet multi disk clutches are used for the dual clutch in the DCT, for the lock-up torque converter or as a launching clutch in the AMT or AT and as switching elements for the planetary gears in the AT.

The durability of a wet clutch mostly depends on the temperature of the disk surfaces during operation. Knowledge of this temperature can be used to optimize cooling and operation of the clutch. This can not only increase the durability, but also lead to better performance. Knowledge of the disk temperature allows an optimization of the control strategy towards shorter coupling times to increase efficiency and driving performance.

1.2 Problem formulation and objectives

To facilitate optimal cooling and operation of the clutch system, the temperature needs to be known online during operation on the test bench or in the vehicle. For online simulation, computational resources for the model are very limited and in the vehicle, only a few sensors are available. Since not only the mean temperature of the disks but also the maximum temperature on the disk surfaces is of interest, the temperature needs to be spatially resolved in radial and axial direction.

The objective is to obtain an accurate estimation of the temperature with little computational effort and little data. The evident solution for this is to combine the accuracy of physical models with the computational efficiency of empirical approaches to a semi-physical model that is capable of estimating the temperature profile in radial direction in every single disk.
Another important aim is the transferability of the model to different clutch systems and applications. The estimation of temperature shall be accurate in all clutch states (open, closed, slipping) and in a wide range of conditions (flow rate, rotational speed, torque, oil properties, ...).

1.3 Overview

In chapter 2, the physical phenomena that are significantly influencing the temperature of the clutch disks are first investigated from a theoretical point of view. Subsequently, simplifications and empirical corrections that allow an implementation which meets the stated objectives are presented. Chapter 3 deals with the parametrisation and validation of the model with measurement data, and also with the qualitative validation of consistency and stability. Chapter 4 gives an overview of the presented approaches and results. Furthermore, an outlook for future work is presented.

2 Modelling

Over the years, many studies about the thermal and mechanical behaviour of multi-disk wet clutches have been conducted. In [1], an extensive CFD (computational fluid dynamics) model to describe the dynamical behaviour of wet clutches has been developed. This model is focused on the multi-phase flow before and during clutch engagement. In [2], a numerical-empirical model to simulate the actuation and friction behaviour of the clutch system is presented. In [3], extensive experiments on a clutch to investigate the friction and temperature behaviour and their dependence on the geometry of the disks, oil flow and other influences have been carried out.

The clutch system considered in this study is schematically illustrated in Figure 2.1. It consists of a stack of friction and separator disks, which are non-rotatably but axially displaceably mounted on the shaft and on the casing, respectively. The friction disks are steel plates with a layer of paper or sinter material, which is radially grooved. The separator disks are smooth steel plates. Oil is pumped through the shaft and lubricates the space between the disks. The (typically hydraulic) actuator can enable clutch engagement by pushing the disks together. The backing holders on both sides of the disk stack ensure a uniform pressure distribution between the disk surfaces. Since the casing of a wet clutch varies a lot for different applications, it is not a part of the model. Its influence is only modelled with an empirical relation.

The measurable boundary conditions are:

- the temperature of the incoming oil $T_{\text{oil,in}}$
- the torque transmitted by the clutch Tq
- the rotational speeds of the friction disk and the separator disk, ω_1 and ω_2, respectively
- the oil volume flow rate Q.

In this chapter, the most important physical phenomena influencing the clutch disk temperature are mathematically described. Furthermore, their significance is estimated and simplifications are made accordingly. In consideration of the limited computation resources, solutions for implementing the phenomena are presented. The main effects and their interaction that will be considered are shown in figure 2.2.
In section 2.1, the behaviour of the oil flow between the disks will be investigated. From the velocity and pressure distributions, the disk distance h, the partition of oil flow in the grooves Q_{g}/Q and the forming of rivulets ϕ_{riv} can be described. Using
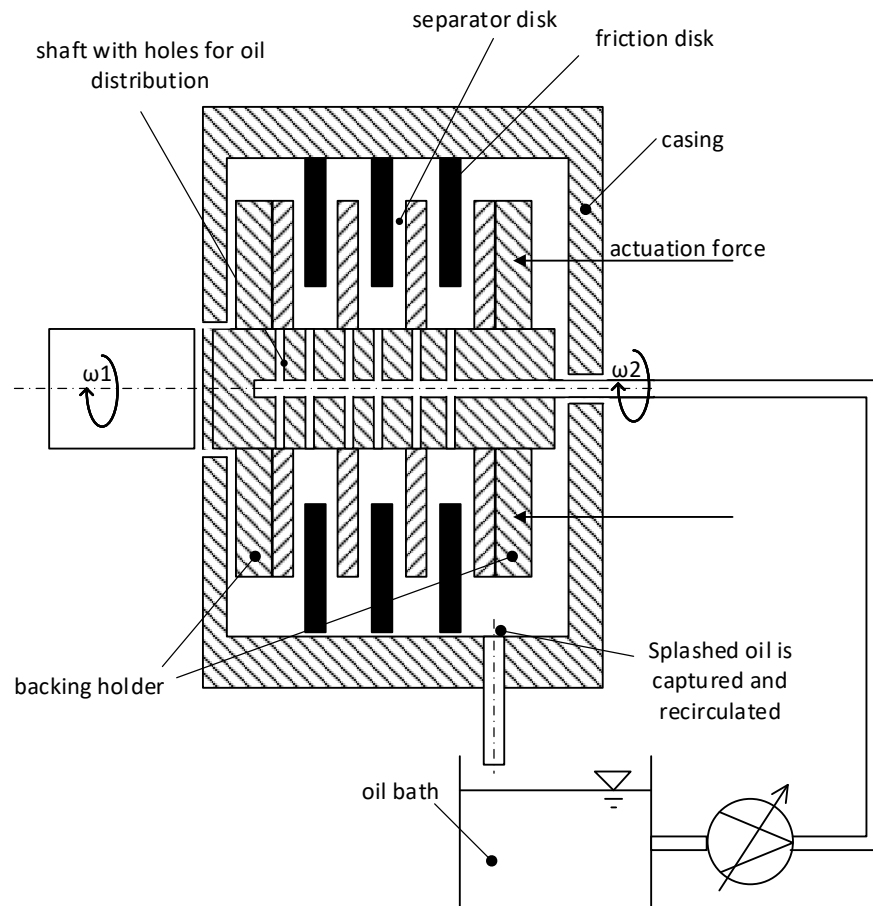
Figure 2.1: Schematic illustration of the considered wet clutch system: Oil is pumped into the shaft and distributed into the stack of disks. The oil flows between the disks and splashes to the casing where it is captured and recirculated. A hydraulic or electric actuator can press the disks together to enable torque transmission
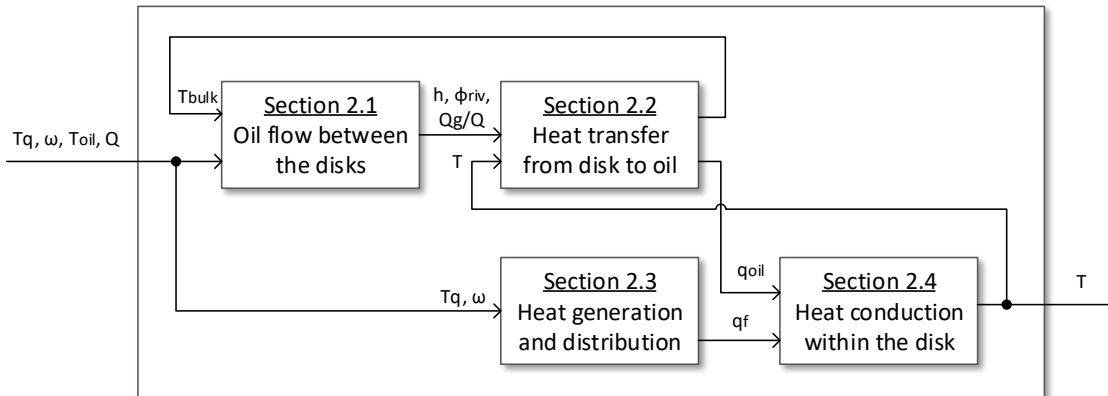
Figure 2.2: Physical phenomena influencing the clutch temperature and their interaction

these results, in section 2.2, the heat transfer from the disks to the oil q_{oil} is estimated, and the resulting oil temperature between the disks T_{bulk} is calculated. In section 2.3, the heat q_{f} generated by friction and viscous flow and its partition to friction and separator disk is described. In section 2.4, the temperature in the disk T and its distribution is estimated.

2.1 Oil flow

Consider a pair of discs as shown in figure 2.3 with distance $h(\varphi) \in [h_{\text{ng}}, h_{\text{g}}]$ to each other, where h_{ng} is the disk distance in the non-grooved area and h_{g} is the disk distance in the grooved area. The grooved friction plate rotates at speed ω_2 and the smooth separator plate rotates at speed ω_1.

Following the simple oil flow model presented in [1], the Reynolds equations in the considered system will be formulated and solved. In contrast to [1], the grooves will be taken into account, and both disks can rotate at different speeds (instead of one disk being stationary). Consequently, the flow will not be rotationally symmetric and the inertia force can also be taken into account for both disks rotating.

2.1.1 Assumptions

To obtain a simple and comprehensive analytical solution for describing the oil flow, several assumptions need to be made.
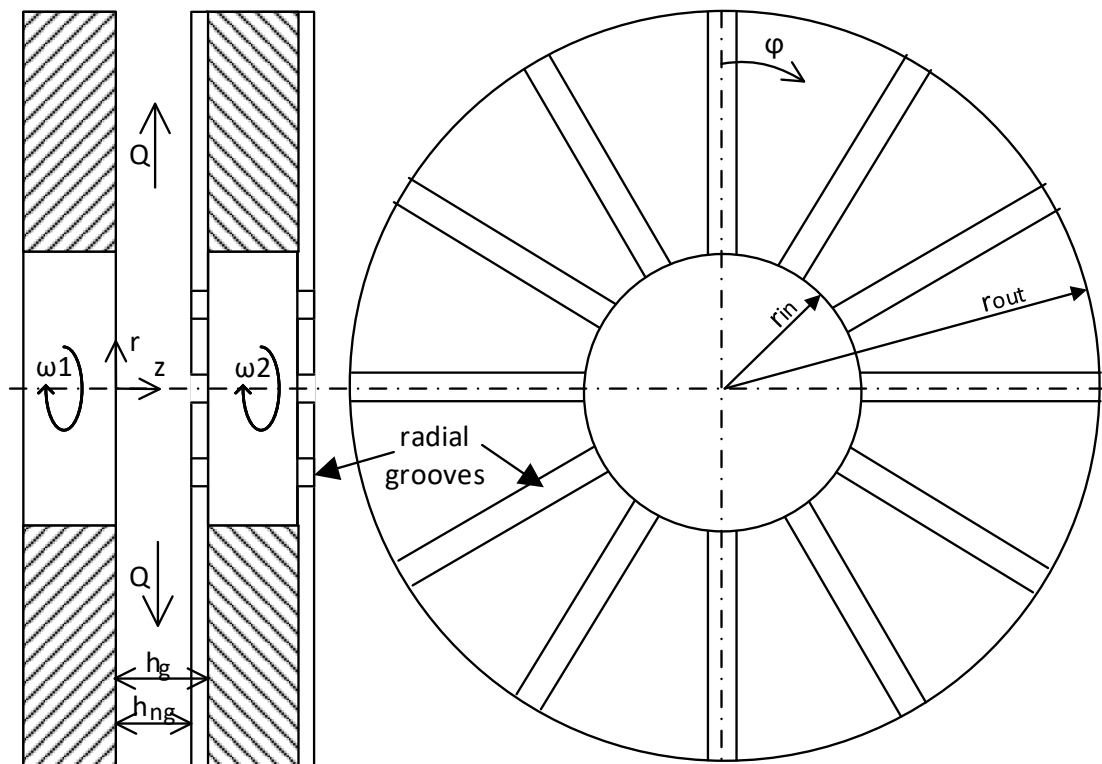
Figure 2.3: Model for considerations regarding the oil flow. The separator disk rotates at speed ω_1, and the radially grooved friction disk rotates at speed ω_2. Between the disks is an oil film with oil volume flow rate Q

- In reality, the oil will flow out through several holes at different angular locations in the shaft. Optimally, the oil will spread in the area between shaft and the beginning of the friction surface, radius r_{in}, and is equally distributed when entering the grooved region. In the presented model, only the flow between r_{in} and r_{out} will be considered, and speed and temperature of the oil entering this region are assumed to be rotationally symmetric with regard to the z axis.
- Although, the oil properties (especially the viscosity) highly depend on the temperature, we assume stationary oil properties equal to the oil properties at the current mean oil temperature. This assumption will later be dropped for particular situations to limit the error.
- The behaviour of a thin fluid film between two solid surfaces can be described with lubrication theories. For a thicker film, hydrodynamic phenomena will become relevant. Reynold's theory of hydrodynamic lubrication (see [4]) describes the case where the film is thick enough to be analysed by hydrodynamics and, at the same time, thin enough so that Reynolds' assumptions hold. This subject is further discussed in [5, p. 11-22].
  It is assumed, that Reynold's theory of hydrodynamic lubrication applies. Therefore, the following assumptions must hold:
    - The oil flow is laminar.
    - The gravity and inertia forces acting on the fluid can be ignored compared to the viscous force.
    - Compressibility of the fluid is negligible. That is, the density of the oil ρ_{oil} is constant.
    - The fluid is Newtonian and the coefficient of viscosity μ_{oil} is constant throughout the area of lubrication.
    - The fluid pressure p does not change along the film thickness h.
    - The rate of change of the velocities v_r and v_φ in the r direction and φ direction is negligible compared with the rate of change in the z direction.
    - There is no slip between the fluid and the solid surface.

Since Reynold's theory neglects inertia forces, the Reynolds equations will be modified such that the inertia force due to the rotational speeds ω_1 and ω_2 is taken into account.

2.1.2 Oil volume flow rate

With the stated assumptions, the Reynolds equations in cylindrical coordinates, as expressed in [5, p. 55f], can be formulated.

$$\mu_{\text{oil}} \frac{\partial^2 v_r}{\partial z^2} = \frac{\partial p}{\partial r} - \rho_{\text{oil}} \frac{v_\varphi^2}{r} \tag{2.1a}$$

$$\mu_{\text{oil}} \frac{\partial^2 v_\varphi}{\partial z^2} = \frac{1}{r} \frac{\partial p}{\partial \varphi} \tag{2.1b}$$

With the second term on the right hand side of (2.1a), the centrifugal force is taken into account.

Considering the Reynolds assumptions, these equations are integrated in z twice.

$$\mu_{\text{oil}} \cdot v_r = \frac{\partial p}{\partial r} \cdot \frac{z^2}{2} - \frac{\rho_{\text{oil}}}{r} \int_0^z \int_0^z v_\varphi^2 \cdot d\tilde{z} d\tilde{z} + z \cdot C_1 + C_2 \tag{2.2a}$$

$$\mu_{\text{oil}} \cdot v_\varphi = \frac{1}{r} \cdot \frac{\partial p}{\partial \varphi} \frac{z^2}{2} + z \cdot C_3 + C_4 \tag{2.2b}$$

$C_{1\ldots4}$ are the integration constants, that will be determined with the boundary conditions.

For easier reading, in the following, the disk distance will be written as

$$h := h(\varphi) \in [h_{\text{ng}}, h_{\text{g}}]. \tag{2.3}$$

With the no-slip boundary conditions $v_r(z = 0) = 0$ and $v_r(z = h) = 0$, equation (2.2a) leads to:

$$v_r = \frac{1}{\mu_{\text{oil}}} \cdot \frac{\partial p}{\partial r} \cdot \frac{z(z-h)}{2} + \frac{\rho_{\text{oil}}}{\mu_{\text{oil}} \cdot r} \left(\frac{z}{h} \int_0^h \int_0^z v_\varphi^2 \cdot d\tilde{z} dz - \int_0^z \int_0^{\tilde{z}} v_\varphi^2 \cdot d\tilde{z} d\tilde{z} \right) \tag{2.4}$$

With the no-slip boundary conditions $v_\varphi(z = 0) = r \cdot \omega_1$ and $v_\varphi(z = h) = r \cdot \omega_2$, equation (2.2b) leads to:

$$v_\varphi = \frac{z(z-h)}{2r \cdot \mu_{\text{oil}}} \cdot \frac{\partial p}{\partial \varphi} + r \cdot \omega_1 + \frac{z}{h} r \cdot (\omega_2 - \omega_1) \tag{2.5}$$

Inserting equation (2.5) into (2.4), the mean radial velocity $\bar{v}_r$ can be calculated.

$$h \cdot \bar{v}_r = \int_0^h v_r \cdot dz = \frac{1}{40} \frac{\rho_{\text{oil}}}{\mu_{\text{oil}}} h^3 \cdot r \cdot (\omega_1^2 + \omega_2^2 + \frac{4}{3} \cdot \omega_1 \cdot \omega_2) - \frac{1}{\mu_{\text{oil}}} \cdot \frac{\partial p}{\partial r} \cdot \frac{h^3}{12}$$
$$+ \frac{\rho_{\text{oil}}}{\mu_{\text{oil}} \cdot r} \left(-\frac{\partial p}{\partial \varphi} \cdot \frac{h^5}{120\mu_{\text{oil}}} \cdot (\omega_1 + \omega_2) + \left(\frac{\partial p}{\partial \varphi} \right)^2 \cdot \frac{h^7}{1120\mu_{\text{oil}}^2 \cdot r^2} \right) \tag{2.6}$$

For easier reading, the characteristic rotational speed Ω is introduced.

$$\Omega^2 = \omega_1^2 + \omega_2^2 + \frac{4}{3} \cdot \omega_1 \cdot \omega_2 \tag{2.7}$$

To simplify the multidimensional partial differential equation (PDE) in (2.6), the method of Non-dimensionalization is performed. For this purpose, first, all variables will be expressed with dimensionless variables and constants. The constants are chosen such that the dimensionless variables will have a magnitude around 1. In a next step, the value of the constant part in each term can be calculated and compared. This values are representative for the impact of the corresponding term on the equation. Therefore, terms where the value is very small can be neglected.

The introduced dimensionless variables are:

$$r^* := \frac{r}{R}, \qquad\qquad\qquad R := (r_{\text{out}} + r_{\text{in}})/2 \tag{2.8a}$$

$$h^* := \frac{h}{H}, \qquad\qquad\qquad H := (h_{\text{ng}} + h_{\text{g}})/2 \tag{2.8b}$$

$$p^* := \frac{p}{\rho_{\text{oil}} \cdot U^2}, \qquad\qquad\qquad U := \frac{Q}{2\pi R H} \tag{2.8c}$$

$$\varphi^* := \frac{\varphi}{2\pi/n_{\text{g}}} \tag{2.8d}$$

$$\bar{v}_r^* := \frac{\bar{v}_r}{U} \tag{2.8e}$$

where n_{g} is the number of radial grooves.

Substituting (2.8) into (2.6) results in:

$$H \cdot h^* \cdot \bar{v}_r = \frac{\rho}{\mu_{\text{oil}}} H^3 \cdot \left[\frac{1}{40} R \cdot \Omega^2 \cdot h^{*3} \cdot r^{*2} + \frac{U^2}{12 \cdot R} \left(-\frac{\partial p^*}{\partial r^*} h^{*3} \right.\right.$$
$$\left.\left. - \frac{H^2(\omega_1 + \omega_2) \cdot \rho_{\text{oil}}}{10 \cdot \mu_{\text{oil}} \cdot 2\pi/n_{\text{g}}} \cdot \frac{1}{r^*}\frac{\partial p^*}{\partial \varphi^*} + \frac{H^4 \cdot 3}{280} \left(\frac{U \cdot \rho_{\text{oil}}}{2\pi \cdot R \cdot \mu_{\text{oil}}} \right)^2 \left(\frac{\partial p^*}{\partial \varphi^*} \right)^2 \frac{1}{(r^*)^2} \right) \right]. \tag{2.9}$$

The last three terms are investigated to find the negligible terms. The constant part of the first term is 1. For the second and third term, exemplary values for dimensions

(a) Clutch open   (b) Clutch closed
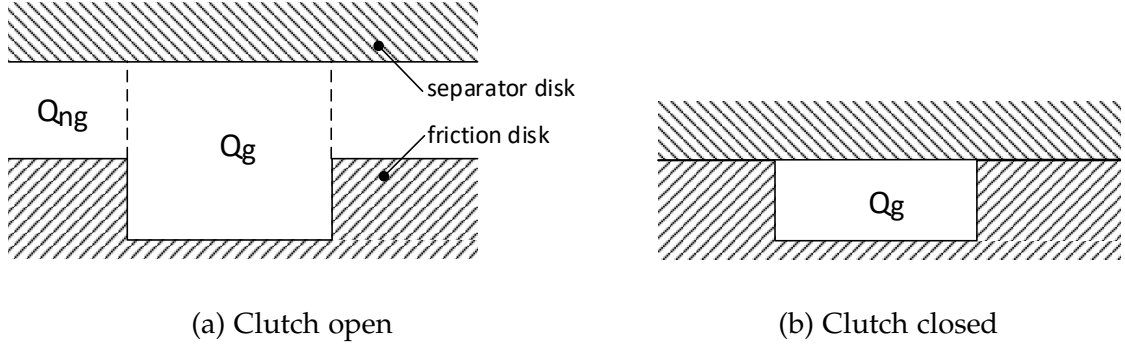
Figure 2.4: The oil flow is split in two independent sections: the oil volume flow in the grooves Q_g and the oil volume flow outside Q_{ng}

and properties from table 3.2 are used to estimate their magnitudes.

$$\frac{H^2}{10} \cdot \frac{(\omega_1 + \omega_2) \cdot \rho_{oil}}{\mu_{oil} \cdot 2\pi/n_g} \approx \frac{(0.2 \text{ mm})^2}{10} \cdot \frac{3000 \text{ rpm} \cdot 857 \text{ kg/m}^3}{0.12 \text{ kg/(m·s)} \cdot 2\pi/60} = 0.056 \qquad (2.10a)$$

$$U = \frac{Q}{2\pi \cdot R \cdot H} \approx \frac{1 \text{ l/min}}{2\pi \cdot 120 \text{ mm} \cdot 0.2 \text{ mm}} = 110.53 \text{ mm/s} \qquad (2.10b)$$

$$\frac{H^4 \cdot 3}{280} \left(\frac{U \cdot \rho_{oil}}{2\pi/n_g \cdot R \cdot \mu_{oil}}\right)^2 \approx \frac{(0.2 \text{ mm})^4 \cdot 3}{280} \left(\frac{66.32 \text{ mm/s}}{2\pi/60 \cdot 120 \text{ mm} \cdot 0.12 \text{ kg/(m·s)}}\right)^2 \qquad (2.10c)$$

$$= 4.07 \cdot 10^{-8}.$$

Consequently, both terms containing the pressure gradient $\partial p^*/\partial \varphi^*$ can be dropped. In the resulting equation, the dimensionless variables are substituted by the original variables. The resulting, simplified PDE is:

$$h \cdot \bar{v}_r = \int_0^h v_r \cdot dz = \frac{1}{40} \frac{\rho_{oil}}{\mu_{oil}} h^3 \cdot r \cdot \left(\omega_1^2 + \omega_2^2 + \frac{4}{3} \cdot \omega_1 \cdot \omega_2\right) - \frac{1}{\mu_{oil}} \cdot \frac{\partial p}{\partial r} \cdot \frac{h^3}{12}. \qquad (2.11)$$

In this equation, the mean radial velocity is not influenced by the oil flow at other angular locations. Therefore, the oil flow in the grooves Q_g and outside Q_{ng} can be considered as two independent sections (see figure 2.4).

The oil volume flow rates in both sections can be calculated with (2.11). However, for the oil volume flow rate in the non-grooved area Q_{ng}, the roughness of disk surface needs to be taken into account.

When the surface roughness R_{RMS} is not very small compared to the lubrication film thickness h ($h/R_{RMS} < 5$), the flow rate will be smaller. In [6], a factor ϕ_p is proposed to account for surface roughness in lubrication flow. For isotropic surfaces where

$h/R_{\text{RMS}} < 5$, the following approximation formula applies:

$$Q_{\text{ng}} := \tilde{Q}_{\text{ng}} \cdot \phi_p \tag{2.12a}$$

$$\phi_p = 1 - e^{0.56h_{\text{ng}}/R_{\text{RMS}}} \tag{2.12b}$$

The surface roughness R_{RMS} is the standard deviation of the combined roughness of both surfaces and $\tilde{Q}_{\text{ng}}$ is the oil volume flow between smooth surfaces.

The resulting oil volume flow rate in the two sections is:

$$Q = \int_0^{2\pi} \int_0^h r \cdot v_r \cdot dz d\varphi = Q_{\text{g}} + Q_{\text{ng}} \tag{2.13a}$$

$$Q_{\text{g}} = 2\pi \cdot x_{\text{g}} \cdot \left(\frac{1}{40} \frac{\rho_{\text{oil}}}{\mu_{\text{oil}}} h_{\text{g}}^3 \cdot r^2 \cdot \Omega^2 - \frac{r}{\mu_{\text{oil}}} \cdot \frac{\partial p}{\partial r} \cdot \frac{h_{\text{g}}^3}{12} \right) \tag{2.13b}$$

$$Q_{\text{ng}} = 2\pi \cdot (1 - x_{\text{g}}) \cdot \left(\frac{1}{40} \frac{\rho_{\text{oil}}}{\mu_{\text{oil}}} h_{\text{ng}}^3 \cdot r^2 \cdot \Omega^2 - \frac{r}{\mu_{\text{oil}}} \cdot \frac{\partial p}{\partial r} \cdot \frac{h_{\text{ng}}^3}{12} \right) \cdot \phi_p \tag{2.13c}$$

Where x_{g} is the ratio of the grooved area on the disk surface to the total area of the disk surface.

Since the pressure gradient in angular direction $\partial p / \partial \varphi$ is negligible regarding its influence on the oil volume flow rate, the pressure gradient in radial direction $\partial p / \partial r$ can be assumed to be the same in both sections. With this equality and (2.13b), the oil volume flow rate in each section can finally be calculated.

$$\frac{\partial p}{\partial r} = \frac{3}{10}\rho_{\text{oil}} r \Omega^2 - \frac{Q_{\text{g}}}{2\pi x_{\text{g}}} \frac{12}{h_{\text{g}}^3} \frac{\mu_{\text{oil}}}{r} = \frac{3}{10}\rho_{\text{oil}} r \Omega^2 - \frac{Q_{\text{ng}}}{2\pi(1 - x_{\text{g}})\phi_p} \frac{12}{h_{\text{ng}}^3} \frac{\mu_{\text{oil}}}{r}$$

$$\stackrel{(2.13a)}{\Longrightarrow} Q_{\text{g}} = Q\frac{1}{(1 - x_{\text{g}})h_{\text{ng}}^3} \left(\frac{\phi_p}{x_{\text{g}}h_{\text{g}}^3} + \frac{1}{(1 - x_{\text{g}})h_{\text{ng}}^3} \right)^{-1} \tag{2.14}$$

2.1.3 Disk distance

During open and slip state of the clutch, the torque Tq results from viscous drag and therefore highly depends on the disk distance h. Thus, with knowledge of the torque, the disk distance can be estimated. The following calculations are based on the approach in [7].

The drag torque Tq_{drag} is

$$Tq_{\text{drag}} = \int_{r_{\text{in}}}^{r_{\text{out}}} \int_0^{2\pi} \sigma_{\varphi z} \cdot r^2 \cdot d\varphi \cdot dr, \tag{2.15}$$

where $\sigma_{\varphi z}$ is the viscous stress defined as

$$\sigma_{\varphi z} = \mu_{\text{oil}} \frac{\partial v_{\varphi}}{\partial z}. \tag{2.16}$$

The angular flow speed v_{φ} is formulated in (2.5) and depends on the still unknown pressure gradient $\partial p / \partial \varphi$. The pressure gradient is calculated in a similiar way as described in [7]: For a large number of grooves, the pressure can be approximated as a piecewise linear function in angular direction in each section (grooved and non-grooved). In other words, the pressure gradients $\partial p / \partial \varphi |_{\text{ng}}$ and $\partial p / \partial \varphi |_{\text{g}}$ are constant.

With the conservation of mass equation in angular direction (applied to the flow relative to the groove),

$$\int_0^{h_{\text{ng}}} (v_{\varphi,\text{ng}} - \omega_2 \cdot r) \cdot dz = \int_0^{h_{\text{g}}} (v_{\varphi,\text{g}} - \omega_2 \cdot r) \cdot dz, \tag{2.17}$$

and the periodicity of the pressure in angular direction,

$$x_{\text{g}} \cdot \left. \frac{\partial p}{\partial \varphi} \right|_{\text{g}} + (1 - x_{\text{g}}) \cdot \left. \frac{\partial p}{\partial \varphi} \right|_{\text{ng}} = 0, \tag{2.18}$$

the pressure gradient $\partial p / \partial \varphi$ can be calculated.

$$\left. \frac{\partial p}{\partial \varphi} \right|_{\text{ng}} = -\frac{6r^2 \mu_{\text{oil}} (h_{\text{g}} - h_{\text{ng}}) \cdot (\omega_1 - \omega_2)}{h_{\text{ng}}^3 + \frac{1 - x_{\text{g}}}{x_{\text{g}}} h_{\text{g}}^3} \tag{2.19a}$$

$$\left. \frac{\partial p}{\partial \varphi} \right|_{\text{g}} = \frac{6r^2 \mu_{\text{oil}} (h_{\text{g}} - h_{\text{ng}}) \cdot (\omega_1 - \omega_2)}{\frac{x_{\text{g}}}{1 - x_{\text{g}}} h_{\text{ng}}^3 + h_{\text{g}}^3} \tag{2.19b}$$

Inserting (2.19) and (2.5) into (2.16) results in:

$$\sigma_{\varphi z} = \mu_{\text{oil}} \cdot (\omega_1 - \omega_2) \cdot r \cdot \left(\frac{x_{\text{g}}}{h_{\text{g}}} + \frac{1 - x_{\text{g}}}{h_{\text{ng}}} + \frac{3(h_{\text{g}} - h_{\text{ng}})^2}{\frac{1}{1 - x_{\text{g}}} h_{\text{ng}}^3 + \frac{1}{x_{\text{g}}} h_{\text{g}}^3} \right) \tag{2.20}$$

The viscosity of the oil μ_{oil} highly depends on the oil temperature and, since the temperature depends on the radial position, the viscosity of the oil μ_{oil} changes with the radial position. To keep the computational effort low, the viscosity is assumed to be linear in radial direction:

$$\mu_{\text{oil}}(r) = \mu_{\text{oil}}(r_{\text{in}}) + (r - r_{\text{in}}) / (r_{\text{out}} - r_{\text{in}}) \cdot (\mu_{\text{oil}}(r_{\text{out}}) - \mu_{\text{oil}}(r_{\text{in}})). \tag{2.21}$$

With (2.15) and (2.20), the relation between drag torque Tq_{drag} and h can finally be formulated:

$$Tq_{\text{drag}} = \left(\mu_{\text{oil}}(r_{\text{in}}) \frac{r_{\text{out}}^4 - r_{\text{in}}^4}{4} + \frac{\mu_{\text{oil}}(r_{\text{out}}) - \mu_{\text{oil}}(r_{\text{in}})}{r_{\text{out}} - r_{\text{in}}} \right) \left(\frac{r_{\text{out}}^5}{5} - \frac{r_{\text{in}}^5}{20} - \frac{r_{\text{in}} \cdot r_{\text{out}}^4}{4} \right)$$
$$\cdot (\omega_1 - \omega_2) \cdot \left(\frac{x_g}{h_g} + \frac{1 - x_g}{h_{ng}} + \frac{3(h_g - h_{ng})^2}{\frac{1}{1-x_g}h_{ng}^3 + \frac{1}{x_g}h_g^3} \right) \tag{2.22}$$

In section 2.3.1, a relation between the drag torque Tq_{drag} between two disks and the torque Tq transmitted by the clutch is formulated and discussed. The relation (2.22) can be either used to estimate the drag torque in the open clutch state, where the disk distance h can be derived from the clutch geometry, or to estimate the disk distance h during closing or slip state, when Tq_{drag} can be derived from Tq.

2.1.4 Forming of rivulets

At low rotation speeds, the fluid transport is mainly caused by the pressure difference $p_{\text{in}} - p_{\text{out}}$ (Poiseuille force) generated by the pump. At high rotation speed, the centrifugal force dominates the Poiseuille force and accelerates the radial speed of the fluid $\bar{v}_r$. Since the oil volume flow rate Q stays constant, rivulets of oil are forming. This phenomenon is discussed in [8] and [9]. The rivulets are surrounded by a mist film of air and oil. Figure 2.5 shows an illustration of the situation.

With (2.13b) and the boundary condition $p(r_{\text{out}}) = p_{\text{out}}$, the pressure $p(r)$ can be calculated.

$$p_{\text{out}} - p(r) = \int_r^{r_{\text{out}}} \frac{\partial p}{\partial r} dr = \frac{3}{10}\rho_{\text{oil}} \frac{r_{\text{out}}^2 - r^2}{2}\Omega^2 - \frac{Q_{ng}}{2\pi} \frac{1}{1 - x_g} \frac{12}{h_{ng}^3} log\left(\frac{r_{\text{out}}}{r} \right) \mu_{\text{oil}} \tag{2.23}$$

Where p_{out} is the overpressure at the outlet - typically 0 N/m^2.

Obviously, the pressure $p(r)$ will decrease with increasing rotational speed Ω. When $p(r)$ reaches values beyond p_{out}, air will flow in from the outside of the disk stack and drive the pressure to p_{out} (see figure 2.6).

This leads to the so called Reynolds cavitation boundary conditions [4]:

$$\left. \frac{\partial p}{\partial r} \right|_{r=r_c} = 0 \tag{2.24a}$$

$$p(r \geq r_c) = p_{\text{out}} \tag{2.24b}$$
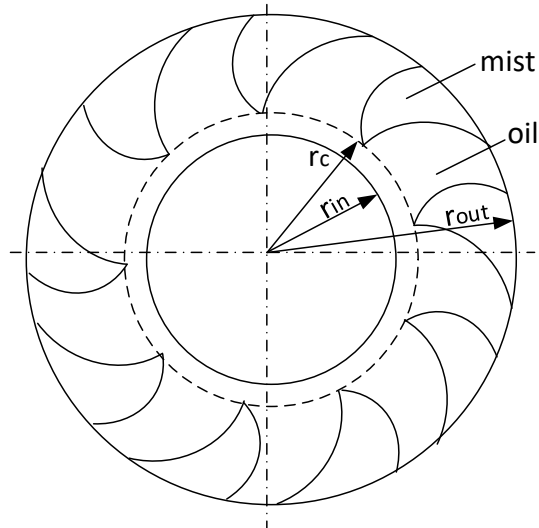
Figure 2.5: Due to the centrifugal force, rivulets of oil between the disks are forming, beginning at radius r_c. Between the rivulets is a mist film of oil and air.
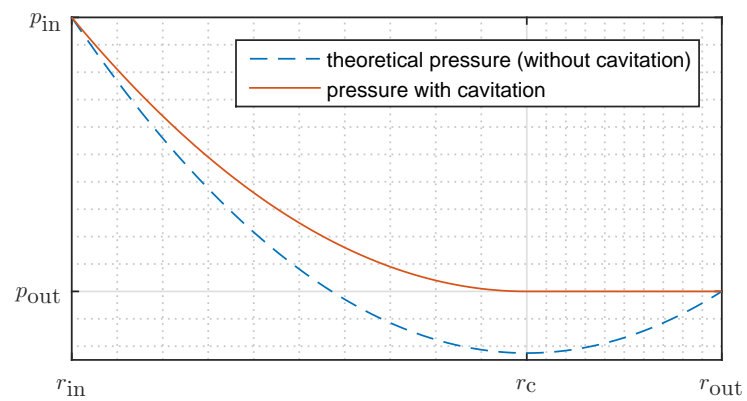
Figure 2.6: Pressure profile of the oil film between the clutch disks. Beginning at radius r_c, rivulets start to form, driving the pressure to p_out

Where r_c is the radius, where the continuous lubrication ends and rivulets start to form. This is illustrated in figure 2.5.

When (2.24a) is applied to (2.14), the radius r_c can be calculated.

$$r_c^2 = \frac{Q_g}{2\pi \cdot x_g} \cdot \frac{12}{h_g^3} \cdot \frac{\mu_{\text{oil}}}{\rho_{\text{oil}} \cdot \Omega^2} \cdot \frac{10}{3} \tag{2.25}$$

Note that this radius is equal in the grooved and non-grooved sections due to the previous claim of equal pressure distribution.

The mean radial speed of the rivulets in the grooved and non grooved section is calculated from (2.11).

$$\bar{v}_{r,i} = \frac{1}{h_i} \cdot \int_0^{h_i} v_{r,i} \cdot dz = \frac{\rho_{\text{oil}} \cdot h_i^2 \cdot r \cdot \Omega^2}{40\mu_{\text{oil}}} - \underbrace{\frac{h_i^2}{12\mu_{\text{oil}}} \cdot \frac{\partial p}{\partial r}}_{\overset{(2.24a)}{=}0}, \, i \in \{g, ng\}, \, r > r_c \tag{2.26}$$

From the conservation of mass, the ratio of the circular segment of rivulets to the total circumference ϕ_{riv} can be calculated.

$$Q_g = \phi_{\text{riv}} \cdot x_g \cdot 2\pi \cdot r \cdot h_g \cdot \bar{v}_{r,g}$$
$$\implies \phi_{\text{riv}}(r) := \frac{Q_g \cdot 20\mu}{x_g \pi r^2 \cdot h_g^3 \cdot \rho_{\text{oil}} \cdot \Omega^2} \tag{2.27}$$

Since this phenomenon will reduce the area of lubrication, the viscous torque and also the heat transfer to the oil at high rotation speeds will decrease. The radius r_c is exemplarily shown in figure 2.7 for different rotational speeds.

2.2 Heat transfer to the oil

As also described in [10, chap. 9], an established method for modelling the heat transfer q_{conv} between a solid body and fluid is to first find the convective heat transfer coefficient h_{conv} for which the following relation applies:

$$q_{\text{conv},i} = h_{\text{conv},i} \cdot (T_s - T_{\text{bulk},i}), \, i \in \{g, ng\}, \tag{2.28}$$

where T_{bulk} is the mean effective oil temperature in the groove

$$T_{\text{bulk},g} = \frac{\int_0^h T \cdot v_r \cdot r \cdot dz}{\int_0^h v_r \cdot r \cdot dz}, \tag{2.29}$$
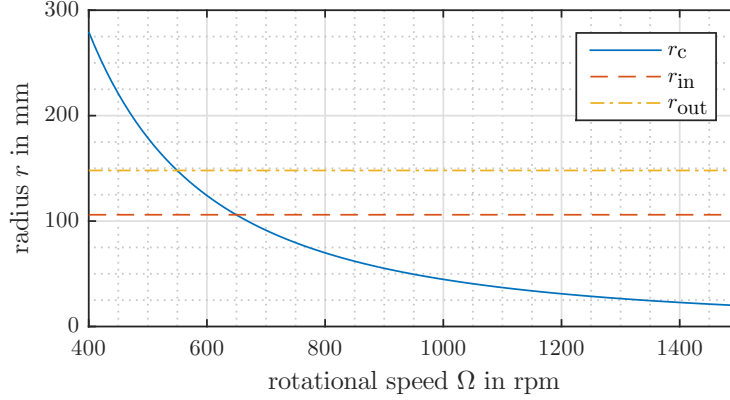
Figure 2.7: Exemplary magnitude of the radius r_c where rivulets start to form depending on the rotational speed Ω. When r_c reaches values beyond the outer radius r_{out}, rivulets start to form. For $r_c < r_{in}$, there are rivulets on the whole surface

or outside

$$T_{\text{bulk,ng}} = \frac{\int_0^h T \cdot v_\varphi \cdot dz}{\int_0^h v_\varphi \cdot r \cdot dz},$$ (2.30)

respectively.

k_{oil} is the thermal conductivity of oil for which the following relation holds:

$$q_{\text{conv}} = - \left. \frac{\partial T}{\partial z} \right|_{z=0} \cdot k_{\text{oil}}$$ (2.31)

With this approach, the temperature distribution in z and in r direction can be investigated separately. Subsections 2.2.2 and 2.2.3 deal with the heat transfer coefficient h_{conv}. In subsection 2.2.4, the temperature distribution in r direction will be estimated, using h_{conv}.

2.2.1 Assumptions

In this section, many strong assumptions are made, that are not all sufficiently justified. For the relations derived in this section, empirical validation is particularly important.

- For considerations regarding the heat transfer coefficient h_{conv}, the system is assumed stationary. For estimating the temperature distribution in r direction, only the time variance of the oil temperature and the surface temperature will be considered. Especially during closing or opening of the clutch, this assumption will lead to a deviation of the result from the real heat transfer, since the squeeze flow is not considered.

- The oil temperature profile is assumed symmetric in z direction. This assumption is applicable if either the surface temperatures of the separator disk and the friction disk do not differ significantly, or the oil temperature in the centre of the flow is not significantly influenced. In the considered system, neither of these conditions can be assumed. Therefore, the arising error will be reduced by a separate term for the heat transfer between both halves of the oil film:

$$q_{\text{conv,oil}} = (T_{\text{bulk,g,1}} - T_{\text{bulk,g,2}}) \cdot h_{\text{c,oil}}, \tag{2.32}$$

where $h_{\text{c,oil}}$ is found empirically.
- The Nusselt number in the grooves and outside will be estimated independently. Therefore, for estimating the heat transfer in the groove, the influence of the non-grooved area is neglected and for estimating the heat transfer in the non-grooved area, the temperature in the groove is assumed constant in z. This is further discussed in subsection 2.2.2.

2.2.2 Nusselt number

The Nusselt number Nu is a dimensionless variable that characterizes the heat transfer. This is further discussed in [10, chap. 9.4]. It is defined as

$$Nu = \frac{h_{\text{conv}} \cdot D_{\text{hyd}}}{k_{\text{oil}}}, \tag{2.33}$$

where D_{hyd} is the characteristic hydraulic diameter, which is 4 times the ratio of the cross section area of the flow to the wetted circumference in this cross section:

$$D_{\text{hyd}} = \frac{4 \cdot 2\pi r \cdot h}{2\pi r \cdot 2} = 2 \cdot h \tag{2.34}$$

From (2.28) and (2.31) follows:

$$h_{\text{conv}} = \frac{\left.\frac{\partial T}{\partial z}\right|_{z=0} \cdot k_{\text{oil}}}{T_{\text{s}} - T_{\text{bulk}}} \tag{2.35}$$

From (2.33) and (2.35) follows that, to calculate the Nusselt number, the temperature gradient is necessary. Therefore, the problem of finding Nu is equal to solving the conservation of thermal energy equation

$$\rho_{\text{oil}} c_{p,\text{oil}} \left(\frac{1}{r} \frac{\partial}{\partial r} (r \cdot v_r \cdot T) + \frac{\partial}{\partial \varphi} \left(\frac{v_\varphi}{r} \cdot T \right) \right) = k_{\text{oil}} \frac{\partial^2 T}{\partial z^2} \tag{2.36}$$

where $c_{p,\text{oil}}$ is the heat capacity of oil. This is a PDE that cannot be solved analytically for the situation as it was described so far. Therefore, several further assumptions and

simplifications need to be made. These are preferably based on the observations from other resources.

In [11], the heat transfer during slip state of the wet clutch was analysed numerically. It was shown that the oil flow can be separated in 2 zones: a recirculation zone in the groove and a stream along the separator plate that can be considered as Couette flow. The Nusselt number in the recirculation zone will increase with increasing Reynolds number of the Couette flow. In [12] the Nusselt number in a general lid driven cavity is numerically investigated. The qualitative results for the Nusselt number in the groove are similar.

Since neither an analytical nor a numerical solution for describing the recirculation zone would be compatible with the limited computational resources presumed in this thesis, only approaches for the Nusselt number in the grooves without rotational speed and the Nusselt number of the Couette flow in the non-grooved area will be presented. The error by neglecting the recirculation flow will be discussed in chapter 3.

In the closed clutch state, the angular flow velocity disappears. Therefore the velocity reduces from (2.4) to

$$v_{r,g} = \frac{Q_g}{2\pi r \cdot x_g} z(h_g - z) \frac{6}{h_g^3}. \tag{2.37}$$

As discussed, the flow in the non-grooved area will be assumed to be a Couette flow. That is, the flow will be solely driven by movement of the walls and not by pressure difference. However, the decrease of the velocity due to the roughness of the friction surface will be considered. This is modelled with the shear flow factor ϕ_s presented in [13].

The coordinate system will be placed on the grooved disk, oriented in the direction of positive relative angular speed $\Delta\omega = |\omega_1 - \omega_2|$. In the resulting Couette flow, the velocity reduces from (2.5) to

$$v_{\varphi,ng} = r \cdot \Delta\omega \cdot \frac{z}{h_{ng}} \cdot \phi_s \tag{2.38}$$

For isotropic roughness on the paper surface and $h_{ng} < 0.02$ mm, the shear flow factor ϕ_s can be calculated with

$$\phi_s = 1 - 1.899 \cdot \left(\frac{h_{ng}}{R_{RMS}}\right)^{-0.02} \cdot \exp\left(-0.92 \cdot \frac{h_{ng}}{R_{RMS}} + 0.05 \cdot \left(\frac{h_{ng}}{R_{RMS}}\right)^2\right). \tag{2.39}$$

Where R_{RMS} is the root-mean square amplitude of the surface roughness. For larger disk distance h_{ng}, the shear flow factor is approximately 1.
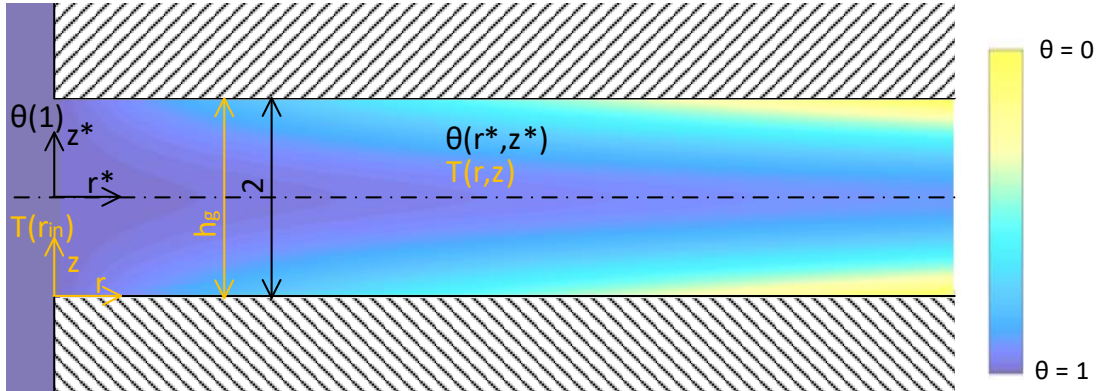
Figure 2.8: Considered system for the Nusselt number in the grooves

For all presented approaches, laminar flow is assumed. As stated in [10, chap. 9.10], this is a valid assumption if the Reynolds number *Re* is smaller than 2300. To check this, the Reynolds number is calculated using exemplary values from table 3.2.

$$Re = \frac{v_r \cdot D_{\text{hyd}} \cdot \rho_{\text{oil}}}{\mu_{\text{oil}}} = \frac{Q \cdot \rho_{\text{oil}}}{\pi \cdot r \cdot \mu_{\text{oil}}} \approx \frac{1 \, \text{l/min} \cdot 857 \, \text{kg/m}^3}{\pi \cdot 120 \, \text{mm} \cdot 0.12 \, \text{kg/ms}} = 0.316 \tag{2.40}$$

To gain an analytical solution of an applicable complexity for the Nusselt number in the grooves, the PDE in (2.36) needs to be further simplified. This can be done for example by assuming constant wall temperature or constant rate of heat transfer. Both approaches will be presented.

Average Nusselt number in the groove with constant wall temperature

With (2.37), (2.36) becomes:

$$\rho_{\text{oil}} c_{p,\text{oil}} \cdot \frac{Q_g}{2\pi r \cdot x_g} z(h_g - z) \frac{6}{h_g^3} \frac{\partial T}{\partial r} = k_{\text{oil}} \cdot \frac{\partial^2 T}{\partial z^2}. \tag{2.41}$$

In the first step, (2.41) is transformed to a more convenient form. This is done by shifting the z-axis of the coordinate system to the centre of the flow, and then transforming the variables to a dimensionless form. The considered system is illustrated in figure 2.8.

19

The following dimensionless variables are introduced:

$$\theta := \frac{T - T_s}{T(r_{in}) - T_s} \tag{2.42a}$$

$$z^* := \frac{z}{h_g/2} - 1 \tag{2.42b}$$

$$r^* := \frac{r}{r^*_{in}}, \qquad r^*_{in} := r_{in} \left(\frac{2\pi r^2_{in}}{Q_g} \frac{4k_{oil}}{3h_g \rho_{oil} c_{p,oil}} \right)^{-1/2} \tag{2.42c}$$

where $T_s = T(z = 0)$ is the surface temperature.

Substituting these variables into (2.41) results in:

$$\frac{1}{r^*}(1 - z^{*2})\frac{\partial}{\partial r^*}\theta = \frac{\partial^2 \theta}{\partial z^2} \tag{2.43}$$

As discussed in 2.2.1, the temperature profile is assumed symmetric. Therefore, the boundary conditions are:

$$\theta(z^* = \pm 1) = 0 \tag{2.44a}$$
$$\theta(r^* = r^*_{in}) = 1 \tag{2.44b}$$

Since the PDE (2.43) with boundary conditions (2.44) is homogeneous, it can be solved by the method of separation of variables. This method is described for example in [14, p.98ff].

With

$$\theta(r^*, z^*) := R(r^*) \cdot Z(z^*), \tag{2.45}$$

(2.43) transforms to two ordinary differential equations.

$$\frac{\partial R(r^*)}{\partial r^*} \cdot \frac{1}{r^* \cdot R(r^*)} = \tilde{\lambda} \tag{2.46a}$$

$$\frac{\partial^2 Z(z^*)}{\partial (z^*)^2} \cdot \frac{1}{Z(z^*) \cdot (1 - (z^*)^2)} = \tilde{\lambda}, \tag{2.46b}$$

where $\tilde{\lambda}$ is the eigenvalue. For physically reasonable results, $\tilde{\lambda}$ must be non-positive. Therefore, the following substitution is applied: $-\lambda^2 := \tilde{\lambda}$.

The ODE in z^* with the boundary condition (2.44a) is a Sturm Liouville problem (this type of problems is described in [14]) with a finite number of eigenvalues λ that lead to non-trivial solutions. In the following, these eigenvalues and their corresponding solutions are indexed with $m \in \mathbb{N}$.

In [15] an approach for calculating the eigenvalues λ_m is presented. The first 3 values are shown in table 2.1.

m	λ_m
0	1.6816
1	5.6698
2	9.6682

Table 2.1: Values of λ_m
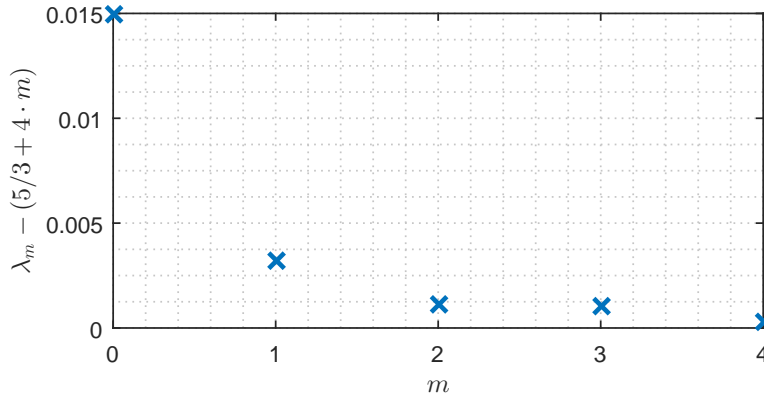
Figure 2.9: The eigenvalues from the Sturm Liouville Eigenvalue problem (2.46) soon converge to the linear function (2.47)

It is also shown in [15] and apparent from figure 2.9, that λ_m will soon converge to

$$\lambda_m \doteq \frac{5}{3} + 4 \cdot m. \tag{2.47}$$

The corresponding solutions will be formulated as a power series

$$Z_m(z^*) = \sum_{k=0}^{\infty} a_{m,k} \cdot (z^*)^k, \tag{2.48}$$

with the recurrence formula

$$a_{m,k} = \frac{\lambda_m}{k(k-1)}(a_{m,k-4} - a_{m,k-2}), \ k > 2 \tag{2.49}$$

Note that only even powers of z will occur due to the symmetry of the temperature profile. From (2.44a), the following condition for $a_{m,k}$ results:

$$\sum_{k=0}^{\infty} a_{m,k} = 0. \tag{2.50}$$

The initial condition for the recurrence formula is chosen as:

$$a_{m,0} := 1. \tag{2.51}$$

A particular solution of the ODE in (2.46a) is

$$R_m(r^*) = A_m \cdot e^{-\frac{\lambda_m^2}{2} r^{*2}}, \tag{2.52}$$

where A_m is a constant that results from the boundary conditions.

Combining (2.48) and (2.52) leads a particular solution for θ_m:

$$\theta_m(r^*, z^*) = R_m(r^*) \cdot Z_m(z^*) = A_m \cdot e^{-\frac{\lambda_m^2}{2} r^{*2}} \cdot \sum_{k=0}^{\infty} a_{m,k}(z^*)^k \tag{2.53}$$

The general solution reads

$$
\begin{aligned}
\theta(r^*, z^*) = R(r^*) \cdot Z(z^*) &= \sum_{m=1}^{\infty} \left(A_m \cdot e^{-\frac{\lambda_m^2}{2} r^{*2}} \cdot \sum_{k=0}^{\infty} a_{m,k}(z^*)^k \right) \\
&= \sum_{m=1}^{\infty} \sum_{k=0}^{\infty} \left(A_m \cdot e^{-\frac{\lambda_m^2}{2} r^{*2}} \cdot a_{m,k}(z^*)^k \right)
\end{aligned}
\tag{2.54}
$$

Applying boundary condition (2.44b) gives

$$
\theta(r^* = r_{\text{in}}^*, z^*) = \sum_{k=0}^{\infty} \left((z^*)^k \cdot \sum_{m=1}^{\infty} \left(A_m \cdot e^{-\frac{\lambda_m^2}{2} r_{\text{in}}^{*2}} \cdot a_{m,k} \right) \right) = 1
$$

$$
\implies \sum_{m=1}^{\infty} \left(A_m \cdot e^{-\frac{\lambda_m^2}{2}(r_{\text{in}}^*)^2} \cdot a_{m,k} \right) = \begin{cases} 0 & k > 0 \\ 1 & k = 0 \end{cases}.
\tag{2.55}
$$

The values for A_m can be estimated by solving (2.55) for a finite sum:

$$
\sum_{m=1}^{M} \left(A_m \cdot e^{-\frac{\lambda_m^2}{2}(r_{\text{in}}^*)^2} \cdot a_{m,k} \right) = \begin{cases} 0 & M - 1 > k > 0 \\ 1 & k = 0 \end{cases}.
\tag{2.56}
$$

This is possible, since the terms of the sum converge to zero, which can be shown by trial.

For calculating the Nusselt number, we are interested in the mean effective oil temperature θ_{bulk}, which results from substituting (2.42a) into (2.29).

$$
\begin{aligned}
\theta_{\text{bulk}} &= \frac{\int_0^1 \theta \cdot (1 - (z^*)^2) \cdot dz^*}{\int_0^1 \cdot (1 - (z^*)^2) \cdot dz^*} \\
&= \sum_{m=1}^{\infty} \frac{3}{2} A_m \sum_{k=0}^{\infty} a_{m,k} \left(\frac{1}{k+1} - \frac{1}{k+3} \right) \cdot e^{-\frac{\lambda_m^2}{2} r^{*2}} \\
&= \sum_{m=1}^{\infty} G_m \cdot e^{-\frac{\lambda_m^2}{2}(r^{*2} - r_{\text{in}}^2)},
\end{aligned}
\tag{2.57a}
$$

$$
\text{with } G_m = \frac{3}{2} A_m \cdot e^{-\frac{\lambda_m^2}{2} r_{\text{in}}^{*2}} \cdot \sum_{k=0}^{\infty} a_{m,k} \left(\frac{1}{k+1} - \frac{1}{k+3} \right).
\tag{2.57b}
$$

m	λ_m	G_m
1	1.6816	0.910
2	5.6698	0.0533
3	9.6682	0.0153

Table 2.2: Values of λ_m and G_m

With (2.56), the values for G_m can be determined. The first three values are shown in table 2.2

To calculate the average Nusselt number $\overline{Nu}_{g,1}$ the conservation of thermal energy equation is formulated again, with (2.29), (2.35) and (2.33):

$$\rho_{\text{oil}} c_{p\text{oil}} \cdot \frac{Q_g}{2\pi r x_g} \cdot \frac{\partial T_{\text{bulk,g}}}{\partial r} = \overline{Nu}_g \frac{k_{\text{oil}}}{2h}(T_s - T_{\text{bulk,g}})$$

$$\xRightarrow{(2.42)} \frac{1}{r^*} \frac{\partial \theta_{\text{bulk}}}{\partial r^*} \frac{8}{3} = -\overline{Nu}_g \cdot \theta_{\text{bulk}}$$

(2.58)

Solving this differential equation, the average Nusselt number $\overline{Nu}_{g,1}$ in the region between r_{in}^* and r_{out}^* can be calculated

$$\overline{Nu}_{g,1} = \frac{8}{3} \ln\left(\frac{\theta_{\text{bulk}}(r_{\text{in}}^*)}{\theta_{\text{bulk}}(r_{\text{out}}^*)}\right) \cdot \left(\frac{r_{\text{out}}^{*2}}{2} - \frac{r_{\text{in}}^{*2}}{2}\right)^{-1}$$

(2.59)

where $\theta_{\text{bulk}}(r_{\text{in}}^*)$ and $\theta_{\text{bulk}}(r_{\text{out}}^*)$ are calculated with equation (2.57a).

Average Nusselt number in the groove with constant rate of heat transfer

Constant rate of heat transfer q_{conv} suggests the assumption of thermally fully developed flow. This means that the shape of the temperature profile in z direction is constant along r. In other words:

$$\frac{\partial^2 T}{\partial r \partial z} = 0.$$

(2.60)

With this assumption, the solution for the Nusselt number becomes very simple. The derivation can also be found in [10, chap. 9.10] for Cartesian coordinates.

With this condition and (2.37), (2.36) can easily be integrated along z:

$$T = -\frac{\rho_{\text{oil}} c_{p,\text{oil}}}{k_{\text{oil}}} \frac{1}{r} \frac{\partial T}{\partial r} \frac{Q}{2\pi}\left(z^3 h_g - \frac{z^4}{2}\right)\frac{1}{h_g^3} + C_1 \cdot z + C_2,$$

(2.61)

where C_1 and C_2 are integration constants.

When assuming a symmetric temperature profile in z, the boundary conditions are

$$\left.\frac{\partial T}{\partial z}\right|_{z=h/2} = 0 \tag{2.62a}$$

$$T(z = 0) = T_{\text{s}}. \tag{2.62b}$$

Inserting this boundary conditions into (2.61) results in:

$$T = -\frac{\rho_{\text{oil}} c_{p,\text{oil}}}{k_{\text{oil}}} \frac{1}{r} \frac{\partial T}{\partial r} \frac{Q}{2\pi} \left((z^3 h_{\text{g}} - \frac{z^4}{2}) \frac{1}{h_{\text{g}}^3} - \frac{z}{2} \right) + T_{\text{s}}, \tag{2.63}$$

and the derivative of the temperature on the disk surface is:

$$\left.\frac{\partial T}{\partial z}\right|_{z=0} = \frac{\rho_{\text{oil}} c_{p,\text{oil}}}{k_{\text{oil}}} \frac{1}{r} \frac{\partial T}{\partial r} \frac{Q}{2\pi} \frac{1}{2}. \tag{2.64}$$

Combining equations (2.33), (2.34) and (2.64), the Nusselt number can be calculated:

$$Nu_{\text{g},2} = \frac{\rho_{\text{oil}} c_{p,\text{oil}} \frac{1}{r} \cdot \frac{\partial T}{\partial r} \cdot \frac{Q}{2\pi} \cdot \frac{1}{2}}{\frac{Q}{2\pi} \frac{\rho_{\text{oil}} c_{p,\text{oil}}}{k_{\text{oil}}} \frac{1}{r} \cdot \frac{\partial T}{\partial r} \cdot \frac{17 h_{\text{g}}}{140}} \cdot \frac{2 h_{\text{g}}}{k_{\text{oil}}} = 8.235 \tag{2.65}$$

This is the Nusselt number for fully developed flow. Checking of applicability of this assumption is done by quantifying the thermal entry length. The thermal entry length $L_{\text{lam,t}}$ characterizes the flow length after which fully developed flow is (almost) reached. If this length is much smaller than the total flow length $L = r_{\text{out}} - r_{\text{in}}$, the assumption of fully developed flow is applicable. In [10, chap. 9.6], an approximate formula for $L_{\text{lam,t}}$ is stated. Using exemplary values from table 3.2 and the Reynolds number Re from (2.40), an estimate can be calculated.

$$L_{\text{lam,t}} = 0.05 \cdot Re \cdot Pr \cdot D_{hyd} = 0.05 \cdot Re \cdot Pr \cdot 2 h_{\text{g}}$$
$$\approx 0.05 \cdot 0.316 \cdot 1510 \cdot 2 \cdot 0.2 \text{ mm} = 9.55 \text{ mm} \tag{2.66a}$$

$$\text{with } Pr = \frac{c_{p,\text{oil}} \cdot \mu_{\text{oil}}}{k_{\text{oil}}} \approx \frac{1990 \text{ J/(kg· K)} \cdot 0.12 \text{ kg/(m· s)}}{0.158 \text{ W/(m· K)}} = 1510 \tag{2.66b}$$

where the Prandtl number Pr is a dimensionless variable that characterizes the ratio of viscous diffusivity to thermal diffusivity. The estimated thermal entry length is not much smaller than the total flow length, which is around 30 mm.

Consequently, the Nusselt number will be corrected for non-developed flow. For this purpose, the formula by Hausen, as stated in [10, chap. 9.10], that provides an approximate solution for the mean Nusselt number over the whole flow length, will be

adapted for cylindrical coordinates and used to estimate the average Nusselt number $\overline{Nu}_{g,2}$.

$$\overline{Nu}_{g,2} = Nu_{g,2} + \frac{0.023\dfrac{D_{hyd}}{L}\left(\dfrac{\mu_{\text{oil}}(r_{\text{out}}) \cdot r_{\text{out}}}{\mu_{\text{oil}}(r_{\text{in}}) \cdot r_{\text{in}}}\right)^{0.14} Re \cdot Pr}{1 + 0.0012\left[\dfrac{D_{hyd}}{L}Re \cdot Pr\right]} \tag{2.67}$$

Two different approaches for estimating the Nusselt number have now been presented. Since neither the surface temperature T_s nor the rate of heat transfer q_{conv} is constant over r, it is important to quantify the error caused by these assumptions. This will be further discussed in chapter 3. However, it is noted that the estimation of the Nusselt number is just a raw approximation, and implementing a complex model for the Nusselt number would not be appropriate.

Both Nusselt numbers $\overline{Nu}_{g,1}$ and $\overline{Nu}_{g,2}$ over the disk distance h_g and the outer radius (starting from r_{in}) are shown in figure 2.10 for exemplary data from table 3.2. Since the magnitude of both is almost constant in a wide range, the Nusselt number will be assumed constant. This will cause that the heat transfer in the entry region will be underestimated. However, since the average Nusselt number of the whole surface is indeed almost constant in h_g, the total heat transfer will not be significantly influenced by this simplification. The average values of the two presented methods are around 7.8 and 8.4. Only with the considerations made in this section, there is no valid reasoning for the best choice of which value to use for the Nusselt number Nu_g. This issue will be treated in chapter 3.

Nusselt number in the non-grooved area with constant wall temperature and a linear velocity profile

For the non-grooved region, it is assumed that the temperature entering this region $T(\varphi = 0)$ is constant in z. For a more accurate boundary condition, knowledge of the recirculation flow would be necessary. The value of $T(\varphi = 0)$ is:

$$T(\varphi = 0) = T_{\text{bulk,ng}}(\varphi = 0) = T_{\text{bulk,g}}(r) \cdot \xi + T_s(r) \cdot (1 - \xi), \tag{2.68}$$

where ξ is found empirically.
The considered situation is illustrated in figure 2.11 The angular flow speed in the non-grooved area (see equation (2.38)) is linear in z. This fact makes the solution for the Nusselt number with constant wall temperature a lot easier.

Substituting (2.38) into (2.36) leads to the PDE:

$$\rho c_{p,\text{oil}}\frac{\partial}{\partial \varphi}\left(\frac{r \cdot \Delta\omega \cdot \frac{z}{h_{\text{ng}}} \cdot \phi_s}{r} \cdot T\right) = k_{\text{oil}}\frac{\partial^2 T}{\partial z^2}, \tag{2.69}$$
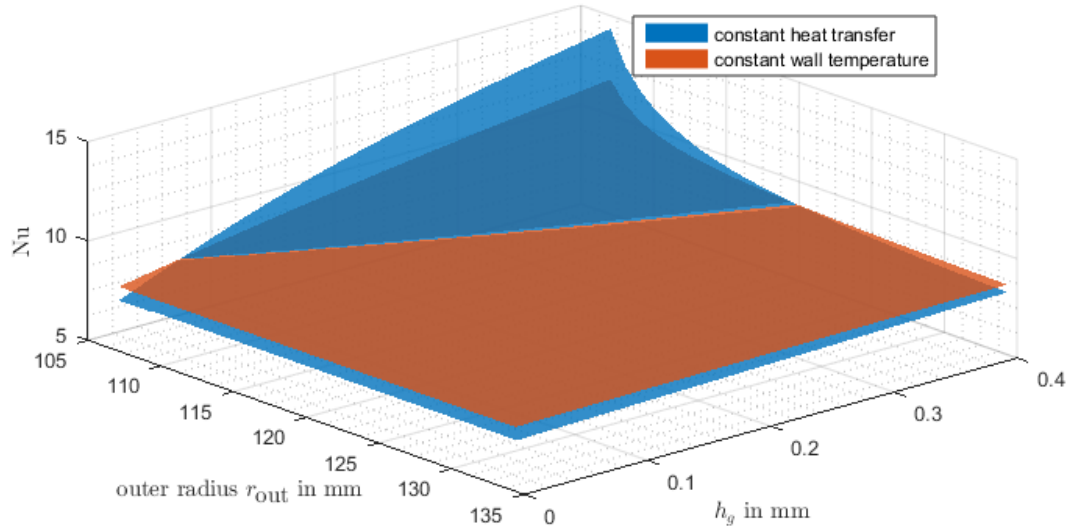
Figure 2.10: The Nusselt number in the grooves can be estimated for example by assuming constant heat transfer on the surface or constant surface temperature. For the exemplary data from table 3.2, they are both almost constant in r and h_g in a wide range

When substituting the following dimensionless variables:

$$\theta := \frac{T - T_s}{T(\varphi = 0) - T_s} \tag{2.70a}$$

$$z^* := \frac{z}{h_{ng}} \tag{2.70b}$$

$$\varphi^* := \varphi \cdot \left(\frac{\rho_{oil} c_{p,oil}}{k_{oil}} \cdot \Delta\omega \cdot h_{ng}^2 \cdot \phi_s \right)^{-1}, \tag{2.70c}$$

this PDE becomes:

$$z^* \frac{\partial\theta}{\partial\varphi^*} = \frac{\partial^2\theta}{\partial(z^*)^2}. \tag{2.71}$$

This equation can be solved by the method of combination of variables if the boundary conditions are compatible. The combined variable is

$$\eta := z^* \cdot (9 \cdot \varphi^*)^{-1/3}. \tag{2.72}$$

The boundary conditions then are:

$$\theta(z^* = 0) = \theta(\eta = 0) = 1 \qquad \Longrightarrow \theta(\varphi^* \to \infty) = 1 \tag{2.73a}$$
$$\theta(\varphi^* = 0) = \theta(\eta \to \infty) = 0 \qquad \Longrightarrow \theta(z^* \to \infty) = 0. \tag{2.73b}$$
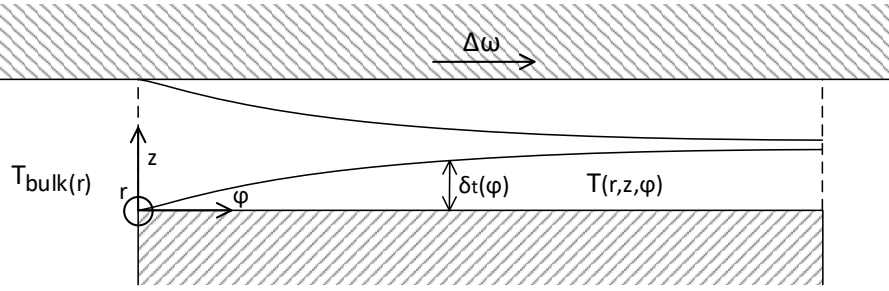
Figure 2.11: Considered system for the Nusselt number in the non-grooved region. On the surface of the disk, a thermal boundary layer with thickness δ_t in which the temperature is significantly influence by the surface will emerge

While boundary condition (2.73a) results from the previous assumption of constant temperature at the beginning of the non-grooved section, for (2.73b) another assumption is needed. For this, the following is considered: Beginning at the entry region, a thermal boundary layer with thickness δ_t will emerge. This is illustrated in figure 2.11. Outside this boundary layer, the temperature is not influenced significantly. Consequently, as long as the boundary layers from both disks do not touch $(2 \cdot \delta_t < h_{ng})$, they can be considered independently. In other words, the influence of the disk opposite to the considered boundary layer can be neglected and the boundary condition $\theta(z^* \to \infty) = 0$ will hold.

The boundary layer thickness $\delta_t(\Delta\varphi \cdot r)$ can be approximated as stated in [10, chap. 9.6]. Using exemplary values from table 3.2, the thickness can be estimated:

$$
\delta_t = 5 \cdot \Delta\varphi \cdot r \cdot \left(\frac{\Delta\omega \rho_{oil}}{\mu_{oil}} \Delta\varphi \cdot r^2 \right)^{-0.5} \cdot Pr^{-0.33}
$$

$$
\approx 5 \cdot 0.06 \cdot 120 \text{ mm} \cdot \left(\frac{2000 \text{ rpm} \cdot 857 \text{ kg/m}^3}{0.12 \text{ kg/ms}} 0.06 \cdot (120 \text{ mm})^2 \right)^{-0.5} \cdot (1510)^{-0.33}
$$

$$
= 0.094 \text{ mm}
$$

$$(2.74)$$

Consequently, this model is not valid in the slip state, for which the Nusselt number will be underestimated. Nevertheless, the Nusselt number for large disk distance h_{ng} can be estimated with the proposed approach.

The PDE (2.71) simplifies to an ODE by inserting the combined variable (2.72):

$$
-3 \cdot \eta^2 \frac{\partial \theta}{\partial \eta} = \frac{\partial^2 \theta}{\partial \eta^2}.
$$

$$(2.75)$$
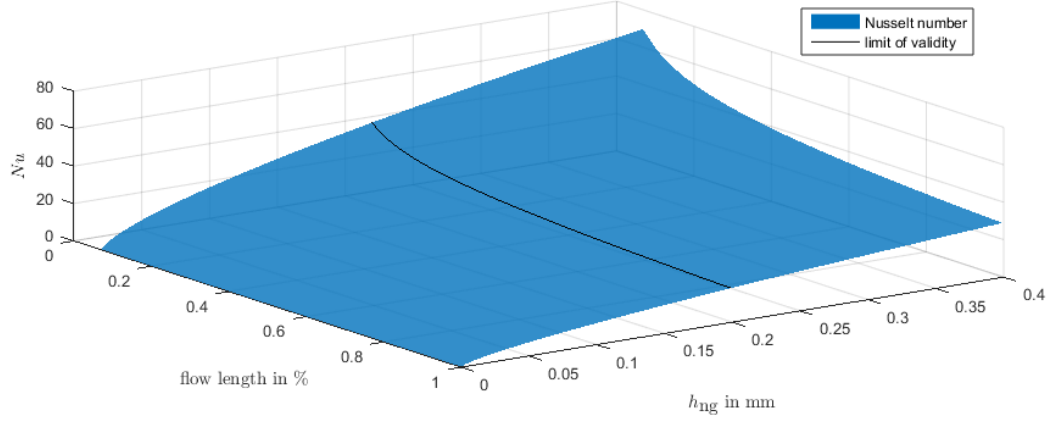
Figure 2.12: The Nusselt number in the non-grooved area significantly depends on the disk distance h_{ng}. With the exemplary data from 3.2, the model is only valid for $h_{\mathrm{ng}} > 0.2mm$

With the boundary conditions (2.73), the solution is:

$$\theta(\eta) = 1 - \frac{\int_{\eta^3}^{\infty} \frac{e^{-\tilde{\eta}}}{\tilde{\eta}^{2/3}} d\tilde{\eta}}{\int_0^{\infty} \frac{e^{-\eta}}{\eta^{2/3}} d\eta} = 1 - \frac{\Gamma(1/3, \eta^3)}{\Gamma(1/3)} \tag{2.76}$$

where $\Gamma(x)$ is the so called Gamma-function and $\Gamma(x, y)$ is the incomplete Gamma-function as described in [16, p.41].

With (2.76), (2.35),(2.33) and (2.70), the Nusselt number can be calculated:

$$\begin{aligned} Nu_{\mathrm{ng}} &= \left. \frac{\partial \theta}{\partial \eta} \right|_{z=0} \cdot (9\varphi^*)^{-1/3} \cdot 2 \\ &= \frac{3}{\Gamma(1/3)} \left(\frac{\rho_{\mathrm{oil}} c_{p,\mathrm{oil}}}{k_{\mathrm{oil}}} \cdot \Delta\omega \cdot h_{\mathrm{ng}}^2 \cdot \phi_{\mathrm{s}} \right)^{1/3} (9\varphi)^{-1/3} \cdot 2. \end{aligned} \tag{2.77}$$

The average Nusselt number between two grooves $\overline{Nu}$ with distance $\Delta\varphi \cdot r$ results in:

$$\overline{Nu}_{\mathrm{ng}} = \frac{1}{\Delta\varphi} \int_0^{\Delta\varphi} Nu_{\mathrm{ng}} \cdot d\varphi = 1.614 \cdot \left(\frac{\rho_{\mathrm{oil}} c_{p,\mathrm{oil}}}{k_{\mathrm{oil}}} \cdot \Delta\omega \cdot h_{\mathrm{ng}}^2 \cdot \phi_{\mathrm{s}} \right)^{1/3} \cdot (\Delta\varphi)^{-1/3} \tag{2.78}$$

The Nusselt number $\overline{Nu}_{\mathrm{ng}}$ over the disk distance h_{ng} and the flow length represented as a percentage of the groove distance $\Delta\varphi$ is shown in figure 2.12 for exemplary data. For this data, the model is valid for $h_{\mathrm{ng}} > 0.2$ mm.

Again, for the same reasoning, the Nusselt number will be assumed constant along the flow length φ. The dependence on the disk distance h_{ng} is not negligible.
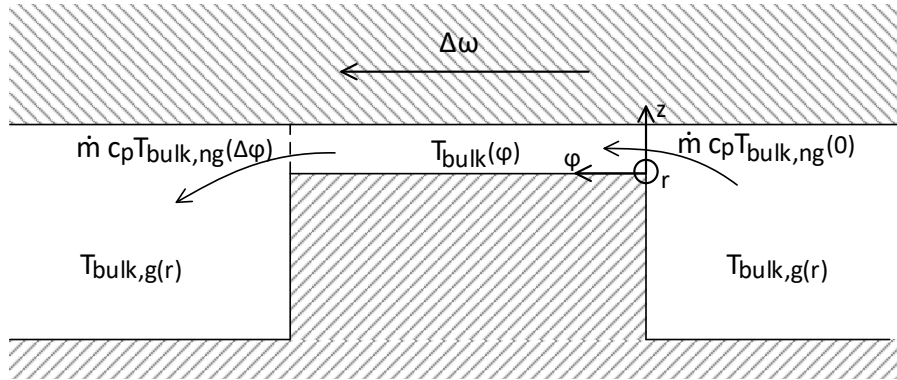
Figure 2.13: Heat is added to the oil in the groove by mass transfer $\dot{m}$ from the non-grooved area

2.2.3 Total heat transfer coefficient

To reduce computational effort, only the bulk temperature in the grooved area and the influence of the non-grooved area on this temperature is calculated. For this purpose, a total heat transfer coefficient $h_{\text{conv,t}}$, representing the combined heat transfer in the grooves and outside is introduced.

$$h_{\text{conv,t}} = h_{\text{conv,g}} \cdot x_{\text{g}} + h_{\text{conv,ng}}, \tag{2.79}$$

where $h_{\text{conv,g}}$ is the heat transfer in the groove calculated with equation (2.33):

$$h_{\text{conv,g}} = Nu_{\text{g}} \cdot \frac{k_{\text{oil}}}{2h_{\text{g}}}, \tag{2.80}$$

and $h_{\text{conv,ng}}$ accounts for the heat added to the oil in the groove by mass transfer from the non-grooved area as illustrated in figure 2.13.

To calculate the bulk temperature of the oil that flows from the non-grooved area into the groove, the conservation of energy equation in angular direction is considered.

With (2.28), (2.30) and (2.33), the conservation of energy in the non-grooved area in angular direction is:

$$\frac{\partial}{\partial \varphi} \int_0^{h_{ng}} \rho_{\text{oil}} c_{p,\text{oil}} \cdot \frac{\Delta \omega}{2} \cdot \phi_{\text{s}} \cdot T_{\text{bulk,ng}}(\varphi) \cdot dz = q_{\text{conv,ng}}$$
$$\dot{=} \overline{Nu}_{\text{ng}} \cdot \frac{k_{\text{oil}}}{2h_{\text{ng}}} \left(T_{\text{s}} - T_{\text{bulk,ng}}(\varphi) \right), \tag{2.81}$$

where $q_{\text{conv,ng}}$ is the convective heat transfer in the non-grooved area.

With the boundary condition $T_{\text{bulk,ng}}(\varphi = 0) = \xi \cdot T_{\text{bulk,g}} + (1 - \xi) \cdot T_{\text{s}}$, the solution to this differential equation is:

$$T_{\text{bulk,ng}}(\varphi) = T_{\text{s}} \cdot (1 - e^{-C \cdot \varphi}) + (\xi \cdot T_{\text{bulk,g}} + (1 - \xi) \cdot T_{\text{s}}) \cdot e^{-C \cdot \varphi}, \tag{2.82a}$$

$$\text{with } C = \frac{k_{\text{oil}}}{\rho_{\text{oil}} c_{p,\text{oil}} \cdot \phi_{\text{s}} \cdot \Delta\omega \cdot h_{ng}^2} \cdot \overline{Nu}_{\text{ng}}. \tag{2.82b}$$

The heat transfer due to mass flow from the non-grooved area to the oil in the groove is:

$$
\begin{aligned}
q_{\dot{m},\text{ng}} = \\
\frac{\Delta\omega}{2} \cdot \phi_{\text{s}} \cdot \rho_{\text{oil}} c_{p,\text{oil}} \cdot h_{\text{ng}} \left(T_{\text{bulk,ng}}(\varphi = \Delta\varphi) - (\xi \cdot T_{\text{bulk,g}} + (1 - \xi) \cdot T_{\text{s}}) \right) \cdot \frac{n_{\text{g}}}{2\pi \cdot r},
\end{aligned}
\tag{2.83}
$$

where n_{g} is the number of grooves. The distance of the grooves $\Delta\varphi$ is:

$$\Delta\varphi = \frac{2\pi r}{n_{\text{g}}}(1 - x_{\text{g}}). \tag{2.84}$$

Substituting (2.82) and (2.84) into (2.83) results in:

$$q_{\dot{m},\text{ng}} = \frac{1}{C \cdot \Delta\varphi}(1 - e^{-C \cdot \Delta\varphi}) \cdot \overline{Nu}_{\text{ng}} \cdot \frac{k_{\text{oil}}}{2h_{\text{ng}}} \cdot (1 - x_{\text{g}}) \cdot \xi \cdot (T_{\text{s}} - T_{\text{bulk,g}}), \tag{2.85}$$

and the corresponding heat transfer coefficient $h_{\text{conv,ng}}$ is

$$h_{\text{conv,ng}} = \frac{1}{C \cdot \Delta\varphi}(1 - e^{-C \cdot \Delta\varphi}) \cdot \overline{Nu}_{\text{ng}} \cdot \frac{k_{\text{oil}}}{2h_{\text{ng}}} \cdot (1 - x_{\text{g}}) \cdot \xi. \tag{2.86}$$

Finally, the total heat transfer coefficient $h_{\text{conv,t}}$ is:

$$h_{\text{conv,t}} = \overline{Nu}_{\text{g}} \cdot \frac{k_{\text{oil}}}{2h_{\text{g}}} x_{\text{g}} + \frac{1}{C \cdot \Delta\varphi}(1 - e^{-C \cdot \Delta\varphi}) \cdot \overline{Nu}_{\text{ng}} \cdot \frac{k_{\text{oil}}}{2h_{\text{ng}}}(1 - x_{\text{g}}) \cdot \xi, \tag{2.87}$$

and the total rate of heat transfer q_{conv} is:

$$q_{\text{conv}} = h_{\text{conv,t}} \cdot (T_{\text{s}} - T_{\text{bulk,g}}). \tag{2.88}$$

2.2.4 Oil temperature distribution in radial direction

As discussed in the subsection 2.2.3, due to the limited computational resources, only the bulk temperature in the groove $T_{\text{bulk,g}}$ will be calculated. For better readability, the subscript g will be omitted for $T_{\text{bulk,g}}$ in this subsection.

When using the heat transfer coefficient $h_{\text{conv,t}}$ (2.87), the oil temperature T_{bulk} can be calculated without considering the z or φ coordinate. For stationary flow, the conservation of energy equation would simplify from a PDE to an ODE in r. Since the surface temperature T_{s} is highly time variant, the transient conservation of energy equation needs to be considered.

For this problem, an analytical solution is not applicable. The most common numerical method for solving a one-dimensional, transient heat transfer problem in a fluid flow would be the finite difference method, as stated in [10].

The quality of the solution of finite difference schemes highly depends on the CFL number (Courant-Friedrichs-Lewy number) as described in [17, p. 106ff].

$$\text{CFL} = \bar{v}_r \frac{\Delta t}{\Delta x} \tag{2.89}$$

Where Δt is the time step and Δx the space step in r direction.

Since the velocity $\bar{v}_r$ will vary in a wide range due to varying disk distance h and oil flow rate Q, a variable step size would be necessary. Another drawback is the high computational effort that is needed for a sufficiently small step size.

For these reasons, a different approach will be attempted in this subsection. The main focus is to preserve the conservation of energy in the entire system. The idea is to approximate the heat transfer q_{conv} with a polynomial such that the change of temperature in the oil and in the disk caused by the approximated rate of heat transfer q_{conv} can be calculated exact. Although the conservation of energy and therefore first law of thermodynamics will hold, the second law of thermodynamics may be violated since the heat transfer will not be modelled exact. The stability of the system will be investigated in chapter 3.

While the Eulerian specification of the flow field, where the flow is observed at specific locations in the field, was used for all previous considerations, in this chapter the Lagrangian specification of the flow field will be used. In the Lagrangian specification of the flow field, one fluid parcel is observed while it flows through space. This is illustrated in figure 2.14. Following the considerations in subsection 2.2.2, not an actual fluid parcel is observed, but rather a fictional bulk segment, extending over the whole disk distance $\bar{h} = x_{\text{g}} \cdot h_{\text{g}} + (1 - x_{\text{g}}) \cdot h_{\text{ng}}$, that moves with the mean flow speed.
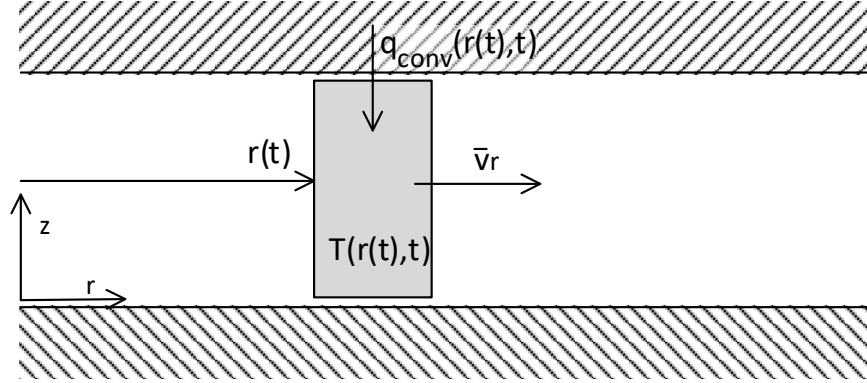
Figure 2.14: In the Lagrangian specification of the flow, one fluid parcel is observed while it flows with velocity $\bar{v}_r$. At each point in time and space, the heat flows to the parcel through heat transfer $q_{\mathrm{conv}}(r(t), t)$

The transient conservation of energy equation in the Lagrangian specification of the field is:

$$\frac{dT_{\mathrm{bulk}}(t, r(t))}{dt} \bar{h} \rho_{\mathrm{oil}} c_{p,\mathrm{oil}} = q_{\mathrm{conv}} \tag{2.90}$$

with $dr(t) = \bar{v}_r \cdot dt$.

This equation is transformed to a more convenient form by introducing a variable dr^* such that $v_r^* = dr^*/dt$ is constant in r. For the oil flow with rivulets, different variables dr_{riv}^* and $v_{r,\mathrm{riv}}^*$ are necessary.

$$v_r^* := \frac{Q}{2\pi\bar{h}}, \qquad\qquad\qquad dr^* = r \cdot dr \tag{2.91a}$$

$$v_{r,\mathrm{riv}}^* := \frac{1}{40} \cdot \frac{\rho_{\mathrm{oil}}}{\mu_{\mathrm{oil}}} \cdot \tilde{h}^2 \cdot \Omega^2, \qquad\qquad dr_{\mathrm{riv}}^* = \frac{dr}{r} \tag{2.91b}$$

Where $\tilde{h}$ is the mean effective disk distance $\tilde{h}^2 = ((1 - x_g) \cdot h_{\mathrm{ng}}^3 + x_g \cdot h_g^3)/\bar{h}$.

The following derivation will be equal for the flow with rivulets and without. For simplicity, the subscript riv will be omitted.

When inserting (2.91) into (2.90) and integrating in time, the change of the bulk temperature T_{bulk} in one time step Δt results in:

$$T_{\mathrm{bulk}}(r^*, t) - T_{\mathrm{bulk}}(r^* - v_r^* \cdot \Delta t, t - \Delta t) = \frac{1}{\rho_{\mathrm{oil}} c_{p,\mathrm{oil}} \cdot \bar{h}} \int_{t-\Delta t}^{t} q_{\mathrm{conv}}(v_r^* \cdot \tilde{t}, \tilde{t}) \cdot d\tilde{t}$$

$$= \frac{1}{\rho_{\mathrm{oil}} c_{p,\mathrm{oil}} \cdot \bar{h} \cdot v_r^*} \int_{r^*-\Delta r^*}^{r^*} q_{\mathrm{conv}}(r^*, r^*/v_r^*) \cdot dr^* \tag{2.92}$$

Due to the discrete time computation of the heat transfer, the following equation holds:

$$q_{\text{conv}}(t - \Delta \tilde{t}) = q_{\text{conv}}(t - \Delta t), \ \forall \Delta \tilde{t} \in (0, \Delta t], \tag{2.93}$$

and (2.92) can be simplified to:

$$T_{bulk}(r^*, t) - T_{bulk}(r^* - \Delta r, t - \Delta t) = \frac{1}{\rho_{\text{oil}} c_{p,\text{oil}} \cdot \bar{h} \cdot v_r^*} \int_{r^* - \Delta r^*}^{r^*} q_{\text{conv}}(r^*, t) \cdot dr^*, \tag{2.94}$$

where $\Delta r = v_r^* \cdot \Delta t$ is the space step.

For expressing time-variant variables f in discrete time, the following notation is introduced:

$$f^t := f(t_0 + \Delta t \cdot t), \ t \in \mathbb{Z} \tag{2.95}$$

The polynomial approximation of the heat transfer q_{conv} is chosen such that it is optimal in the least-squares sense. As it is derived in [18, p. 251ff], such an approximation is achieved by projecting the function to any orthogonal polynomial space. The Chebyshev polynomials are orthogonal polynomials used for this purpose. This is derived in [18, p.239f]. Therefore when using the Chebyshev nodes for polynomial interpolation, the resulting polynomial will be optimal in the least squares sense.

The n Chebyshev nodes in the interval $[r_{\text{in}}^*, r_{\text{out}}^*]$ are:

$$r_{\text{cheb},k}^* = \frac{r_{\text{in}}^* + r_{\text{out}}^*}{2} + \frac{r_{\text{out}}^* - r_{\text{in}}^*}{2} \cdot \cos(\frac{2k-1}{2n}\pi), \ k \in \{1, ..., n\}. \tag{2.96}$$

The heat transfer q_{conv} is approximated with a polynomial of order n.

$$q_{\text{conv}}^t(r^*) := \sum_{k=0}^{n} (r^* - r_{\text{in}}^*)^k \cdot \tilde{a}_k^t \tag{2.97}$$

Therefore, its antiderivative $F_{q_{\text{conv}}}$ will be of order $n + 1$.

$$F_{q_{\text{conv}}}^t(r^*) = \int q_{\text{conv}} \cdot dr^* := \sum_{k=0}^{n+1} (r^* - r_{\text{in}}^*)^k \cdot a_k^t \tag{2.98}$$

With this and (2.95), (2.94) results in:

$$T_{\text{bulk}}^t(r^*) = \frac{1}{\rho_{\text{oil}} c_{p,\text{oil}} \cdot h \cdot v_r^*} \left(F_{q_{\text{conv}}}^{t-1}(r^*) - F_{q_{\text{conv}}}^{t-1}(r^* - \Delta r^*) \right) + T_{\text{bulk}}^{t-1}(r^* - \Delta r^*). \tag{2.99}$$

As a result, T_{bulk} will be a polynomial of order n.

$$T_{\text{bulk}}^t(r^*) := \sum_{k=0}^{n} (r^* - r_{\text{in}}^*)^k \cdot b_k^t \tag{2.100}$$

The coefficients b_k can be calculated with (2.99). The linear system of equations, exemplary for $n = 3$, is:

$$
\begin{pmatrix} b_0 \\ b_1 \\ b_2 \\ b_3 \end{pmatrix}^t = \begin{pmatrix} 1 & -\Delta r^* & (\Delta r^*)^2 & -(\Delta r^*)^3 \\ 0 & 1 & -2\Delta r^* & 3(\Delta r^*)^2 \\ 0 & 0 & 1 & -3\Delta r^* \\ 0 & 0 & 0 & 1 \end{pmatrix} \cdot \begin{pmatrix} b_0 \\ b_1 \\ b_2 \\ b_3 \end{pmatrix}_{t-1} +
$$
$$
\frac{1}{\rho_{\text{oil}} c_{p,\text{oil}} \cdot h \cdot v_r^*} \begin{pmatrix} \Delta r^* & -(\Delta r^*)^2 & (\Delta r^*)^3 & -(\Delta r^*)^4 \\ 0 & 2\Delta r^* & -3(\Delta r^*)^2 & 4(\Delta r^*)^3 \\ 0 & 0 & 3\Delta r^* & -6(\Delta r^*)^2 \\ 0 & 0 & 0 & 4\Delta r^* \end{pmatrix} \cdot \begin{pmatrix} a_1 \\ a_2 \\ a_3 \\ a_4 \end{pmatrix}_{t-1}
$$
$$(2.101)$$

Since T_{bulk} is a polynomial of order n, with (2.88), the problem of approximating q_{conv} can be shifted to the polynomial approximation of a fictional surface temperature $T_{\text{s,f}}$.

$$
T_{\text{s,f}}^t := \sum_{k=0}^{n} (r^* - r_{\text{in}}^*)^k \cdot c_k^t \tag{2.102}
$$

$$
q_{\text{conv}}^t = h_{\text{conv}} \cdot \sum_{k=0}^{n} (r^* - r_{\text{in}}^*)^k \cdot (c_k^t - b_k^t) \tag{2.103}
$$

Note that polynomial approximation is a linear operation and therefore, least squares optimal approximation of the surface temperature implies least squares optimal approximation of the heat transfer.

The following boundary condition for T_{bulk} must be satisfied:

$$
T_{\text{bulk}}^t(r^* = r_{\text{in}}^*) = b_0^t = T_{\text{oil,in}}^t, \tag{2.104}
$$

where $T_{\text{oil,in}}$ is the temperature of the incoming oil. With (2.88) and (2.99), (2.104) becomes:

$$
\int_0^{-\Delta r} T_{\text{s,f}}^t(-\Delta r) dr^* = \left(T_{\text{bulk}}^{t-1}(-\Delta r^*) - T_{\text{oil,in}}^t \right) \frac{\rho_{\text{oil}} c_{p,\text{oil}} \cdot h \cdot v_r^*}{h_{\text{conv,t}}} + \int_0^{-\Delta r} T_{\text{bulk}}^t dr^*
$$
$$(2.105)$$

To satisfy (2.105), the approximation of the fictional surface temperature must be adapted accordingly. The Vandermonde Matrix for the polynomial interpolation, as described in [18, p. 147], is extended by the boundary condition (2.105). The resulting
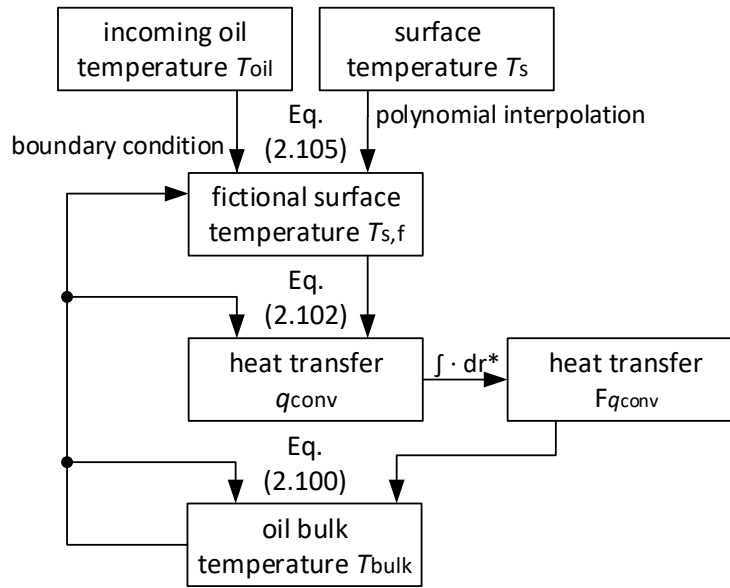
Figure 2.15: Relations between the variables used for calculating the oil bulk temperature and the convective heat transfer from the disk to the oil q_{conv}. From the polynomial interpolation of the surface temperature and the boundary condition (2.105), the fictional surface temperature is calculated in (2.106). From the conservation of energy, the relations between $T_{\mathrm{s,f}}$, T_{bulk} and q_{conv} are formulated in (2.101) and (2.103)

equation, exemplary for $n = 3$, is:

$$
\begin{pmatrix}
1 & r^*_{\mathrm{cheb},1} & \left(r^*_{\mathrm{cheb},1}\right)^2 & \left(r^*_{\mathrm{cheb},1}\right)^3 \\
1 & r^*_{\mathrm{cheb},2} & \left(r^*_{\mathrm{cheb},2}\right)^2 & \left(r^*_{\mathrm{cheb},2}\right)^3 \\
1 & r^*_{\mathrm{cheb},3} & \left(r^*_{\mathrm{cheb},3}\right)^2 & \left(r^*_{\mathrm{cheb},3}\right)^3 \\
-\Delta r^* & \frac{(-\Delta r^*)^2}{2} & \frac{(-\Delta r^*)^3}{3} & \frac{(-\Delta r^*)^4}{4}
\end{pmatrix}
\cdot
\begin{pmatrix}
c_0 \\ c_1 \\ c_2 \\ c_3
\end{pmatrix}
$$
$$
=
\begin{pmatrix}
T_{\mathrm{s}}\left(r^*_{\mathrm{cheb},1}\right) \\
T_{\mathrm{s}}\left(r^*_{\mathrm{cheb},2}\right) \\
T_{\mathrm{s}}\left(r^*_{\mathrm{cheb},3}\right) \\
\left(T^{t-1}_{\mathrm{bulk}}(-\Delta r^*) - T^t_{\mathrm{oil,in}}\right)\frac{\rho_{\mathrm{oil}} c_{p,\mathrm{oil}} \cdot h \cdot v^*_r}{h_{\mathrm{conv,t}}} + \int_0^{-\Delta r} T_{\mathrm{bulk}} dr^*
\end{pmatrix}. \tag{2.106}
$$

In figure 2.15, the relations between the calculated variables are summarized. In figure 2.16, the surface temperature of the clutch T_{s}, the fictional temperature $T_{\mathrm{s,f}}$ and the bulk temperature T_{bulk} are shown for exemplary data from table 3.2 for $n = 6$. At $r \leq r_{\mathrm{in}}$, the correction of the fictional surface temperature for the boundary condition (2.105) is evident.
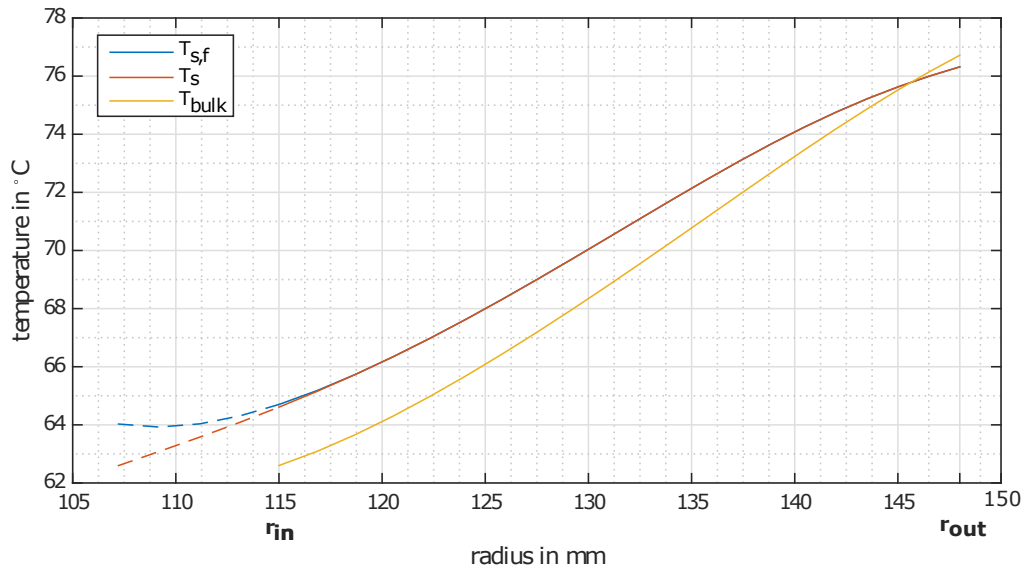
Figure 2.16: Surface temperature of the clutch T_s and resulting bulk temperature T_{bulk} and fictional surface temperature $T_{s,f}$. At $r \leq r_{in}$, the correctio of the fictional surface temperature for the boundary condition (2.105) is evident. At $r > 145$, the oil temperature profile disagrees with the second law of thermodynamics, due to the approximation error

2.3 Heat generation and distribution

The heat q_{gen} is generated by friction between the disks and viscous dissipation in the oil between the disks. The total heat generation on the disk surface equals the input of mechanical power into the system, which is:

$$\int_{r_{in}}^{r_{out}} \int_{0}^{2\pi} q_{gen} \cdot r \cdot d\varphi \cdot dr = Tq_{drag} \cdot \Delta\omega + Q \cdot (p_{out} - p_{in}). \tag{2.107}$$

In normal clutch operation (that is, the magnitude of the oil volume flow is in an appropriate range), the second term is insignificantly small and will therefore be neglected.

The drag torque Tq_{drag} can be calculated from the torque transmitted by the clutch Tq. Due to the axial force loss, the drag torque is different in each pair of disks. This will be discussed in subsection 2.3.1. The distribution of the generated heat in radial direction depends on the pressure distribution between the disks and will be estimated in subsection 2.3.2. The heat is not distributed to the friction and the steel disks equally, which will be discussed in subsection 2.3.3
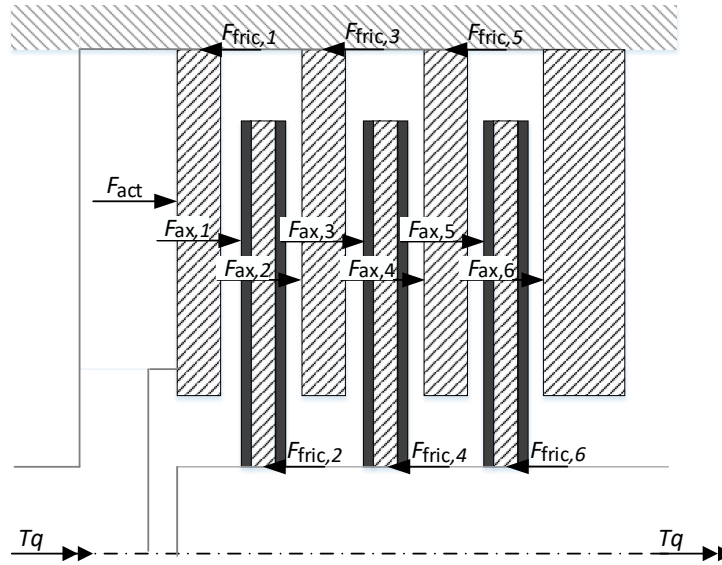
Figure 2.17: Friction between the disks and the splined shaft or casing due to the transmitted torque Tq reduces the axial force F_{ax} that pushes the disks together

2.3.1 Axial force loss

The actuation force F_{act} to close the clutch, generates an axial force F_{ax} on each pair of disks. Due to friction force F_{fric} between the disks and the splined shaft or casing, where the disks are mounted, the axial force will decrease with each disk on the stack. This is illustrated in figure 2.17.

As long as the disks do not touch (that is, when the clutch is open or slipping), the axial force equals the integral of the pressure in the oil over the surface area:

$$F_{ax} = \int_{r_{in}}^{r_{out}} 2\pi \cdot r \cdot p(r) \cdot dr. \tag{2.108}$$

In (2.14), the pressure gradient $\frac{\partial p}{\partial r}$ has been formulated as a function of the oil volume flow in the grooves Q_g and the characteristic rotation speed Ω. The pressure $p(r)$ can be calculated by integrating (2.14) in r with the boundary condition $p(r_{out}) = p_{out}$:

$$p(r) = p_{out} - \frac{3}{20}\rho_{oil} \cdot (r_{out}^2 - r^2) \cdot \Omega^2 + \ln\left(\frac{r_{out}}{r}\right)\frac{12 \cdot Q_g}{2\pi \cdot x_g \cdot h_g^3} \cdot \mu_{oil}. \tag{2.109}$$

With (2.108) and (2.109), it is apparent, that the oil flow rate Q and the disk distance h depend on the axial force. When recalling the relation between the drag torque Tq_{drag} and disk distance h (see (2.22)), it is obvious, that the drag torque is lower when the axial force is lower.

When the clutch closes, the asperities on the disk surfaces get in contact. The relation between the drag torque and the axial force then becomes more complex. Therefore, considering the goals discussed in 1.2, an empirical model for this problem is more suitable than a physical model. For example in [19], the contact pressure and drag torque due to the axial force are estimated based on empirical methods.

However, since also the friction force F_{fric} cannot easily be modelled with physical relations due to the imperfect contact in the splines and vibrations, not the relation between drag torque and axial force, but the drag torque itself will be estimated with an empirical model.

The drag torque Tq_{drag} in the disk pair i is:

$$Tq_{\text{drag},i} = \zeta \cdot Tq_{\text{drag},i-1}, \tag{2.110}$$

where ζ is an empirical value. From $\sum_{i=1}^{n} Tq_{\text{drag},i} = Tq$ results:

$$Tq_{\text{drag},i} = \frac{\zeta^i}{\sum_{j=0}^{n-1} \zeta^j} Tq, \ i \in \{0, 1, ..., n\}, \tag{2.111}$$

where n is the number of disk pairs.

The dependence of the axial force loss on the oil flow Q is neglected. In other words, the oil flow is assumed to be equal in each pair of disks.

2.3.2 Heat distribution in radial direction

The friction coefficient μ_{fric} characterizes the relation between the contact pressure of the disks p and the friction force $F_{f,s}$ on the surface.

$$F_{f,s} = \mu_{\text{fric}} \cdot p. \tag{2.112}$$

The generated heat can then be expressed as:

$$q_{\text{gen}} = \mu_{\text{fric}} \cdot r \cdot \Delta\omega \cdot p(r). \tag{2.113}$$

Inserting (2.113) into (2.107) results in:

$$Tq_{\text{drag}} = \int_{r_{\text{in}}}^{r_{\text{out}}} \mu_{\text{fric}} \cdot 2\pi \cdot r^2 \cdot p(r) \cdot dr. \tag{2.114}$$

According to [20], in an unworn, accurately manufactured clutch, with rigid backing holders, the contact pressure can be assumed constant in r and φ.

Therefore, the integral in (2.114) can be solved and the result is used to express μ_{fric} in (2.113). The generated heat q_{gen} then results in:

$$q_{\text{gen}} = \frac{Tq_{\text{drag}} \cdot \Delta\omega}{2\pi} \cdot \frac{3 \cdot r}{r_{\text{out}}^3 - r_{\text{in}}^3} \tag{2.115}$$

2.3.3 Partition of the friction heat

The friction heat is generated in the interface between friction and separator disk. The fraction of the generated heat that will flow to the friction disk depends on the material properties of the disks. Assuming perfect contact on the non-grooved surface between the disks means, that the temperature on the surface of each disk is equal. It is shown in many studies (for example [20], [21]), that this assumption is valid. Therefore, the partition of the heat transfer can be calculated as stated in [22], where the temperature and heat distribution of two bodies in perfect contact, with a heat source in the interface, is calculated analytically.

The heat transfer to the separator disk q_s and the heat transfer to the friction disk q_f are:

$$q_s = \frac{s}{1+s} \cdot q_{gen} \tag{2.116a}$$

$$q_f = \frac{1}{1+s} \cdot q_{gen} \tag{2.116b}$$

$$\text{with} \quad s = \frac{A_s}{A_f} \cdot \sqrt{\frac{k_s \cdot \rho_s \cdot c_{p,s}}{k_f \cdot \rho_f \cdot c_{p,f}}}, \tag{2.116c}$$

where k_s, ρ_s and $c_{p,s}$ are the thermal conductivity, the density and the heat capacity of the separator disk. k_f, ρ_f and $c_{p,f}$ are the thermal conductivity, the density and the heat capacity of the friction disk.
A_f is the area of heat input on the friction disk, which equals the non-grooved area of the disk. The area of heat input on the separator disk A_s is its total surface area. Therefore, (2.116c) becomes:

$$s = \frac{1}{(1 - x_g)} \cdot \sqrt{\frac{k_s \cdot \rho_s \cdot c_{p,s}}{k_f \cdot \rho_f \cdot c_{p,f}}}. \tag{2.117}$$

Note, that q_f is the heat transfer rate averaged in angular direction. Actually, the heat is only generated on the non-grooved area, where the heat transfer $q_{f,ng}$ is

$$q_{f,ng} = \frac{q_f}{1 - x_g} \tag{2.118}$$

2.4 Heat conduction within the disk

Now that the convective heat transfer to the oil q_{conv} and the heat transfer from the generated heat q_s and $q_{f,ng}$ are calculated, the boundary conditions for the heat transfer problem within the disk can be formulated and the temperature distribution in the disk can be estimated. The considered system is shown in figure 2.18. To enable
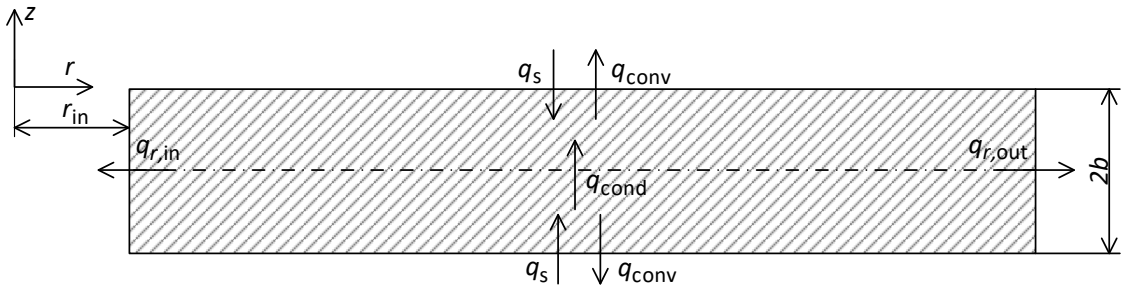
Figure 2.18: The temperature distribution in the separator disk of width $2b$ results from the heat transfer on the surface. At the inner and outer radius, heat is transferred in radial direction from the disk to the oil or the casing. In z direction, there is heat transfer due to convection to the oil (q_{conv}) and due to friction or viscous dissipation (q_{s} or q_{f})
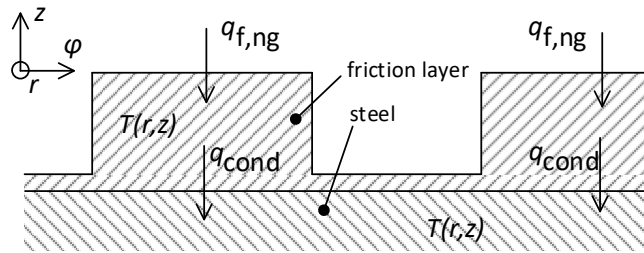
Figure 2.19: The heat from friction and viscous dissipation $q_{\text{f,ng}}$ will flow into the non grooved surface area of the friction disk. Nevertheless, the temperature under the grooves is assumed constant in angular direction.

implementing a generic number of disk pairs, the disk is split at the halve disk width b and modelled separately. The conductive heat transfer q_{cond} between these halves is an additional boundary condition.

The temperature distribution is assumed constant in angular direction. In the separator disk, this is a valid assumption since the disk is rotationally symmetric. In the friction disk, the generated heat will first flow into the non-grooved area and then distribute in the whole disk volume. This is illustrated in figure 2.19. When the conductivity of the friction layer and the steel disk is large enough, the temperature can still be assumed constant in angular direction. This will be further discussed in chapter 3.

When neglecting the temperature gradient in angular direction, the conservation of energy equation in the separator and the friction disk becomes:

$$\rho(z)c_p(z)\frac{\partial T}{\partial t} = \frac{k(z)}{r}\frac{\partial}{\partial r}\left(r\frac{\partial T}{\partial r}\right) + \frac{\partial}{\partial z}\left(k(z)\frac{\partial T}{\partial z}\right), \tag{2.119}$$
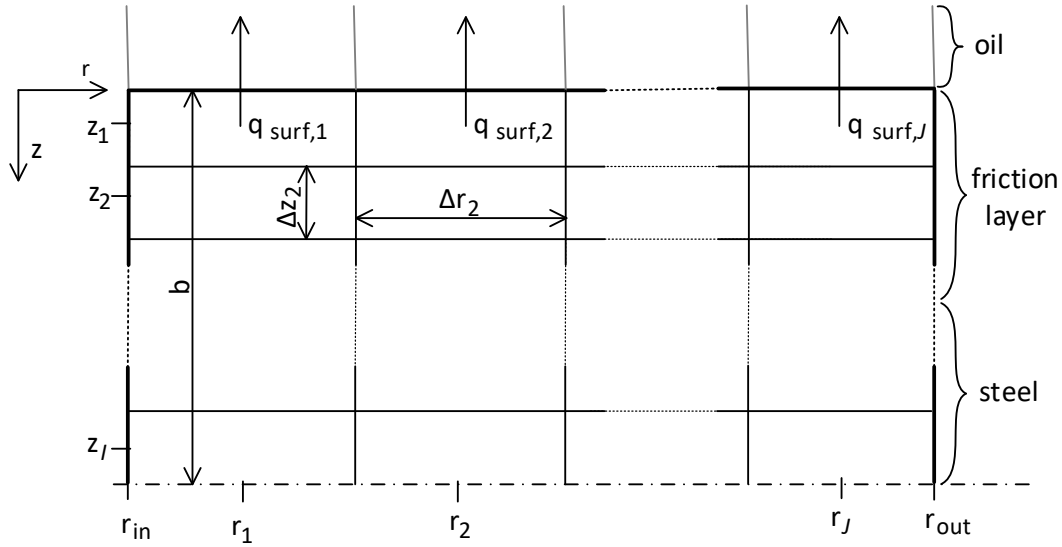
Figure 2.20: The heat conduction problem in the disk is solved with the FDM with I elements in z direction and J elements in r direction.

where ρ, c_p and k are the density, heat capacity and thermal conductivity of the disk material. In the friction disk, these values depend on z, since the friction layer has properties different from the steel disk.

The boundary conditions are:

$$k \cdot \left.\frac{\partial T}{\partial z}\right|_{z=0} = q_{\text{conv}} - q_s \tag{2.120a}$$

$$k \cdot \left.\frac{\partial T}{\partial z}\right|_{z=b} = q_{\text{cond}} \tag{2.120b}$$

$$k \cdot \left.\frac{\partial T}{\partial r}\right|_{r=r_{\text{in}}} = q_{\text{r,in}} \tag{2.120c}$$

$$k \cdot \left.\frac{\partial T}{\partial r}\right|_{r=r_{\text{out}}} = q_{\text{r,out}} \tag{2.120d}$$

This PDE will be solved numerically with the Finite Difference Method (FDM). The considered system for the friction disk is shown in figure 2.20.

The following notation for discrete time and space is introduced:

$$f_{i,j}^k = f(t = t_0 + k \cdot \Delta t \cdot k, z = z_i, r = r_j)$$
$$f_{i+1/2} = f(z = z_i + \Delta z_i/2) \tag{2.121}$$
$$i \in \{1, 2, ...I\}, \, j \in \{1, 2, ...J\}, \, k \in \mathbb{Z}$$

where Δt is the time step, and z_i and r_j are the positions of the FDM elements as shown in figure 2.20. $f_{i,j}^k$ corresponds to an element of the grid and $f_{i+1/2}^k$ corresponds to the boundary between two elements. Therefore, while the width of an element is Δz_i, the distance between two elements is $\Delta z_{i+1/2} = \Delta z_i/2 + \Delta z_{i+1}/2$.
The gird in r direction is chosen such that the finite volumes are equal at each radial position.

$$r_j \cdot \Delta r_j = r_{j+1} \cdot \Delta r_{j+1} \tag{2.122}$$

The grid in z direction is chosen such that an element boundary is on the boundary between friction layer and steel. The finite volumes in each material are chosen to be of equal size.

Since, in the friction disk, the thermal conductivity $k(z)$ is discontinuous in z at the boundaries of the finite volumes, the finite difference for $k\frac{\partial T}{\partial z}$ can be modified to improve accuracy. The discrete heat transfer between two volumes $q_{\text{cond},i+1/2}$ is:

$$q_{\text{cond},i+1/2} = k_i \frac{T_{i+1/2} - T_i}{\Delta z_i/2} = k_{i+1} \frac{T_{i+1} - T_{i+1/2}}{\Delta z_{i+1}/2} := u_{i+1/2}(T_{i+1} - T_i) \tag{2.123}$$

where $u_{i+1/2}$ is the thermal transmittance between the volumes i and $i+1$. From (2.123) results:

$$u_{i+1/2} = \left(\frac{\Delta z_{i+1}}{2k_{i+1}} + \frac{\Delta z_i}{2k_i} \right)^{-1} \tag{2.124}$$

With this, the finite difference can be calculated:

$$k \cdot \left. \frac{\partial T}{\partial z} \right|_{z=z_{i+1/2}} \doteq u_{i+1/2} \cdot (T_{i+1} - T_i) \tag{2.125}$$

With forward differencing in time and the modified central difference approximation of the second derivative in space, (2.119) becomes

$$\rho_i c_{p,i} \frac{T_{i,j}^{k+1} - T_{i,j}^k}{\Delta t} = \frac{1}{\Delta z_i} \left[\left(T_{i+1,j}^k - T_{i,j}^k \right) \cdot u_{i+1/2} - \left(T_{i,j}^k - T_{i-1,j}^k \right) \cdot u_{i-1/2} \right] \\ + \frac{k_i}{r_j \Delta r_j} \left(r_{j+1/2} \frac{T_{i,j+1}^k - T_{i,j}^k}{r_{j+1} - r_j} - r_{j-1/2} \frac{T_{i,j}^k - T_{i,j-1}^k}{r_j - r_{j-1}} \right), \tag{2.126}$$

with the boundary conditions

$$\left(T_{1,j}^k - T_{0,j}^k\right) \cdot u_{1-1/2} = q_{\text{surf},j}^k \tag{2.127a}$$

$$\left(T_{I+1,j}^k - T_{I,j}^k\right) \cdot u_{I+1/2} = q_{\text{cond},j}^k \tag{2.127b}$$

$$k_i \frac{T_{i,1}^k - T_{i,0}^k}{r_1 - r_0} = q_{r,\text{in},i}^k \tag{2.127c}$$

$$k_i \frac{T_{i,J+1}^k - T_{i,J}^k}{r_{J+1} - r_J} = q_{r,\text{out},i}^k . \tag{2.127d}$$

With (2.98), (2.115) and (2.116) the mean heat transfer on the elements surface for the separator disk $q_{\text{surf},s,j}^k$ and for the friction disk $q_{\text{surf},f,j}^k$ can be calculated.

$$
\begin{aligned}
q_{\text{surf},s,j}^k &= \frac{1}{r_{j+1/2}^2 - r_{j-1/2}^2} - \int_{r_{j-1/2}}^{r_{j+1/2}} (q_{\text{conv}}^k(r) - q_s^k(r)) \cdot r \cdot dr \\
&= \frac{1}{r_{j+1/2}^2 - r_{j-1/2}^2} \left(F_{q_{\text{conv}}}^k(r_{j+1/2}^*) - F_{q_{\text{conv}}}^k(r_{j-1/2}^*) \right) \\
&\quad - \frac{r_{j+1/2}^3 - r_{j-1/2}^3}{(r_{\text{out}}^3 - r_{\text{in}}^3) \cdot (r_{j+1/2}^2 - r_{j-1/2}^2)} \cdot \frac{Tq_{\text{drag}}\Delta\omega}{\pi} \cdot \frac{s}{1+s}
\end{aligned}
\tag{2.128a}
$$

$$
\begin{aligned}
q_{\text{surf},f,j}^k &= \frac{1}{r_{j+1/2}^2 - r_{j-1/2}^2} - \int_{r_{j-1/2}}^{r_{j+1/2}} (q_{\text{conv}}^k - q_f^k) \cdot r \cdot dr \\
&= \frac{1}{r_{j+1/2}^2 - r_{j-1/2}^2} \left(F_{q_{\text{conv}}}^k(r_{j+1/2}^*) - F_{q_{\text{conv}}}^k(r_{j-1/2}^*) \right) \\
&\quad - \frac{r_{j+1/2}^3 - r_{j-1/2}^3}{(r_{\text{out}}^3 - r_{\text{in}}^3) \cdot (r_{j+1/2}^2 - r_{j-1/2}^2)} \cdot \frac{Tq_{\text{drag}}\Delta\omega}{\pi} \cdot \frac{1}{1+s} ,
\end{aligned}
\tag{2.128b}
$$

where r_j^* is the radial position r_j transformed according to (2.91).

The radial rates of heat transfer $q_{r,\text{in},i}^k$ and $q_{r,\text{out},i}^k$ depend on the assembly of the clutch and on the casing, which can not be generalized. Therefore, these heat transfers will be modelled with an empiric relation:

$$q_{r,\text{in},i}^k = u_{\text{in}} \cdot (T_{i,1}^k - T_{\text{oil,in}}) \tag{2.129a}$$

$$q_{r,\text{out},i}^k = u_{\text{out}} \cdot (T_{i,J}^k - T_{\text{oil,in}}) \tag{2.129b}$$

where u_{in} and u_{out} has to be found empirically.

The conductive heat transfer between the two halves of the disks is:

$$q_{\text{cond},j}^k = \tilde{T}_{I,j}^k - T_{I,j}^k \cdot \frac{k_s}{\Delta z_I}, \tag{2.130}$$

where $\tilde{T}$ is the temperature in the other halve of the disk.

Finally, when solving (2.126) and (2.127) for $T_{i,j}^{k+1}$, the temperature in the disks can be calculated incrementally in time.

3 Validation

In the presented model, many empirical relations and simplifications were used. Therefore, correctness of the model and its components need to be validated by comparison with data from measurements. A complete validation of all components would require a large amount of measurements and thus an effort that goes beyond the scope of this thesis. Therefore, the model will be validated with measurements only to a limited extend. However, qualitative validation of the behaviour of the model and its components will be conducted. Since many parameters need to be identified with measurement data, in section 3.2, a sensitivity analysis is performed to rate the accuracy of the model in a different setup, when no parametrization can be performed.

3.1 Qualitative validation and analysis of stability

In this section, the stability of the model in different artificial scenarios will be investigated. Among others, this will give a notion of appropriate values for the time- and space step. Also, the correctness of some of the models components is validated qualitatively by comparison to results from literature and to a simple stationary model. The investigated components are the heat transfer from the disk to the oil and the heat conduction within the disk. For the oil flow between the disks and the heat generation and distribution, no qualitative validation is conducted.

3.1.1 Heat transfer to the oil

In subsection 2.2.4, the rate of heat transfer from the disk to the oil was approximated with a polynomial function. This model can become unstable or highly inaccurate. Therefore, correct choice of the order of the polynomial approximation and the time step is crucial. Also, pre-processing of the input data can help to ensure stability. In the following, the reasons for inaccuracy or instability are discussed:

Neglecting the recirculation flow in the grooves

As discussed in subsection 2.2.2, during slip state, a recirculation flow will emerge in the grooves. In the model, only the flow in radial direction has been considered for estimating the Nusselt number and the convective heat transfer coefficient $h_{\mathrm{conv,t}}$. Moreover, the Nusselt number in the grooves was only calculated for constant rate of heat transfer or constant wall temperature on the surface and the Nusselt number in the non-grooved area was only calculated for open clutch state.
These simplifications will be compensated with parametrization of Nu_{g} and the empirical factor ζ. In the following, the qualitative relations will be compared to literature, where mainly empirical relations to model the total heat transfer coefficient $h_{\mathrm{conv,t}}$ were used.
In [21], the total Nusselt number Nu was modelled as a function of the Reynolds and Prandtl number. In [23], the convective heat transfer coefficient was modelled with a constant empiric Nusselt number and as a function of the oil properties and the square root of the angular velocity. [24] used a simple analytical solution for the heat transfer on a flat plate:

$$h_{\mathrm{conv,t}} = 0.332 \cdot \frac{k_{\mathrm{oil}}}{r} \sqrt{Re_\omega} \cdot Pr^{1/3}, \tag{3.1}$$

were Re_ω is the Reynolds number resulting from the rotational speed difference $\Delta\omega$. All these solutions have in common, that the oil flow in radial direction is neglected (that is, the heat transfer is zero at 0 rpm). In [24], although the grooves are not considered at all, the results are acceptable. The reason is, that starting at low rotational speeds, the rate of convective heat transfer in the non-grooved area is much larger than in the grooved area. The actual error by neglecting the recirculation flow can only be determined with measurements.

In figure 3.1, the rate of convective heat transfer according to [24] and the rate of convective heat transfer in the proposed model is shown. Since the convective heat transfer in the presented model depends on many parameters such as geometry and oil volume flow rate, the graph in 3.1 only fits quite well with the simple relation from [24] for a particular range of parameters. Also, to fit with the assumption of no convective heat transfer at 0 rpm, the grooves need to be removed from the model (that is, $x_{\mathrm{g}} = 0$). However, the qualitative trend of the rate of convective heat transfer in the presented model matches with the proportionality to $\sqrt{\omega}$, as it is stated in many literature, quite well.

Explicit integration in discrete time

The heat transfer problem is solved with explicit time integration. A criterion for the stability of this solution is the Courant-Friedrichs-Lewy (CFL) condition, as described
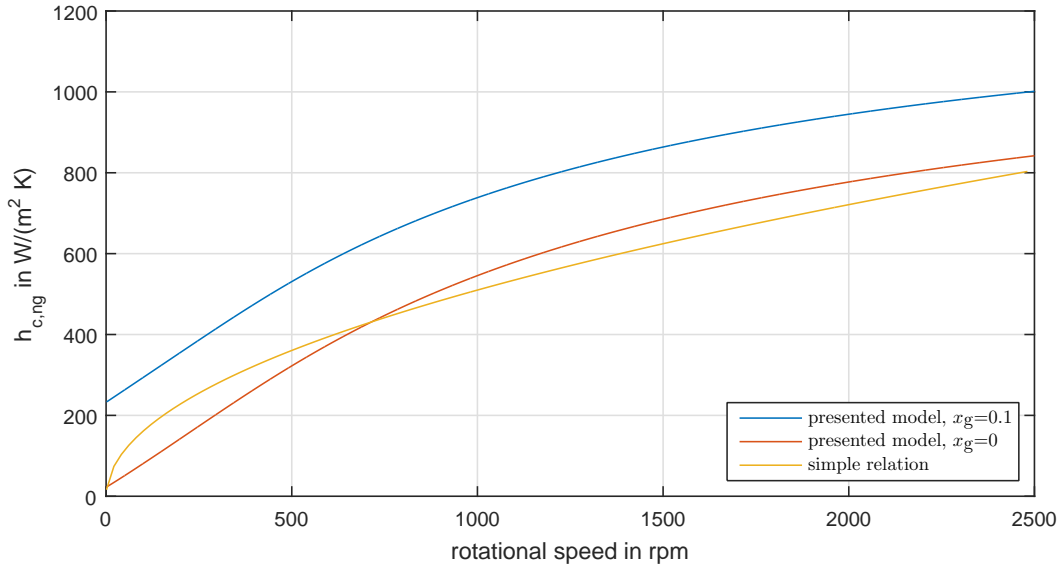
Figure 3.1: The convective heat transfer from the disk to the oil is simulated for different rotational speeds. This result can be compared to the convective heat transfer when the width of the grooves reaches 0 and to a simple relation for the convective heat transfer as described in [24].

in [17, p. 106ff].

$$u_{\mathrm{p}} \cdot \frac{\Delta t}{\Delta x} \overset{!}{<} 1 \tag{3.2}$$

Where u_{p} is the propagation speed of the state variable (here the temperature T) and Δx is the space step. For the present model, the respective finite difference equation is:

$$\frac{T_{\mathrm{bulk,g}}^{k} - T_{\mathrm{bulk,g}}^{k-1}}{\Delta t} = u_{\mathrm{p}} \cdot \frac{T_s - T_{\mathrm{bulk,g}}^{k-1}}{\Delta x} = \frac{h_{\mathrm{conv,t}}}{\rho_{\mathrm{oil}} \cdot c_{p,\mathrm{oil}}} (T_s - T_{\mathrm{bulk,g}}^{k-1}) \tag{3.3}$$

Using exemplary values from 3.2, the propagation rate $u_{\mathrm{p}}/\Delta x$ can be estimated:

$$\frac{u_{\mathrm{p}}}{\Delta x} = \frac{h_{\mathrm{conv,t}}}{\rho \cdot c_p \cdot \bar{\bar{h}}} \approx \frac{2000 \mathrm{W}/(\mathrm{m}^2 \cdot \mathrm{K})}{857 \ \mathrm{kg/m}^3 \cdot 1990 \ \mathrm{J}/(\mathrm{kg \cdot K}) \cdot 0.1 \ \mathrm{mm}} = 11.76 \ \mathrm{Hz} \tag{3.4}$$

With (3.2) and (3.4), the condition for the time step can be formulated:

$$\Delta t < 0.085 \ \mathrm{s} \tag{3.5}$$

Polynomial approximation of the heat transfer

The rate of heat transfer was approximated with a polynomial function. Therefore, equalization of the temperatures of the oil and the disk is not guaranteed, even though

47

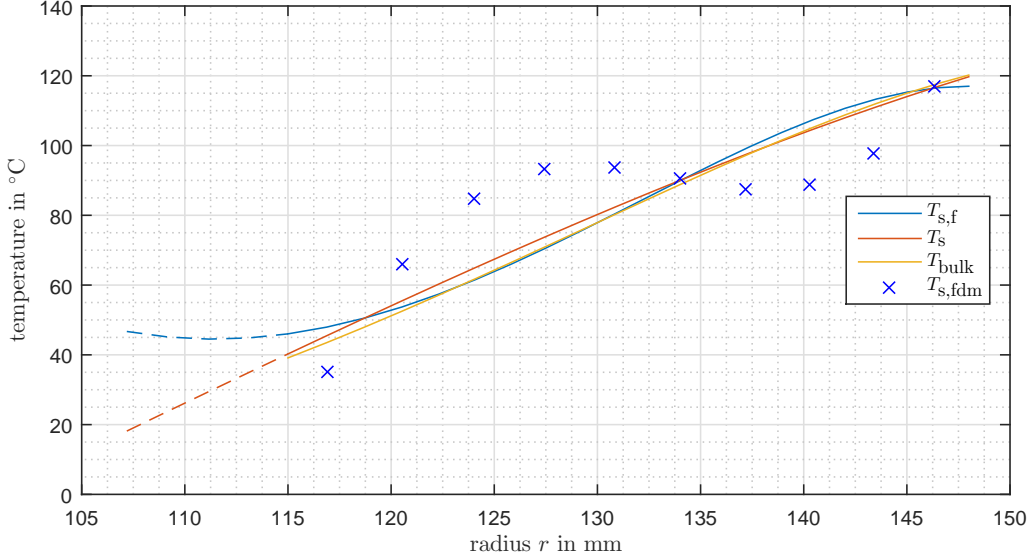Figure 3.2: Extending the polynomial interpolation T_s of the surface temperature $T_{s,fdm}$ of order $n = 2$ by the boundary condition results in the fictional surface temperature $T_{s,f}$ of order $n = 3$. The order of the interpolation is not high enough, which results in waves in the surface temperature $T_{s,fdm}$.

the CFL condition is met. In figure 3.2, the surface temperatures and the oil bulk temperature are shown for a polynomial order of the rate of heat transfer $n = 3$. Apparently, the difference between the polynomial approximation of the surface temperature to the surface temperature resulting from the heat conduction in the disk is large. The reason is, that the polynomial order of the surface temperature T_s is not sufficient to reproduce the actual surface temperature $T_{s,fdm}$. At location, where the surface temperature is underestimated, also the rate of heat transfer to the oil will be underestimated. Consequently, the surface temperature at this location will increase and thus, also the error of underestimation will increase. This phenomenon creates the waviness of the surface temperature $T_{s,fdm}$ as seen in figure 3.2. The amplitude of these waves is limited due to the heat conduction in radial direction within the disk.

In figure 3.3, the error between the polynomial approximation of the surface temperature T_s and the surface temperature resulting from the heat conduction in the disk is shown for different polynomial orders n. The mean square error between T_s and $T_{s,fdm}$ is almost halved with each increase of the order. However, the computational effort increases with n, especially because the matrix in (2.106) needs to be inverted. Considering this trade-off, the order $n = 6$ is chosen.
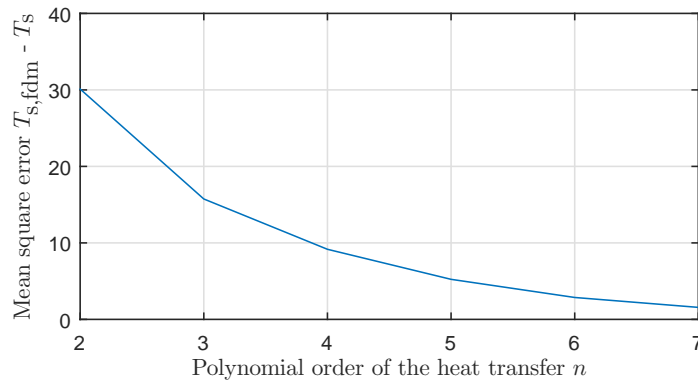
Figure 3.3: The mean squared error between the polynomial interpolation of the surface temperature T_s and the surface temperature $T_\text{s,fdm}$ almost halves with each increment of the order n.

Time variance of input parameters

In subsection 2.2.4, most of the input variables where assumed constant in time. A change of the oil volume flow rate Q will lead to different values for the flow speed and therefore the space step Δr will change (see (2.91)). The behaviour of the presented model in this situation has not been investigated so far. The relevant quantity for this investigation is the change of the input variables from one time step to another. The following tests are conducted with a constant time step $\Delta t = 0.01s$. The encountered limits of the slew rates can be scaled linearly by the time step.

In figure 3.4, the rate of convective heat transfer from the disk to the oil when the oil volume flow rate is changed from 3 l/min to 13 l/min with a slew rate of 10 (l/min)/s is shown. At the beginning, the model is in a stationary state. In the time slot between 1 s and 2 s, the oil volume flow rate is increased. Consequently, the rate of heat transfer increases too, which causes the disk temperature to decrease and the rate of heat transfer falls until the stationary state is reached again. Therefore, the rate of heat transfer $q_\text{conv}(r_{2-6})$ behaves as expected. However, the rate of heat transfer at the outer radius r_8 shows oscillations that are not expected in reality. Apparently, these oscillations result from the error caused by assuming constant input variables. For a higher slew rate, these oscillations will increase. Therefore, a rate limiter for the oil volume flow rate will be used. Similar behaviour can be seen in the artificial situation, where only the disk distance h_ng changes with an opening time of 200 ms.

A change of the oil temperature or other input parameters does not show any critical behaviour. An exception to this is the start of the forming and dissolving of rivulets. In the model presented in subsection 2.2.4, a continuous transition from a continuous oil flow to rivulets is not possible due to the non-linear change of the coordinate r^* (see equation (2.91)). It is not even possible, to model the situation where part of the
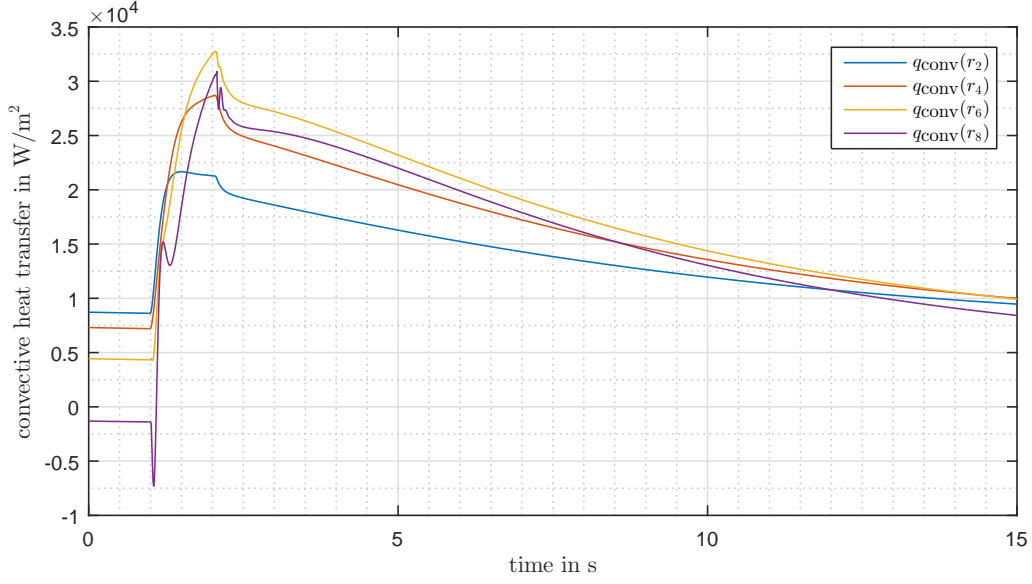
Figure 3.4: The convective heat transfer from the disk to the oil on different radial locations is simulated during a change of the oil volume flow rate from 3 to 13 (l/min) in the timeslot between 1 s and 2 s.

flow is continuous and the other part contains rivulets. For this situation, a simpler, stationary model will be derived:

The stationary conservation of energy in radial direction is:

$$\rho \cdot c_p \frac{1}{r} \frac{\partial}{\partial r} \left(T_{\text{bulk}} \int_0^{\bar{h}} r \cdot v_r \cdot dz \right) = h_{\text{conv,t}} \cdot (T_s - T_{\text{bulk}}). \tag{3.6}$$

With the dimensionless radius r^* and average radial velocity v_r^* as defined in (2.91), (3.6) becomes:

$$\frac{\partial T_{\text{bulk}}}{\partial r^*} = \frac{h_{\text{conv,t}} \cdot (T_s - T_{\text{bulk}})}{\rho \cdot c_p \cdot \bar{h} \cdot v_r^*}. \tag{3.7}$$

The surface temperature is interpolated linearly:

$$T_{s,j}^{\text{int}} = T_{s,j} + (r^* - r_j^*) \cdot \frac{T_{s,j+1} - T_{s,j-1}}{r_{j+1} - r_{j-1}} \tag{3.8}$$

Solving the differential equation (3.6) and inserting (2.27) results in:

$$T_{\text{bulk},j+1/2} = (1 - e^C) \cdot T_{s,j} + e^C \cdot T_{\text{bulk},j-1/2} + \frac{T_{s,j+1} - T_{s,j-1}}{2} \left(\frac{1 + e^C}{2} + \frac{1 - e^C}{C} \right),$$

$$\text{with } C = \frac{2\pi}{Q \cdot \rho \cdot c_p} h_{\text{conv,t}} \cdot \phi_{\text{riv}}^2 (r = r_i) \cdot (r_{i+1}^* - r_i^*)$$

$$\tag{3.9}$$
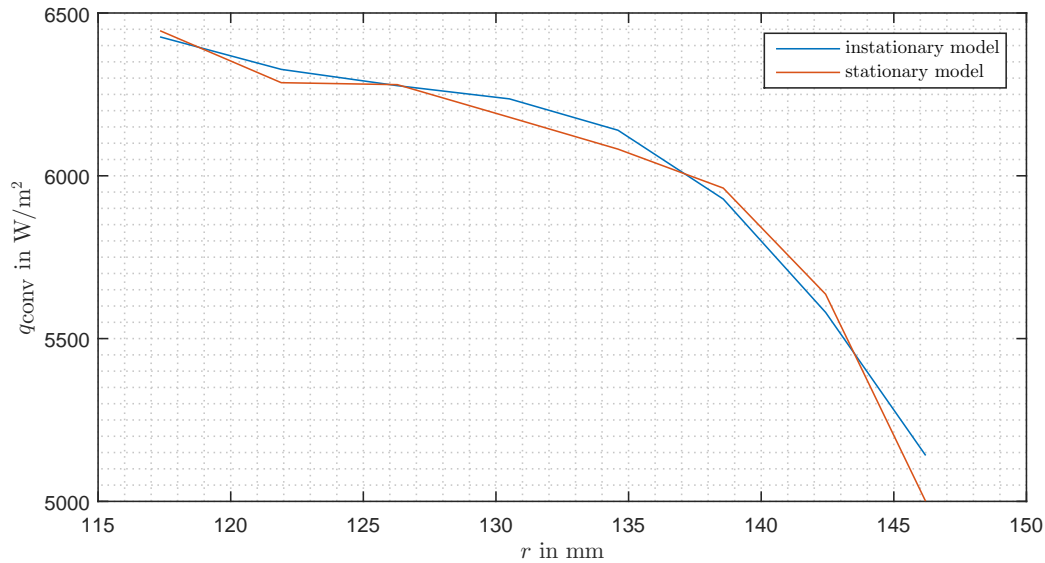
Figure 3.5: The convective heat transfer from the disk to the oil on different radial locations is simulated in a stationary state both using the presented instationary model (see subsection 2.2.4) and the stationary model presented in this subsection

In a stationary test setup, this model should give similar values for the rate of convective heat transfer as the model presented in subsection 2.2.4. Exemplary results for the rate of heat transfer during stationary state are shown in figure 3.5. The difference between the shown profiles is in a range that is to be expected from the different interpolation methods for the surface temperature.

3.1.2 Heat conduction within the disk

The accuracy and stability of calculating the heat conduction within the disk depends on the grid used for the FDM. When the grid elements are too large, the model will be inaccurate and when the elements are too small, the model will be unstable.

Maximum element size

The maximum grid size used for the FDM to obtain accurate results depends on the temperature gradient in the disk. This relation can be described with the Biot number, as described in [10, chap. 7.4]. The Biot number Bi is defined as the ratio of conductive resistance in the solid to convective resistance at the surface.

$$Bi = \frac{h_{\mathrm{conv,t}} \cdot L_{\mathrm{c}}}{k} \tag{3.10}$$

Where L_c is the characteristic length defined as the ratio of the volume of the solid to its surface area and k is the thermal conductivity of the solid.

When the Biot number is much less than 1, the temperature distribution in the element can be assumed to be uniform. The larger the Biot number, the larger the error due to space discretization will be. Technically this criterion is for convective heat transfer only. However, when the generated heat q_{gen} is in the same order of magnitude, the considerations can be also applied in the present situation.

To check if a resolution of the temperature in z direction is necessary in the steel disk or the friction layer, the characteristic length L_c is based on the half width of the steel disk b_s or the thickness of the friction layer made of sintered material b_{si} or paper b_p respectively.

$$L_c = \frac{(r_{out}^2 - r_{in}^2)\pi \cdot b}{(r_{out}^2 - r_{in}^2)\pi} = b \tag{3.11}$$

Using exemplary data from 3.2 and an exemplary value for $h_{conv,t}$ from simulations, the Biot numbers for a steel disk Bi_s, a paper based friction layer Bi_p and a copper based sintered friction layer Bi_{si} are estimated.

$$Bi_s = \frac{h_{conv,t} \cdot b_s}{k_s} \approx \frac{2000 \text{ W}/(\text{m}^2 \cdot \text{K}) \cdot 1.15 \text{ mm}}{50 \text{ W}/(\text{m} \cdot \text{K})} = 0.046 \tag{3.12a}$$

$$Bi_{si} = \frac{h_{conv,t} \cdot b_{si}}{k_{si}} \approx \frac{2000 \text{ W}/(\text{m}^2 \cdot \text{K}) \cdot 0.575 \text{ mm}}{1.5 \text{ W}/(\text{m} \cdot \text{K})} = 0.767 \tag{3.12b}$$

$$Bi_p = \frac{h_{conv,t} \cdot b_p}{k_p} \approx \frac{2000 \text{ W}/(\text{m}^2 \cdot \text{K}) \cdot 0.475 \text{ mm}}{0.4 \text{ W}/(\text{m} \cdot \text{K})} = 2.37 \tag{3.12c}$$

Consequently, the temperature need not be resolved in z direction in the separator steel disk or the steel disk of the friction disk. For the friction layer, at least a small number of elements would be appropriate to obtain accurate results.

The temperature gradient in angular direction has been neglected. The characteristic length to quantify the error caused by this assumption, the characteristic length is:

$$L_c = \frac{\Delta\varphi \cdot (r_{out} + r_{in})/2 \cdot (r_{out} - r_{in}) \cdot b}{2 \cdot (r_{out} - r_{in}) \cdot b} = \Delta\varphi \cdot (r_{out} + r_{in})/4. \tag{3.13}$$

And, with exemplary data from 3.2, the Biot number is:

$$Bi_{ang,s} = \frac{h_{conv,t} \cdot L_c}{k_s} \approx \frac{2000 \text{ W}/(\text{m}^2 \cdot \text{K}) \cdot 3.78 \text{ mm}}{50 \text{ W}/(\text{m} \cdot \text{K})} = 0.151$$

$$Bi_{ang,si} = \frac{h_{conv,t} \cdot L_c}{k_{si}} \approx \frac{2000 \text{ W}/(\text{m}^2 \cdot \text{K}) \cdot 3.78 \text{ mm}}{1.5 \text{ W}/(\text{m} \cdot \text{K})} = 5.04$$

$$Bi_{ang,p} = \frac{h_{conv,t} \cdot L_c}{k_p} \approx \frac{2000 \text{ W}/(\text{m}^2 \cdot \text{K}) \cdot 3.78 \text{ mm}}{0.4 \text{ W}/(\text{m} \cdot \text{K})} = 18.9$$

$$\text{with } L_c \approx 0.063 \cdot 120 \text{ mm}/2 = 3.78$$

(3.14)

Consequently, resolving the temperature in the steel disk in angular direction is not necessary. The Biot numbers of the friction layer $Bi_{ang,si}$ and $Bi_{ang,p}$ are very large. However, it is possible, that the temperature gradient will be compensated by the constant temperature in the steel disk and by the oil. Therefore, to determine if the presented model will still give accurate results, further empirical or numerical investigations are necessary.

Minimum element size

The heat conduction within the disk is solved by the FDM with explicit time integration. Therefore, the CFL condition for stability (as described in 3.1.1) can be formulated. The relevant CFL conditions (see (3.2)) for the heat conduction in the paper based friction disc in r and z direction are:

$$\Delta t \leq \frac{\rho_s \cdot c_{p,s} \cdot \Delta r^2}{k_s} \tag{3.15a}$$

$$\Delta t \leq \frac{\rho_p \cdot c_{p,p} \cdot \Delta z^2}{k_p} \tag{3.15b}$$

$$\Delta t \leq \frac{\rho_s \cdot c_{p,s} \cdot \Delta z^2}{k_s} \tag{3.15c}$$

The CFL condition in r direction of the friction layer is not relevant since the thermal diffusivity $\rho_p \cdot c_{p,p}/k_p$ is much smaller than the thermal diffusivity of steel.

For exemplary data from 3.2 and the time step $\Delta t = 0.05$ s, the maximum numbers of elements in z direction n_z and in r direction n_r can be calculated. Since the temperature in the steel disk will not be resolved in z direction, the CFL condition (3.15c) is used

Variable	chosen value	limiting effects
time step Δt	0.01 s	time variance of input variables CFL condition computational resources
polynomial order n	6	polynomial approximation computational resources
rate limiter for Q	3 (l/min)/s	discrete time step
FDM elements in z direction n_z in the friction layer	2	Biot number CFL condition
FDM elements in r direction n_r	8	computational resources

Table 3.1: Parameters chosen after the qualitative validation

to find a condition for the maximum time step.

$$n_{z,\mathrm{p}} \leq b_{\mathrm{p}} \cdot \left(\frac{\rho_{\mathrm{p}} \cdot c_{p,\mathrm{p}}}{k_{\mathrm{p}} \cdot \Delta t} \right)^{\frac{1}{2}} \approx 0.475 \text{ mm} \left(\frac{1799\mathrm{kg/m^3} \cdot 740.7 \text{ J/(kg·K)}}{0.4 \text{ W/(m·K)} \cdot 0.05 \text{ s}} \right)^{\frac{1}{2}} = 3.88 \quad (3.16a)$$

$$n_r \leq (r_{\mathrm{out}} - r_{\mathrm{in}}) \cdot \left(\frac{\rho_{\mathrm{s}} \cdot c_{p,\mathrm{s}}}{k_{\mathrm{s}} \cdot \Delta t} \right)^{\frac{1}{2}} \approx 30 \text{ mm} \cdot \left(\frac{7850 \text{ kg/m^3} \cdot 500 \text{ J/(kg·K)}}{50 \text{ W/(m·K)} \cdot 0.05 \text{ s}} \right)^{\frac{1}{2}} = 37.6$$
$$(3.16b)$$

$$\Delta t \leq \frac{\rho_{\mathrm{s}} \cdot c_{p,\mathrm{s}} \cdot b_{\mathrm{s}}^2}{k_{\mathrm{s}}} \approx \frac{7850\mathrm{kg/m^3} \cdot 500 \text{ J/(kg·K)} \cdot (0.73 \text{ mm})^2}{50 \text{ W/(m·K)}} = 0.042 \text{ s} \quad (3.16c)$$

According to the results in subsubsection 3.1.2, a number of elements in z direction larger than 3 would not be appropriate anyway. A number of elements in r direction larger than 37 would not be appropriate considering the computational effort. Therefore, the only relevant criterion in (3.16) is the maximum time step $\Delta t \leq 0.042$ s.

In table 3.1, appropriate parameters for the model are summarized.

3.2 Validation with measurement data

For the validation with measurement data, the model will first be parametrized for the clutch used in the measurements. The parametrized model is then used to estimate the temperature during the measurements and the results are compared to the measured temperature. Also, to rate the transferability of the model, the sensitivity of the model to its parameters is analysed. In the last sub-subsection, all results from this subsection are discussed.

3.2.1 Test bench and clutch parameters

The clutch used for validation has a stack of 3 paper based friction disks and 4 separator disks. The test bench is schematically illustrated in figure 3.6. On the test bench, one side of the clutch is attached to an electric motor while the other is stationary. The oil is conditioned to a preferably constant temperature $T_{oil,in}$ and pumped with a variable volume flow Q into the clutch. The measured variables are:

- the temperature of the incoming oil $T_{oil,in}$
- the torque transmitted by the clutch Tq
- the rotational speed ω_2
- a temperature in each friction disk $\hat{T}_1, \hat{T}_2$ and $\hat{T}_3$.

The radial or axial location of the temperature sensor in the disks is not known and the oil volume flow rate Q was not measured. Furthermore, the properties of the friction layer as well as the geometry or thermal behaviour of the casing are unknown.

All modelling parameters of the clutch and variables needed for the exemplary calculations in chapter 2, as well as their known or expected values are listed in table 3.2.
The exact properties of the friction layer are not known, but in literature ([20], [25], [26]), exemplary values are given. The friction disks are not radially grooved but have a waffle grooving, as described in [3]. Therefore, for n_g and x_g, characteristic values that fit with a radially grooved pattern will be used. It will have to be verified, if the model can still be valid for the waffle groove pattern.
The depth of the grooves $h_g - h_{ng}$ is not known, but can not be greater than the thickness of the friction layer.
In chapter 2, only a range of possible values for the Nusselt number in the grooves Nu_g has been derived. Its approximative value will be identified with measurement data. The geometrical or thermal properties of the casing of the clutch are not known. The properties of the oil (10W40) are specified as a function of the temperature. For the radial thermal transmittances u_{in} and u_{out}, a maximum can be roughly estimated from the tooth geometry of the disks.

3.2.2 Measuring procedure

Stationary and dynamic measurements have been conducted at different loads and oil temperatures. In the following, these are described shortly.
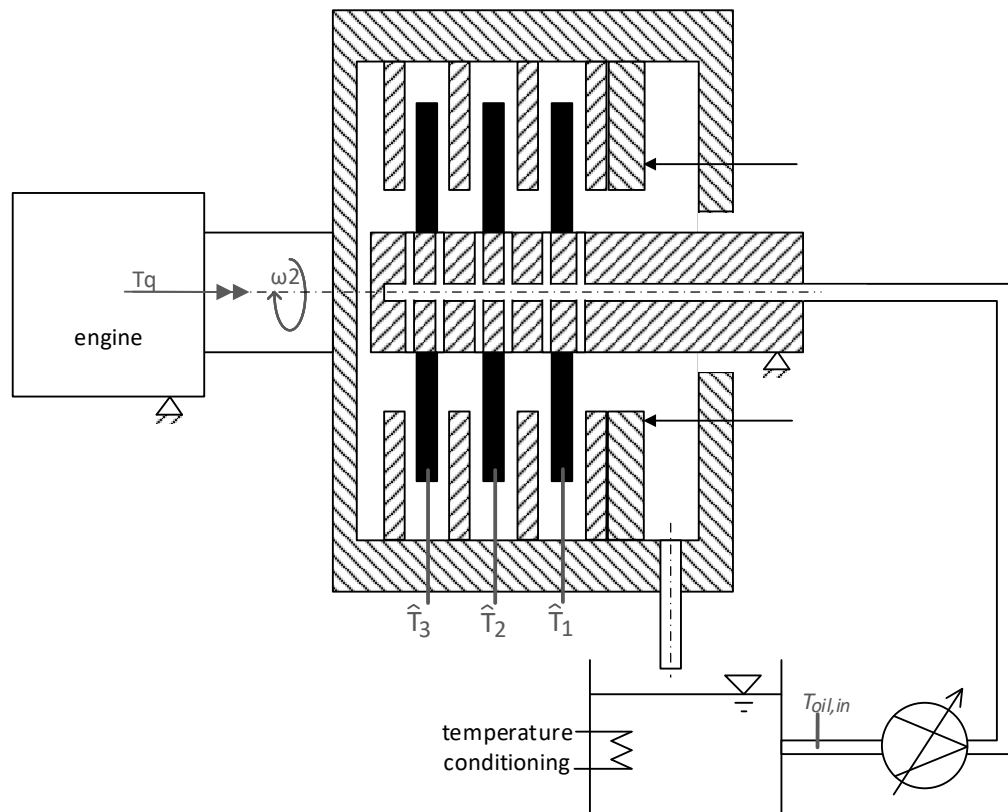
Figure 3.6: Schematic illustration of the test bench: The disk stack consists of 3 paper based friction disks and 4 separator disks. One side of the clutch is attached to an electric motor (speed ω_2), while the other is stationary ($\omega_1 = 0$). The oil is conditioned to the temperature $T_{\text{oil,in}}$ and pumped with oil volume flow rate Q into the clutch. Temperature sensors are attached to the friction disks ($\hat{T}_1$, $\hat{T}_2$, $\hat{T}_3$) and the oil bath ($T_{\text{oil,in}}$). Also, the torque Tq and the rotational speed ω_2 at the motor are measured.

Variable	Symbol	Value	Source
Inner radius of the friction surface	r_in	115 mm	
Outer radius of the friction surface	r_out	148 mm	
Thickness of the steel in the friction disk	$b_\text{p,s}$	1.45 mm	
Thickness of the friction layer	b_p	0.475 mm	data sheet
Thickness of the separator disk	b_s	2.3 mm	
Number of grooves	n_g	$50 - 80$	
Ratio of grooved area	x_g	$0.2 - 0.4$	
Disk distance of the open clutch	h_ng	0.2 mm	
Depth of the grooves	$h_\text{g} - h_\text{ng}$	≤ 0.475 mm	
Radial thermal transmittance of the casing	$u_\text{in}, u_\text{out}$	< 3000 W/(m^2· K)	
Heat capacity of steel C60	c_{ps}	500 J/(kg·K)	
Thermal conductivity of steel C60	k_s	50 W/(m· K)	[27]
Density of steel C60	ρ_s	7850 kg/m^3	
Heat capacity of the paper friction layer	$c_{p,p}$	≈ 740.7 J/(kg·K)	
Thermal conductivity of the paper friction layer	k_p	$0.2 - 0.6$ W/(m· K)	[20], [25], [26, p. 11]
Density of the paper friction layer	ρ_p	≈ 1799 kg/m^3	
Heat capacity of engine oil 10W40	$c_{p,\text{oil}}$	1990-2450 J/(kg·K)	[28]
Thermal conductivity of oil 10W40	k_oil	0.158 W/(m·K)	
Kinematic viscosity of oil 10W40 (at $0 - 200°C$)	$\mu_\text{oil}/\rho_\text{oil}$	10 - 840 mm^2/s	[29]
Density of oil 10W40 (at $0 - 200°C$)	ρ_oil	808 - 876 kg/m^3	
Oil volume flow rate	Q	6 l/min	exemplary
Relative rotation speed	$\Delta\omega$	2000 rpm	
Nusselt number in the grooves	Nu_g	7.8 - 8.4	
Coefficient for the temperature in the non-grooved area	ξ	0 - 1	Chapter 2
Heat transfer between the disks	$h_\text{c,oil}$		
Axial thermal transmittance of the casing	$u_\text{ax,in}, u_\text{ax,out}$	unknown	
Axial force loss	ζ	0.998 - 0.918	[30]

Table 3.2: Modelling parameters of the clutch

Figure 3.7: Stationary measurement points at 15 different loads in separate runs for both engine oil and ATF

Stationary measurements

In the stationary measurements, the clutch is in slipping state with constant torque and rotational speed until the temperature in the clutch becomes approximately constant.

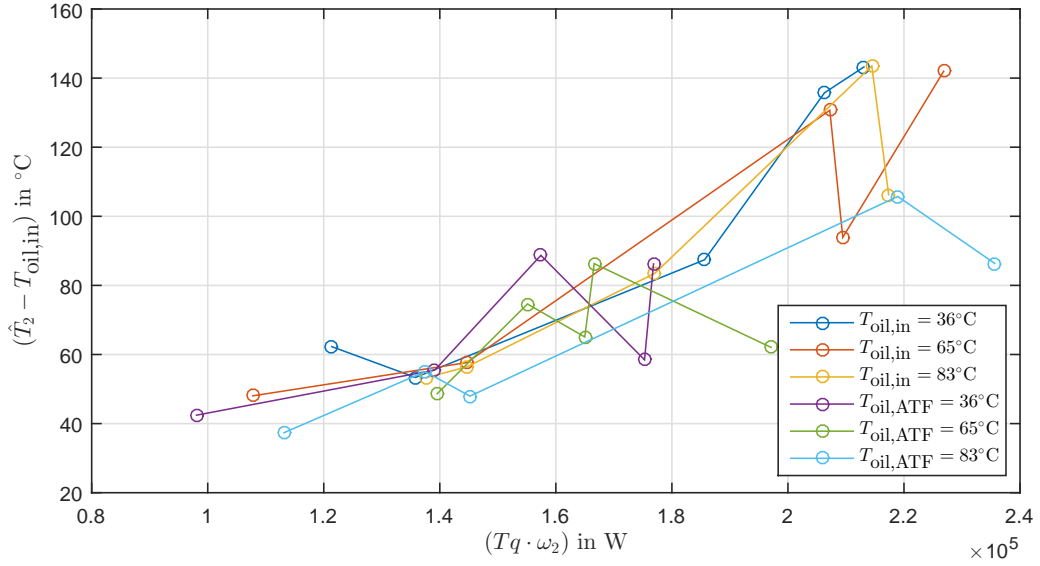30 stationary measurements were conducted with different loads and oil temperatures. The first 15 stationary points were measured in separate runs while the others were measured in 3 runs of several stationary points each. They can be classified in 3 values of incoming oil temperature: 36°C, 65°C and 83°C. The incoming oil temperature $T_{\mathrm{oil,in}}$ during one measuring run was approximately constant.
The same measurements have also be conducted with an automatic transmission fluid (ATF) instead of engine oil. Since several parameters differ for these measurements, they will only be used for the identification of the axial force loss ζ and the axial thermal transmittance $u_{\mathrm{ax,in}}$ and $u_{\mathrm{ax,out}}$.

The first 15 stationary points with engine oil and with ATF are shown in figure 3.7 and the second 15 stationary points are shown in figure 3.8. The approximately constant proportionality factor between temperature $\hat{T}_2$ and dissipation power $Tq \cdot \omega_2$ indicates that the oil volume flow rate Q is constant during one measuring run.
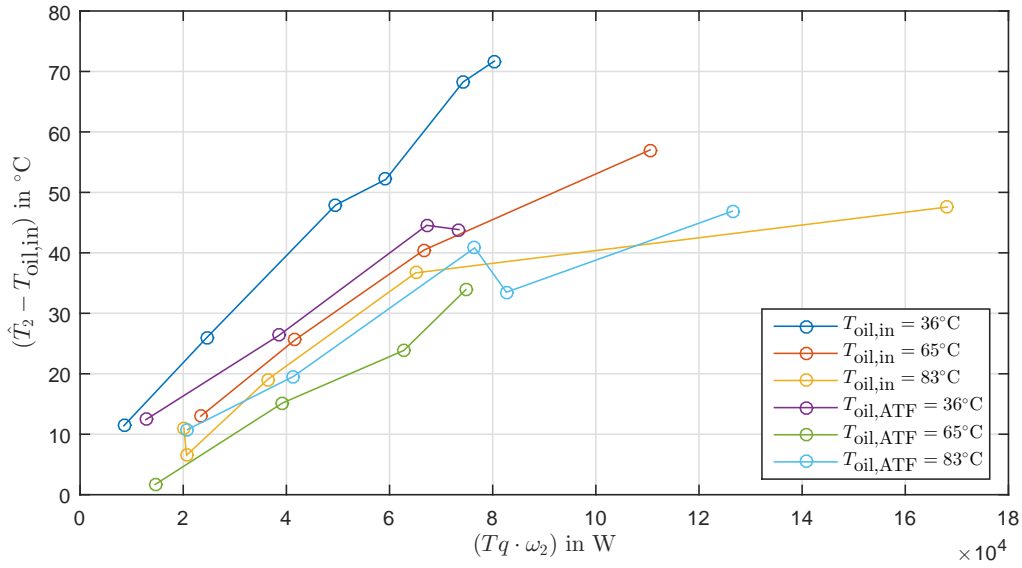
Figure 3.8: Stationary measurement points at 15 different loads in 3 runs for both engine oil and ATF

Dynamic measurements

In the dynamic measurements, the clutch is first open at constant rotational speed and then actuated, such that the torque reaches and keeps a desired, constant value. The rotational speed is then decreased until it reaches 0 and the torque drops to almost 0. The clutch is then opened again and the rotational speed is increased to the initial value. An exemplary sequence of dynamic measurements is shown in figure 3.9.

Dynamic measurements are conducted in 3 runs of different incoming oil temperatures. The rotational speed while the clutch is open is $\omega_2 = 1000$ rpm in all measurements. In each run, 4 different loads are tested. The oil volume flow rate Q is assumed constant during each run.

3.2.3 Parametrization

As mentioned, several parameters needed for the model are not known and need to be identified with measurement data. For an unbiased validation, independent measurement data, that has not been used for parametrization is needed. To keeping the bias of the validation down, only a part of the available measurement data is used for parametrization and the rest is used for validation. Despite the oil volume flow rate Q was treated as an input to the model, it has not been measured on this test bench. When assuming constant oil volume flow rate during one run of measurements, the
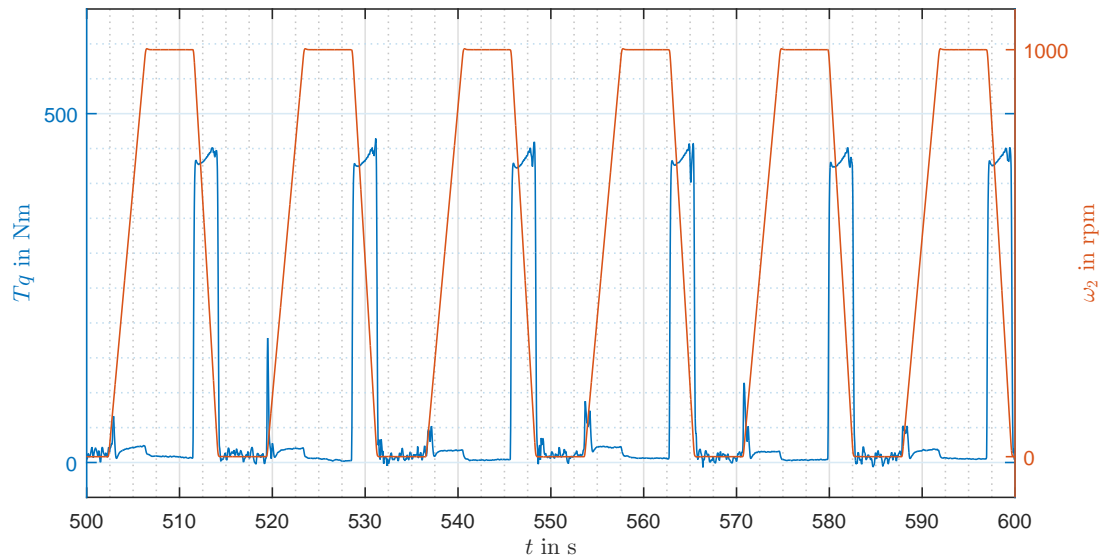
Figure 3.9: Exemplary sequence of dynamic measurements. The clutch is first open at constant rotational speed and then actuated, such that the torque reaches and keeps a desired, constant value. The rotational speed is then decreased until it reaches 0 and also the torque drops to approximately 0. The clutch is then opened again and the rotational speed is increased to the initial value.

oil volume flow rate can be estimated using only the parametrization dataset and treated as known input for the validation.

First, using only stationary measurements, the axial force loss ζ will be estimated. Then, the rest of the parameters will be estimated using both stationary and dynamic measurements.

Parametrization with stationary measurements

The empiric factor ζ for the axial force loss (defined in (2.110)) and the axial thermal transmittance to the casing $u_{\text{ax,in}}$, $u_{\text{ax,out}}$ (see (2.129)) will be estimated by comparing the temperatures of the 3 friction disks to each other. In figure 3.10 and 3.11, the temperatures of all 3 friction disks during the stationary measurements are shown.

Due to the axial heat transfer to the casing from disk 1 and disk 3, the temperature is expected highest in disk 2 and due to the axial force loss, the temperature in disk 1 is expected to be higher than the temperature in disk 3. The measurements in figure 3.10 match this expectation, while in figure 3.11, several measurement points differ from this expectation. Apparently, at low load points as in figure 3.11, other influences outweigh these effects since both the friction force F_{fric} (which is proportional to the
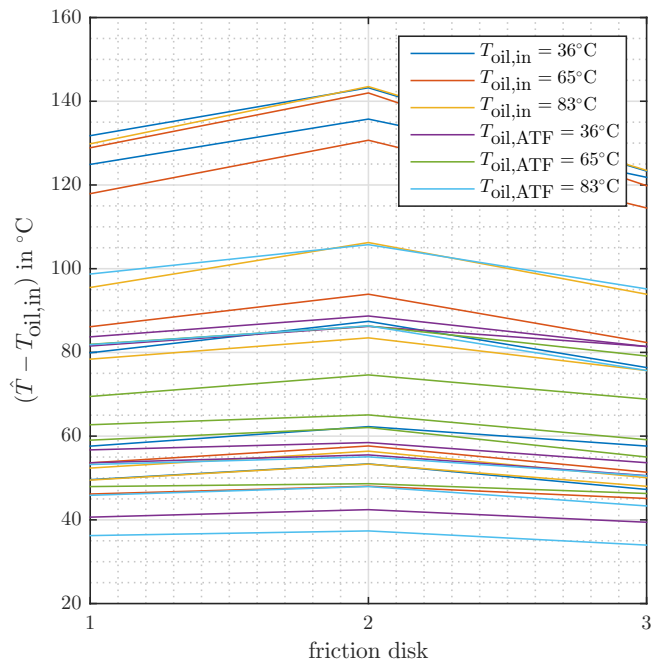
Figure 3.10: Temperature in all 3 friction disks during the stationary measurements in separate runs
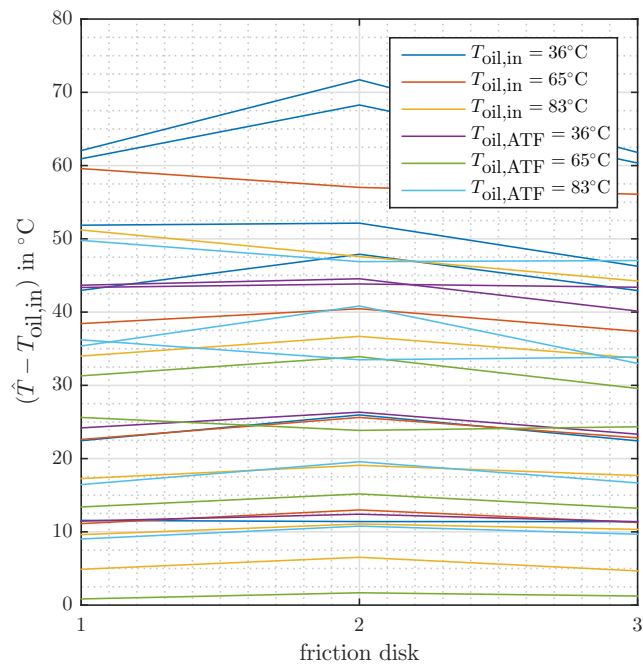

Figure 3.11: Temperature in all 3 friction disks during the stationary measurements in 3 runs

axial force loss) and the rate of axial heat transfer are very low. Therefore, to estimate ζ, $u_{\mathrm{ax,in}}$ and $u_{\mathrm{ax,out}}$, only the measurements shown in figure 3.10 are used.

The axial heat transfer from a friction pair to the casing is assumed uniform on the disk surface. The total rate of axial heat transfer to the casing is estimated with:

$$Q_{\mathrm{ax,in}} = u_{\mathrm{in}} \cdot (\hat{T}_1 - T_{\mathrm{oil,in}}) \cdot (r_{\mathrm{out}}^2 - r_{\mathrm{in}}^2)\pi \tag{3.17a}$$

$$Q_{\mathrm{ax,out}} = u_{\mathrm{out}} \cdot (\hat{T}_3 - T_{\mathrm{oil,in}}) \cdot (r_{\mathrm{out}}^2 - r_{\mathrm{in}}^2)\pi, \tag{3.17b}$$

From the stationary measurements, Q_{ax} will be estimated and with (3.17), the thermal transmittance can then be calculated.

As discussed in chapter 2, the value for ζ is assumed equal for every disk and can be calculated from the difference of the drag torques transmitted at the disk interfaces. To estimate ζ from the temperatures in the friction disks, a relation between the temperatures and the drag torque at each disk needs to be found. In stationary state, the dissipation power at each disk i equals the heat that is emitted from the disk $Q_i(\hat{T}_i)$. With (2.111), (2.110) and (2.116), the dissipation power results in:

$$Q_i = Tq \cdot \zeta^{2i} \cdot \frac{1 + \zeta}{\sum_{j=0}^{n-1} \zeta^j} \cdot \omega_2 \tag{3.18}$$

The emitted heat $Q_i(\hat{T}_i)$ is split in a function $\hat{Q}(\hat{T})$, that is assumed independent of the disk position and the axial heat transfer $Q_{\mathrm{ax}}(\hat{T}_i)$.

$$Q_1(\hat{T}_1) = \hat{Q}(\hat{T}_1) + Q_{\mathrm{ax,in}} \tag{3.19a}$$

$$Q_2(\hat{T}_2) = \hat{Q}(\hat{T}_2) \tag{3.19b}$$

$$Q_3(\hat{T}_3) = \hat{Q}(\hat{T}_3) + Q_{\mathrm{ax,out}}, \tag{3.19c}$$

When linearising the function $\hat{Q}(\hat{T})$ in the interval $[\hat{T}_1, \hat{T}_3]$, the following approximations can be formulated:

$$\hat{Q}(\hat{T}_3) - \hat{Q}(\hat{T}_1) \doteq \left.\frac{\partial \hat{Q}}{\partial \hat{T}}\right|_{\hat{T}_2} \cdot (\hat{T}_3 - \hat{T}_1) \tag{3.20a}$$

$$\hat{Q}(\hat{T}_2) - \hat{Q}(\hat{T}_1) \doteq \left.\frac{\partial \hat{Q}}{\partial \hat{T}}\right|_{\hat{T}_2} \cdot (\hat{T}_2 - \hat{T}_1). \tag{3.20b}$$

With (3.18) and (3.19), the derivative can be expressed as:

$$\left.\frac{\partial \hat{Q}}{\partial \hat{T}}\right|_{\hat{T}_2} = \left.\frac{\partial Tq \cdot \omega_2}{\partial \hat{T}}\right|_{\hat{T}_2} \cdot \zeta^2 \cdot \frac{1 + \zeta}{\sum_{j=0}^{n-1} \zeta^j}, \tag{3.21}$$

where $\left.\frac{\partial Tq}{\partial \hat{T}}\right|_{\hat{T}_2}$ is estimated with a linear regression of $\hat{T}_2 - T_{\text{oil,in}}$ and $Tq \cdot \omega_2$ in all stationary measurements.

Combining equation (3.18)-(3.21) results in:

$$Tq(\zeta^4 - 1) + (Q_{\text{ax,in}} - Q_{\text{ax,out}}) \cdot \frac{1}{\omega_2} \cdot \frac{1 + \zeta}{\sum_{j=0}^{n-1} \zeta^j} = \left.\frac{\partial Tq}{\partial \hat{T}}\right|_{\hat{T}_2} \cdot \zeta^2 \cdot (\hat{T}_3 - \hat{T}_1) \tag{3.22a}$$

$$Tq(\zeta^2 - 1) + Q_{\text{ax,in}} \cdot \frac{1}{\omega_2} \cdot \frac{1 + \zeta}{\sum_{j=0}^{n-1} \zeta^j} = \left.\frac{\partial Tq}{\partial \hat{T}}\right|_{\hat{T}_2} \cdot \zeta^2 \cdot (\hat{T}_2 - \hat{T}_1) \tag{3.22b}$$

Since the presented model leads to only 2 independent equations (3.22), the axial heat transfer is assumed to be equal on both sides of the disk stack $Q_{\text{ax}} := Q_{\text{ax,in}} = Q_{\text{ax,out}}$. Then, (3.22a) becomes:

$$Tq \cdot (\zeta^4 - 1) = \left.\frac{\partial Tq}{\partial \hat{T}}\right|_{\hat{T}_2} \cdot \zeta^2 \cdot (\hat{T}_3 - \hat{T}_1), \tag{3.23}$$

and ζ can be estimated. The results for all considered measurements are shown in figure 3.12. The mean value of all ζ is 0.996. The total axial force reduction for the last friction surface $(1 - \zeta^5) \cdot 100$ % is 2.49 %. Since this value is very low, the errors due to the simplifications made in this chapter will make little contribution to the total error. In [30], the loss of drag torque has been investigated. The percentage of the torque reduction with a stack of 6 disks ranges from 1 % to 35 %. The value in the presented model is therefore within the expected range.

With (3.22b), the rate of axial heat transfer Q_{ax} can be estimated. In figure 3.13, the results for the rate of axial heat transfer are shown. Recalling (3.17), the thermal transmittance $u_{\text{ax}} := u_{\text{ax,in}} \doteq u_{\text{ax,out}}$ is estimated with

$$u_{\text{ax}} = \frac{dQ_{\text{ax}}}{d\hat{T}_2} \frac{1}{(r_{\text{out}}^2 - r_{\text{in}}^2)\pi}, \tag{3.24}$$

where $\frac{dQ_{\text{ax}}}{d\hat{T}_2}$ is the linear regression without intercept from the results in figure 3.13. As can be seen in figure 3.13, a linear regression with intercept would fit the results a lot better. This suggests an offset error in the rate of axial heat transfer.

The results for the axial thermal transmittance is $u_{\text{ax}} = 1577$ W/(m²·K).

Parametrization with stationary and dynamic measurement data

To reduce the computational effort, the influence of the axial heat transfer on the middle disk is neglected for the parameter identification. The model can then be reduced to a single pair of disks.
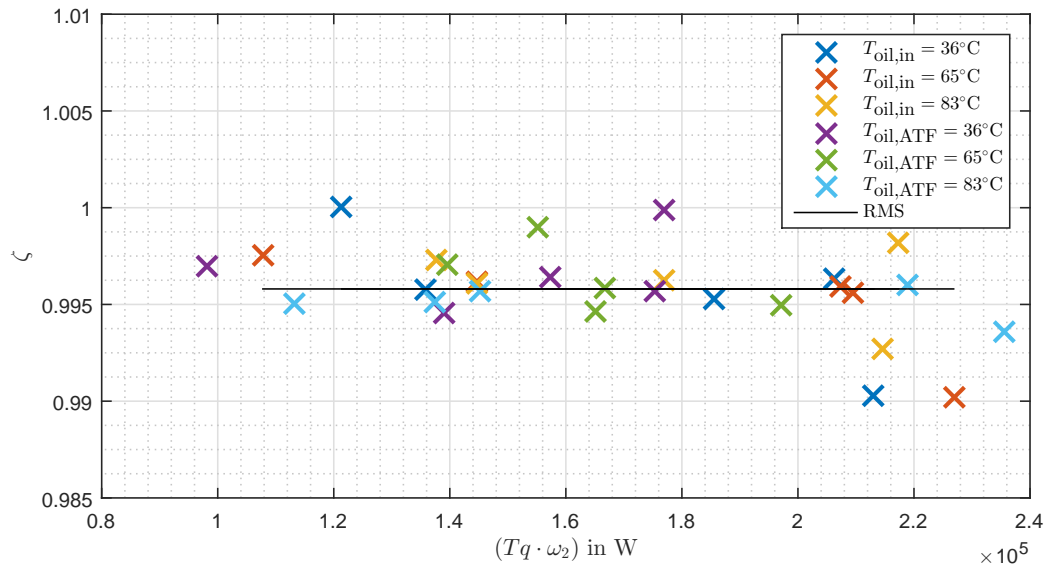
Figure 3.12: The estimated empirical constant ζ for the axial force loss for all considered stationary measurements and the RMS value.
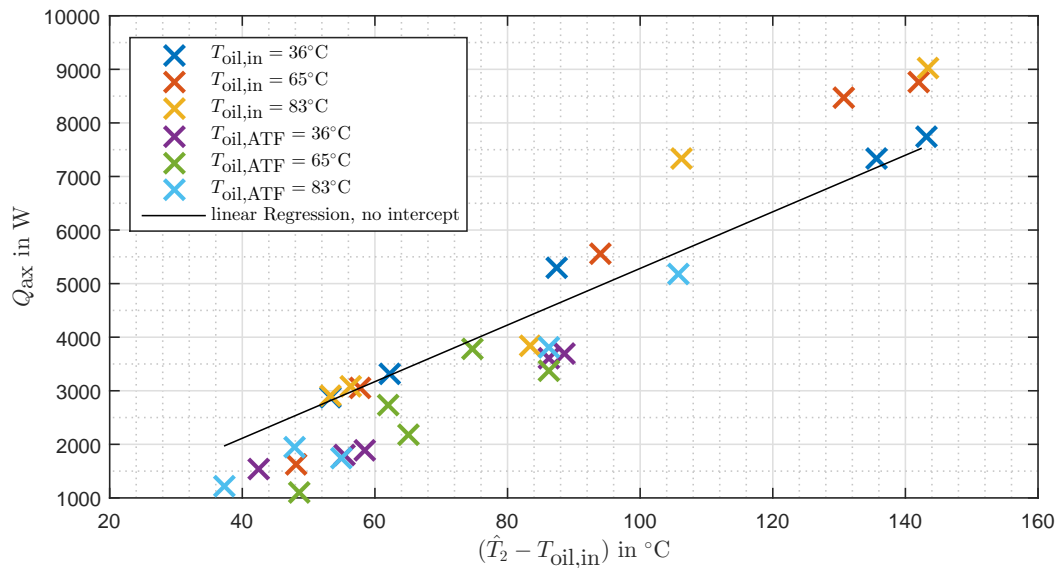

Figure 3.13: The estimated rate of axial heat transfer to the casing for all considered stationary measurements and the linear regression without intercept.

The remaining unknown parameters (as listed in table 3.3) are determined iteratively, minimizing the error of the temperature of the middle paper disk in 1 load of each dynamic measurement run as well as the temperature error in all stationary measurements. The other loads of each dynamic measurement run will be used for validation.

The identified parameters and their expected range of values are listed in table 3.3 and will be discussed in subsection 3.2.5.

Parameter	value	expected range
number of grooves n_g	60	50 - 80
Ratio of grooved area x_g	0.4	0.2 - 0.4
Depth of the grooves $h_g - h_{ng}$	0.25 mm	0.25 - 0.48 mm
Heat capacity and density of the paper friction layer $\rho_p \cdot c_{p,p}$	$1.33 \cdot 10^6$ J/(m^{3}K)	$\approx 1.33 \cdot 10^6$ J/(m^{3}K)
Thermal conductivity of the paper friction layer k_p	0.2 W/(m·K)	0.2 - 0.6 W/(m· K)
Nusselt number in the grooves Nu_g	8.4	7.8 - 8.4
Heat transfer between the disks $h_{c,oil}$	1.2	0.1 - 10
Coefficient for the temperature in the non-grooved area ζ	0.5	0 - 1

Table 3.3: Identified parameters and their expected range of values

The temperature estimation with the parametrized model is shown exemplary for one dynamic measurement sequence in figure 3.14. The position of the temperature sensor is not known, but the measured temperature fits best with the estimated temperature in the inner half of the friction layer (in axial direction) and at radial position $r = 139$ mm. For all following considerations, it is assumed that the temperature was measured at this location and the estimated temperature at this location will be referred as T. The RMS error between the measured and estimated temperature at this location is 1.58 K and the positive and negative maximum error is 5.67 K and -5.62 K respectively. In figure 3.15, the results are shown for one sequence of stationary measurements. In the 4 stationary points, the RMS error of the final temperature is 1.01 K with positive and negative maximum error of 0.9 K and $-1.3K$ respectively.

3.2.4 Validation

To validate the model, first, the estimation error for the present test setup is quantified. Then, to rate the accuracy of the model for other clutches, where the empiric or not exactly known parameters (see table 3.3) are not adjusted, the sensitivity of the model to this parameters is estimated.

Figure 3.14: Resulting temperature estimation from the parametrized model in the inner half of the friction layer T and in the steel disk under the friction layer T_s, and the measured temperature $\hat{T}$ in the middel friction disk.
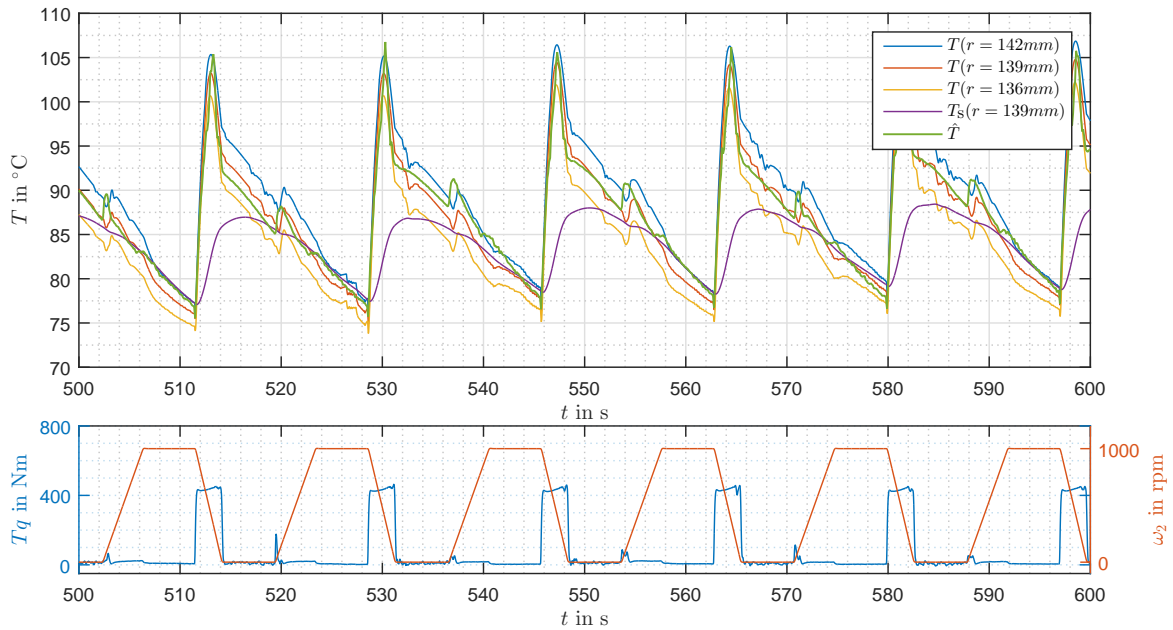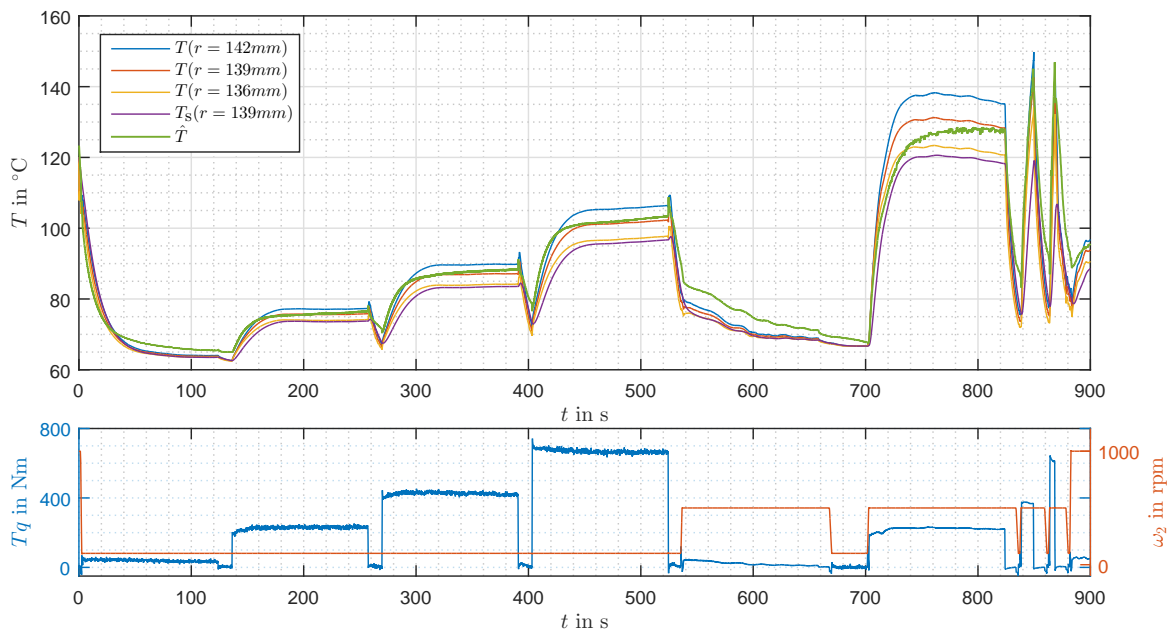

Figure 3.15: Resulting temperature estimation from the parametrized model in the inner half of the friction layer T and in the steel disk under the friction layer T_s, and the measured temperature $\hat{T}$ in the middle friction disk (the exact location is not known).
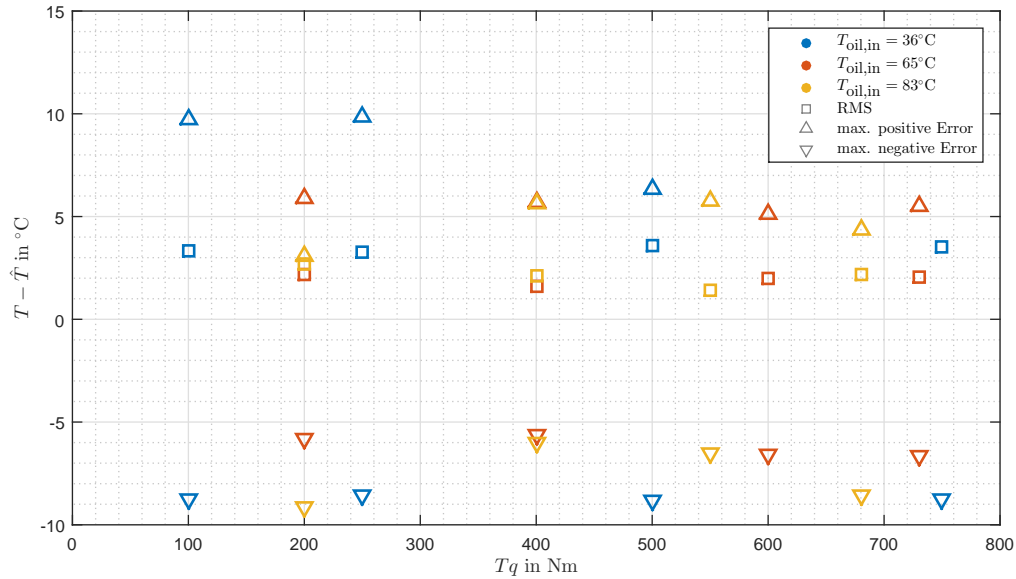
Figure 3.16: Temperature estimation error in all dynamic measurements.

Estimation error

With the parametrized model, the temperature was estimated in all dynamic and stationary measurements. The estimation error for the dynamic measurements is shown in figure 3.16. The total RMS error is 2.61 K and the maximum positive error is 10.27 K. In the stationary measurements, the final temperature in each stationary point has an RMS error of 1.65 K and a maximum positive error of 2.5 K.

Sensitivity analysis

The sensitivity of the model to the parameters in table 3.3 is estimated by comparing the estimation error for varied parameters to the estimation error for the original parametrization. To get an estimate of how much these parameters can vary in reality, measurements on different clutches would be necessary. However, to find the sensitivity of the model to an equal variation of each parameter, consecutively, each parameter is increased and decreased by 20 %. The results are shown in figure 3.17 for the dynamic measurements used for parametrization. The largest error results from an increase of the depth of the grooves $h_{\mathrm{g}} - h_{\mathrm{ng}}$, which increases the RMS error by 38 %. Some variations even decrease the error, since the stationary measurements are not considered for the sensitivity analysis.
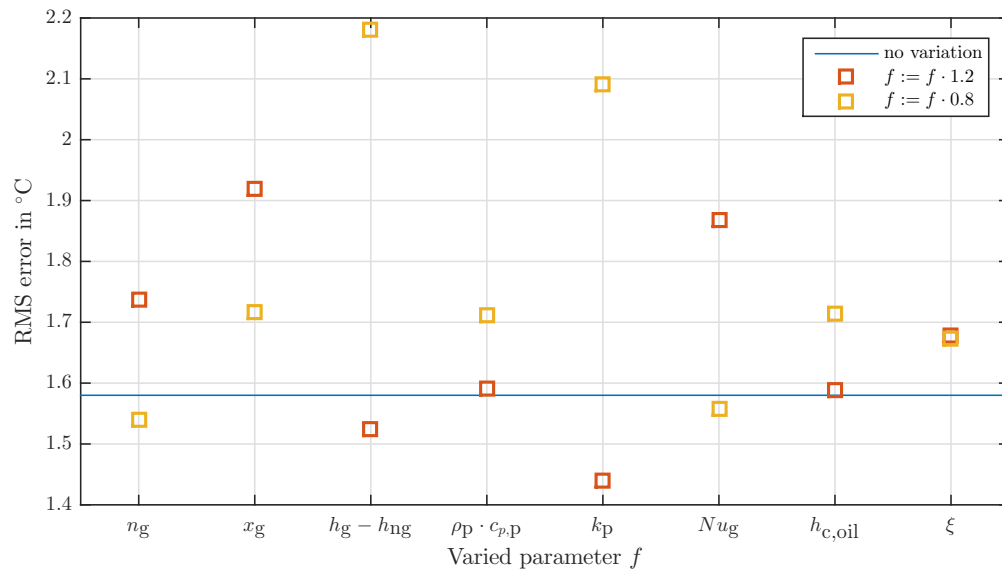
Figure 3.17: Change of the RMS error when parameters of the model are varied. Consecutively, each parameter f is increased or decreased by 20 %.

3.2.5 Discussion

As discussed in the beginning of this chapter, the presented measurement data is not sufficient for a full validation of the model. Therefore, it is particularly important to clarify what conclusions can be made from the presented validation and what remains still uncertain.

During the identification of the parameters for the axial force loss and the rate of axial heat transfer, many restrictive simplifications were made, which led to a large variance of the values for ζ (see figure 3.12) and the rate of axial heat transfer (see figure 3.13). Moreover, since the casing of the clutch and its behaviour regarding the axial force loss and axial heat transfer differ in each clutch, the found parameters will have to be adjusted for every clutch. However, the rate of axial heat transfer from the paper disks to the casing is very low and will therefore have no big influence to the accuracy of the model.

Using also measurement data from dynamic test runs, all parameters in table 3.3 have been found within the expected range. However, the influence of some parameters on the result is redundant. For example, a bigger groove depth $h_\mathrm{g} - h_\mathrm{ng}$ would lead to similar results as a larger ratio of the grooved area x_g combined with a lower Nusselt number in the grooves Nu_g. Therefore, the correct parametrization of the model requires much effort. A purely empirical model with a number of parameters that requires similar effort would likely result in an even better accuracy. However, the sensitivity of the parameters would be much larger than in the presented model.
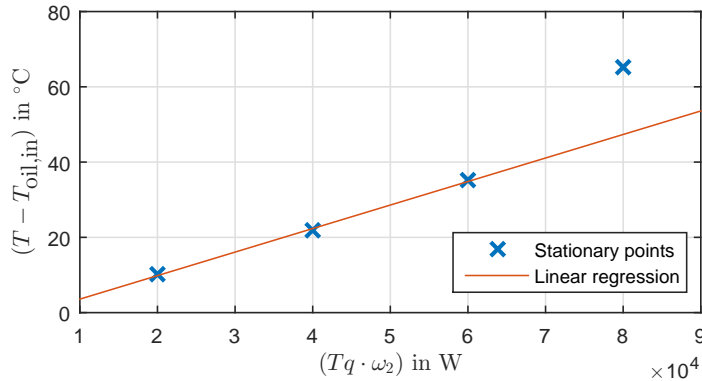
Figure 3.18: In the first 3 stationary points from the sequence in figure 3.15, the relation between temperature and power is linear. However, in the last stationary point, the temperature is higher. The reason is the high rotational speed which causes rivulets to form.

Another advantage of this model compared to an empirical model is, that it can help to understand the physical background of the disk temperature behaviour. The estimated temperature profile over the time qualitatively equals the measured temperature profile most of the time, as can be seen in figure 3.14. For these temperature profiles, the model provides an insight in the oil flow and heat transfer. For example, in the test run shown in figure 3.15, the following two phenomena can be seen:

- When the clutch opens ($t = 260$ s, 390 s, 512 s), there is a sharp upper peak in temperature. This results from the increased heat transfer coefficient $h_{\mathrm{conv,t}}$ due to the increased disk distance h_{ng}, which causes the steel disk to heat the oil even more, which also increases the temperature of the friction disk.
- In figure 3.18, the stationary points from the sequence in figure 3.15 are shown. In the first 3 stationary points, the power $Tq \cdot \omega_2$ is approximately proportional to the temperature difference $T - T_{\mathrm{oil,in}}$. In the last stationary point ($t = 820$ s, $Tq \cdot \omega_2 = 8 \cdot 10^4$ W), the temperature is higher. The reason is, that, due to the high rotational speed ω_2, rivulets are forming and therefore, the rate of convective heat transfer decreases.

The RMS error of the temperature estimation of the parametrized model was very low for all tested measurement sequences. However, especially regarding the thermal stress limits, the maximum positive error is more important.

The sensitivity of the model was analysed by varying each parameter by 20 %. With this variation, the estimation errors still remain in a range that is acceptable for the intended application. However, no estimation of the actual variance of the parameters in different test setups was made. Especially the heat transfer coefficient $h_{\mathrm{c,oil}}$ and the coefficient ξ could possibly vary in a vast range.

4 Summary, conclusions and outlook

4.1 Summary and conclusions

In chapter 1, an overview of this thesis was given and its motivation was discussed shortly.

In chapter 2, a semi-physical model was developed, that provides an estimate of the disk temperature under consideration of many physical phenomena regarding the oil flow between the disks, the convective and conductive heat transfer and generation and distribution of the friction heat. Despite neglecting some effects of minor influence and approximating some phenomena with empirical relations, the complexity of the model is still high. Therefore, defining the numerical procedures to implement the developed relations was a difficult trade-off between accuracy and computational efficiency. However, the chosen procedures can be parametrized depending on the specific application to either increase the accuracy of estimation or decrease the required computational resources.

In chapter 3, first the consistency and stability of the model was determined with numerical analysis and qualitative validation of selected model components. The parameters of the numerical methods need to be chosen with great care to ensure both stable and accurate results. However, correctly parametrized, the model and its components provide estimations of the oil flow and heat transfer that are internally consistent and also consistent with literature.
With measurement data from a test bench, the model was validated empirically. For this, many empirical parameters and unknown properties needed to be estimated with measurements. However, the sensitivity to most of these parameters was rather low. The estimated temperature profile in time of the parametrized model qualitatively equals the measured temperature profile most of the time and also the estimation error was low.

The intention of this thesis was to make a model for estimating the temperature in the disks that can be used to optimize cooling and operation of the clutch system. Due to the requirements to minimize costs, the components are designed closer and closer to their performance limits. An accurate model is therefore necessary to ensure the durability and availability of the clutch system and to design the system at its limits. Also, computational efficiency, transferability and a wide scope of validity is important.

The most critical scope of operation is close to maximum load, where knowledge of the disk temperature is important to prevent overheating and maximizing the durability. The presented model provided good estimates for the temperature maxima with low positive errors. However, further validation with a wider range of measurements is important to ensure that this accuracy will also apply to higher loads.

4.2 Outlook

As discussed, the validation carried out so far, could be expanded with further measurements. To rate the validity and accuracy of the model and its components, further measurements under different conditions as well as the measurement of other quantities are required. Furthermore, some physical effects in the clutch were not investigated so far. The model can possibly be improved by considering these effects.

4.2.1 Consideration of further physical phenomena

In chapter 2, many assumptions and simplifications were made. While many of them where sufficiently justified, the influence of others is still not validated. Some physical phenomena that should be investigated are:

- The clutch disks reach the highest temperature while or immediately after the clutch is closed. Therefore, a correct model for this situation is most important. In the presented model, the time variance of the disk distance h_{ng} was not considered. While the clutch closes, a squeeze flow emerges, that has a great influence on the cooling of the clutch.
- Paper based friction material has a significant permeability, which influences the oil flow and consequently also the heat transfer. The oil flow between the disks with a permeable friction layer was investigated for example in [31].
- The model was developed for a radially grooved friction layer. However, various other patterns are also common. For example the waffle, spiral or swirl pattern as shown in figure 4.1. In [7], the flow model for radial grooves was generalized to grooves with an arbitrary orientation.
- The oil flow was only investigated in the friction surface area. The temperature and flow velocity was assumed to be uniform when entering this region. In reality, the oil is distributed through several holes in the shaft and will therefore not be rotationally symmetric at the beginning of the friction surface.
- The contact pressure on the disk surfaces was assumed uniformly distributed. In reality, the pressure distribution will not be uniform due to deformation, production tolerance and wear. This leads to a different distribution of the
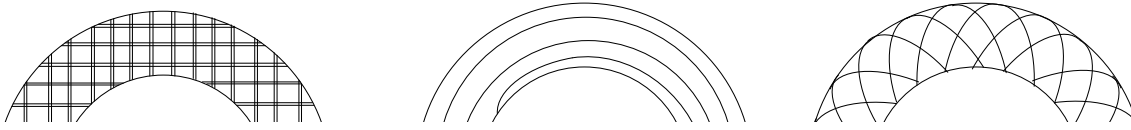
Figure 4.1: Common groove patterns for friction disks: waffle, spiral and swirl (from left to right)

friction heat. For a dry friction clutch, the contact pressure distribution was investigated for example in [32].

- As discussed in chapter 2, due to the axial force loss, the disk distance and consequently also the oil volume flow will be different between each pair of disks. The influence of this effect and its significance have not been investigated in this thesis.

4.2.2 Validation with measurement data

In chapter 3, validation of the model by comparison to measurement data was already conducted. However, these measurement data should be supplemented by further measurements. The model needs to be tested in a wider range of situations and not only the temperature estimation but also the models components need to be validated. This can be done by comparing the model with results from extensive numerical simulations or from measurements on a test bench.

In the following, possible measurement setups and procedures are proposed.

Validation of the oil flow model

In section 2.1, the oil flow was investigated to gather relations for calculating the disk distance h_{ng}, the forming of rivulets ϕ_{riv} and the partition of the oil flow Q_g/Q. The validity of these relations could be verified on an adaptation of the test bench used in chapter 3 as shown in figure 4.2. To reduce the effect of axial force loss, only 1 friction disk is used. Especially for validation of the forming of rivulets, both rotational speeds ω_1 and ω_2 can be specified. The (directly or indirectly) measured variables are:

- the temperature of the incoming oil $T_{oil,in}$
- the torque transmitted by the clutch Tq
- the rotational speed of the friction disk and the separator disk, ω_1 and ω_2 respectively
- the oil volume flow rate Q.
- the disk distance h
- the pressure at the inlet p_{in}

The disk distance h can be determined by measuring the displacement of the piston for closing the clutch. For example in [1], this approach is used and its noise factors are investigated and suppressed. The pressure p_{in} should be measured as close to the clutch as possible to minimize the error caused by pressure loss between the sensor and the disks. This problem is dealt with in [9].

With this test bench, the relation between the drag torque and the disk distance (2.22) can be validated with the measured values for Tq, h, ω_1 and ω_2 in different operation conditions. The forming of rivulets can be tested when measuring the Ω - p_{in} characteristic and comparing it to (2.27). With equation (2.14), the partition of the oil flow Q_g/Q and also the inlet pressure p_{in} can be calculated. With measurement results for the inlet pressure p_{in}, the validity of this equation can be investigated. Especially the following statements should be verified:

- With constant oil volume flow rate Q, the inlet pressure p_{in} does not significantly depend on the difference $\omega_1 - \omega_2$, as long as Ω is constant.
- In open or slipping clutch state with continuous lubrication, the drag torque Tq does not significantly depend on the oil volume flow rate Q
- When rivulets are forming (that is, $p_{in} \lesssim 0$), the torque Tq decreases with the relation $Tq \propto \Omega^{-2}$

Validation of the heat transfer and generation

To validate the heat transfer and generation in the clutch, the test bench used in chapter 3 could be extended by adding temperature sensors to the separator disks and the temperature of the oil splashing out of the disks $T_{oil,out}$.

As it was also conducted in [11] the rate of convective heat transfer can be approximated with temperature measurements of the disk and the oil. The average total convective heat transfer coefficient $h_{conv,t}$ can be estimated with

$$h_{conv,t} \doteq \frac{Q \cdot \rho_{oil} c_{p,oil} \cdot (T_{oil,out} - T_{oil,in})}{\Delta T_{LMTD} \cdot 2\bar{h}^2} \tag{4.1a}$$

$$\Delta T_{LMTD} = [(T(r_{out}) - T_{oil,out}) - (T(r_{in}) - T_{oil,in})] \ln\left(\frac{T(r_{in}) - T_{oil,in}}{T(r_{out}) - T_{oil,out}}\right), \tag{4.1b}$$

where $T(r_{out})$ and $T(r_{in})$ are the temperatures measured at the outer and inner radius of the separator disk respectively.
By comparing these results to the results of the model presented in chapter 2, the accuracy of the presented model can be quantified.

The distribution of the generated heat mainly depends on the distribution of the contact pressure between the disks. In chapter 2, this distribution was assumed constant. The error caused by this assumption can be quantified by comparing the
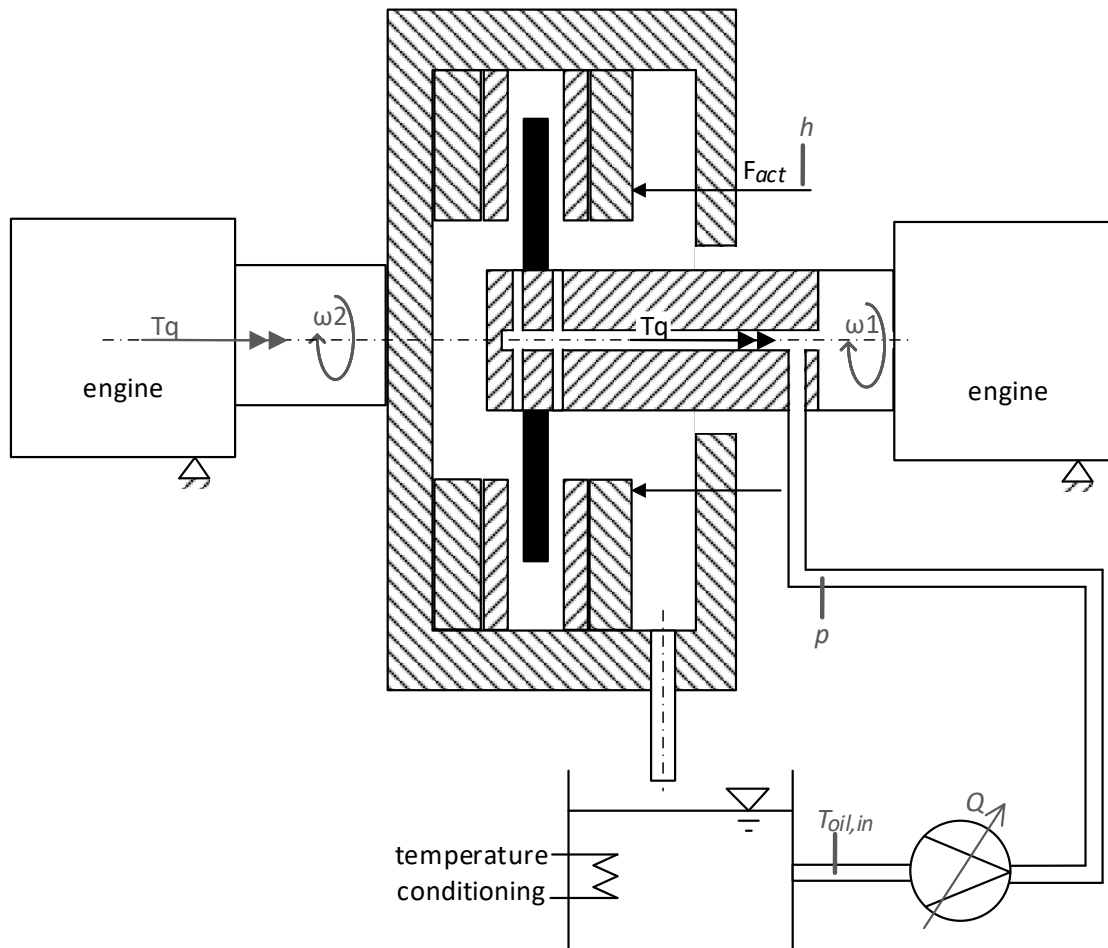
Figure 4.2: Proposed test bench for validating the oil flow model: To reduce the effect of axial force loss, only 1 friction disk is used. Especially for validation of the forming of rivulets, both rotational speeds ω_1 and ω_2 can be specified. The disk distance h is measured indirectly by measuring the displacement of the actuating piston.

temperature difference $T(r_{\mathrm{out}}) - T(r_{\mathrm{in}})$ to the estimation of this temperature difference in the model.

Validation of the complete model

As it was done in chapter 3, the complete model can be validated by comparing the estimated temperature in the disks to the measured values. However, as already discussed, the test bench and the measuring procedure had several issues. The following improvements would lead to a better validation:

- The properties of the friction material (such as density, specific heat capacity and thermal conductivity) are determined beforehand.
- The locations of the temperature sensors in the disks are known.
- The temperature is not only measured in the friction disks but also in the separator disks.
- The oil volume flow rate Q is measured.
- Measurements are also conducted on higher loads and at different rotational speeds.
- Measurements are conducted with at least 2 different clutches of different size

Symbols

Variable	Symbol	Unit
Coordinates		
Radial coordinate	r	m
Axial coordinate	z	m
Angular coordinate	φ	rad
Time	t	s
Indices		
Groove	g	
Non-grooved (between the grooves)	ng	
Separator disk / Surface	s	
Friction disk	f	
Paper material	p	
Sinter material	si	
Geometry		
Disk distance	h	m
Standard deviations of roughness	R_{RMS}	m
Ratio of grooved area to non-grooved area	x_g	-
Hydraulic diameter	D_{hyd}	m
Thermal entry length	$L_{lam,t}$	m
Thermal boundary layer thickness	δ_t	m
Number of grooves	n_g	-
Disk width	b	m
Material properties		
Density	ρ	kg/m^3
Specific heat capacity	c_p	J/(kg·K)
Dynamic viscosity	μ	kg/(m· s)
Thermal conductivity	k	W/(m·K)
Thermal transmittance	u	W/(m^2·K)
Oil flow properties		
Oil volume flow	Q	m^3/s
Flow velocity	v	m/s

Ratio of wetted area to total area	ϕ_{riv}	-
Pressure flow factor	ϕ_p	-
Shear flow factor	ϕ_{s}	-

Dimensionless variables

Nusselt number	Nu
Reynolds number	Re
Prandtl number	Pr
Normalized temperature	θ
Normalized radius	R
Normalized disk distance	H
Normalized velocity	U

Other variables

Rotational speed	ω	rad/s
Characteristic rotational speed	Ω	rad/s
Pressure	p	N/m^2
Shear stress	$\sigma_{\varphi z}$	N/m^2
Force	F	N
Axial force loss	ζ	-
Friction coefficient	μ_{fric}	m^2
Torque	τ	N· m
Temperature	T	K
Heat transfer	q	W/m^2
Antiderivative of the heat transfer	$F_{q_{\mathrm{conv}}}$	W/m
Axial heat transfer on the whole surface area	Q_{ax}	W
Convective heat transfer coefficient	h_{conv}	$W/(m^2 \cdot K)$
Coefficient for the temperature in the non-grooved area	ξ	-

Bibliography

[1] J. Cho. "A multi-physics model for wet clutch dynamics." PhD thesis. The University of Michigan, 2012.

[2] G. Rao. "Modellierung und Simulation des Systemverhaltens nasslaufender Lamellenkupplungen." PhD thesis. Technische Universität Dresden, 2010.

[3] K. A. Snima. "Kenngrößen und Belastungsgrenzen von nasslaufenden Lamellenkupplungen unter Dauerschlupfbeanspruchung." PhD thesis. Universität Karlsruhe, 2005.

[4] O. Reynolds. "IV. On the Theory of Lubrication and its Application to Mr. Beauchamp Tower's Experiments, including an Experimental Determination of the Viscosity of Olive Oil." In: *Philosophical Transactions of the Royal Society of London* (1885).

[5] Y. Hori. *Hydrodynamic Lubrication*. Tokyo: Springer, 2006. ISBN: 9784431279013.

[6] N. Patir and H. S. Cheng. "An Average flow Model for Determining Effects of Three-Dimensional Roughness on Partial Hydrodynamic Lubrication." In: *Journal of Lubrication Technology* 100.1 (1978), pp. 12–17.

[7] M. M. Razzzaque and T. Kato. "Effects of a Groove on the Behavior of a Squeeze Film Between a Grooved and a Plain Rotating Annular Disk." In: *Journal of Tribology* 121.4 (1999), pp. 808–815.

[8] S. A. Pahlovy, S. F. Mahmud, and M. Ogawa. "Development techniques of high efficiency with low drag torque automatic transmission friction disk." In: *16th International CTI Symposium Automotive Transmissions, HEV and EV Drives*. Berlin, 2017.

[9] S. Iqbal et al. "Model for Predicting Drag Torque in Open Multi-Disks Wet Clutches." In: *ISRN Tribology* 136.2 (2013).

[10] M. Thirumaleshwar. *Fundamentals of heat and mass transfer*. Mumbai: Pearson Education, 2009. ISBN: 9789332503397.

[11] P. Payvar. "Laminar heat transfer in the oil groove of a wet clutch." In: *International Journal of Heat and Mass Transfer* 34.7 (1991), pp. 1791–1798.

[12] R. M. Abdel-Wahed, S. V. Patankar, and E. M. Sparrow. "Fully developed laminar flow and heat transfer in a square duct with one moving wall." In: *Letters in Heat and Mass Transfer* 3.5 (1976), pp. 355–364.

[13] N. Patir and H. S. Cheng. "Application of Average Flow Model to Lubrication Between Rough Sliding Surfaces." In: *Journal of Lubrication Technology* 101.2 (1979), pp. 220–230.

[14] Y. Pinchiver and J. Rubinstein. *An Introduction to Partial Differential Equations.* New York: Cambridge University Press, 2005. ISBN: 9780521848862.

[15] J. Schenk and J. M. Dumore. "Heat transfer in laminar flow through cylindrical tubes." In: *Applied Scientific Research, Section A* 4.1 (1953), pp. 39–51.

[16] N. M. Temme. *Special functions : An Introduction to the Classical Functions of Mathematical Physics.* Amsterdam: Wiley-Interscience, 1996. ISBN: 9780471113133.

[17] D. Duffy. *Finite Difference Methods in Financial Engineering: A Partial Differential Equation Approach.* Chichester: John Wiley & Sons, Ltd, 2006. ISBN: 9781118673447.

[18] S.D. Conte and Carl de Boor. *Elementary numerical analysis.* 3rd ed. New York: McGraw-Hill Book Company, 1980. ISBN: 9780070662285.

[19] L. Guoqiang, M. Biao, and L. Heyan. "Research of Torque Response Characteristics During the Engagement of Wet Clutches." In: *International Conference on Mechanical Engineering and Material Science* Mems (2012), pp. 295–298.

[20] M. Mansouri et al. "Thermal and Dynamic Characterization of Wet Clutch Engagement With Provision for Drive Torque." In: *Journal of Tribology* 123.2 (2001), p. 313.

[21] G. Chen, K. Baldwin, and E. Czarnecki. "Real Time Virtual Temperature Sensor for Transmission Clutches." In: *SAE International Journal of Engines* 4.1 (2011), pp. 1523–1535.

[22] R. C. Xin and W. Q. Tao. "Analytical Solution for Transient Heat Conduction in Two Semi-infinite Bodies in Contact." In: *Journal of Heat Transfer* 116.1 (1994), pp. 224–228.

[23] Z. Zhigang, S. Xiaohui, and G. Dong. "Dynamic Temperature Rise Mechanism and Some Controlling Factors of Wet Clutch Engagement." In: *Mathematical Problems in Engineering* 2016 (2016), pp. 1–12.

[24] J. Liu et al. "Amelioration and Finite Element Analysis for Oil Groove of a Wet Clutch Friction Disk." In: *2nd International Conference on Electronic & Mechanical Engineering and Information Technology* (2012), pp. 1891–1895.

[25] T. C. Jen and D. J. Nemecek. "Thermal analysis of a wet-disk clutch subjected to a constant energy engagement." In: *International Journal of Heat and Mass Transfer* 51.7-8 (2008), pp. 1757–1769.

[26] L. Lu and N. A. Bakar. *Manufacturing Engineering and Intelligent Materials.* Guangzhou: International Conference on Manufacturing Engineering and Intelligent Materials, 2015. ISBN: 9781315681573.

[27] R. Gomeringer et al. *Tabellenbuch Metall*. Haan-Gruiten: Verlag Europa-Lehrmittel, 2014. ISBN: 978-3-8085-1726-0.

[28] "Thermal Properties Materials Database." In: *thermtest.com/materials-database*. Mar. 2018.

[29] "Anton Paar Wiki: viscosity table and viscosity chart." In: *wiki.anton-paar.com*. Mar. 2018.

[30] W. Beisel. "Untersuchungen zum Betriebsverhalten nasslaufender Lamellenkupplungen." PhD thesis. TU Berlin, 1983.

[31] E. J. Berger, F. Sadeghi, and C. M. Krousgrill. "Analytical and Numerical Modeling of Engagement of Rough, Permeable, Grooved Wet Clutches." In: *Journal of Tribology* 119.1 (1997), p. 143.

[32] O. I Abdullah, J. Schlattmann, and M. Lytkin. "Effect of Surface Roughness on the Thermoelastic Behaviour of Friction Clutches." In: *FME Transactions* 43 (2015), pp. 241–248. DOI: 10.5937/fmet1503241A.